Doctoral Thesis

An Improvement of the SPH Method for Landslide Hazard Prediction and Mitigation

July, 2016

NGUYEN Tien Cuong

Doctoral Thesis reviewed
by Ritsumeikan University

An Improvement of the SPH Method for Landslide Hazard Prediction and Mitigation

(斜面崩壊の予知と減災のための SPH 法の改善)

July 2016
2016 年 7 月

NGUYEN Tien Cuong
グエン　ティエン　クオン

Principal referee: Professor FUKAGAWA Ryoichi
主査：深川　良一教授

ACKNOWLEDGEMENT

First of all, I would like to express my deepest gratitude to my supervisor professor, Prof. Ryoichi Fukagawa, Professor at the Graduate School of Science and Engineering, Ritsumeikan University, for all of the very strong support and the encouragement during my PhD study in the last five years. Thank you for giving me the opportunity go to the Ritsumeikan University and having freedom to select my research topic.

I would like to sincerely thank Dr. Ha H. Bui, Senior Lecturer at Department of Civil Engineering, Monash University, Australia, for all of the opportunity and continuous supports. The theoretical work on SPH presented in my thesis was based on the research framework that was originally developed by Dr. Ha H. Bui. Therefore, I could not complete my study, especially the study on SPH simulation without the support from Dr. Ha H. Bui. With me, he is a good friend of mine and also a dedicated teacher, together with Prof. Fukagawa, mentoring and monitoring me throughout the years. Thanks to that I have achieved good results in my work.

I would like to thank Prof. Hoang Van Lai, Professor at Institute of Mechanics, Vietnam Academy of Science and Technology for his support and encouragement to complete this work. I also would like to thank the committee members, Prof. John C. Wells and Prof. Kazuyuki Izuno, Professors at Graduate School of Science and Engineering, Ritsumeikan University, for their time to read and comment my thesis.

I would like to thank JSPS (Japan Society for the Promotion of Science) for their financial supports by RONPAKU fellowship ID number VNM11010.

I also would like to give my special thanks to my parents, my lovely wife and my children for the care, and the encouragement enabled me to complete this research.

And finally, I would like to say "thank you very much" with all my heart to all of my colleagues and friends in Vietnam and Japan for the encouragement and kind helps during last five years.

NGUYEN TIEN CUONG, Ritsumeikan University

March, 2016

ABSTRACT

In this dissertation, I focus on improving Smoothed Particles Hydrodynamics (SPH) method approach, in order to predict the landslide process with purpose of mitigating the hazard. Currently, in numerical simulation of geotechnical problems using SPH approach, researchers have to use artificial viscosity to stabilize the model. But it is difficult to identify two unknown parameters because these parameters will be different for each different problem. In this thesis, a new SPH approach combining viscous damping with stress/strain regularisation is proposed for simulation of granular flows. This improvement helps to eliminate the need to use artificial viscosity during the calculation. The results of numerical model show that beside the good failure kinematic simulation of the slope, the forecast of stress distribution during slope demolition is also exact. This is a significant step of SPH approach, because in the previous calculation results of other researchers, the stress field was so noisy and had low accuracy.

To verify the improvement of the model, I have made a series of experiments on the failure of 2D granular columns, as recorded in detail by a high-speed camera. The results of SPH simulation have been compared with the experimental ones in terms of both space and time. This is the first time the SPH approach to soil mechanics problem, has been verify in both space and time. Based on my experimental results, I analyzed and identified a number of empirical formulas of the failure process of 2D granular columns. These formulas predict the farthest distance that the granular columns can run out failure based on their original dimensions.

Also in this dissertation, the reduction of landslide possibility is studied both by experiment and numerical simulation using the above SPH approach. The experiments, relating to two dimensional retaining wall (2D) using rectangular blocks, are also recorded in detail by high-speed camera. The results of this experiment show in detail the types of failure mechanism of retaining wall system. This is a complete and reliable set of data on the box-shaped retaining wall failure mechanism that other researchers can use to verify their numerical models. The failure mechanisms of this retaining wall system have been accurately simulated by SPH approach.

NGUYEN TIEN CUONG, Ritsumeikan University

March, 2016

CONTENTS

CHAPTER 1

INTRODUCTION

Landslides are a dangerous threat. It may be natural disasters such as landslides of mountain, soil – rock, snow ice, etc. and also disasters caused by human. Especially under the current effects of global climate change, the natural landslides have been becoming more complicated, increased both in number and scale. Recent years, landslides concentrated in Asian countries as Vietnam (Tran Thuc et al., 2015), India, China (see Figure 1.1), Japan (see Figure 1.2), Afghanistan (see Figure 1.3), etc.

Figure 1.1: *Landslide in Quangdong, China 2015 (source from http://mashable.com)*

Figure 1.2: *Landslide in Hiroshima, Japan 2014 (source from http://www.thetimes.co.uk)*

Figure 1.3: *Landslide in Afghanistan 2014 (source from http://www.theatlantic.com)*

There are many reasons that cause landslide, but can be divided into two basic ones as follows:

The first type is caused by an imbalance of the slope. This kind often happens when there are impacts that make change to slope as activities that change the status of slope's foot. In addition, this can occurs due to the impact of external forces such as earthquakes or overloaded pressures on slope. In this case, the road landslides caused by over-loaded vehicles in mountainous areas are an example.

The second one is caused by change in mechanical and physical characteristics of the slope itself that lead to imbalance. This type includes phenomena as mountain landslide caused by heavy or the long-timed rain or avalanche caused by temperature change, etc.

In this thesis, I focus on studying the post-flow failure characteristics. This study can help prevent or reduce damages of the first type. The natural and artificial slopes are usually structured in debris such as landslide of soil- structured slopes, sliding in the storage of tablet drugs or in the storage of agricultural products as corn, rice, etc. So, to research this issue, the two-dimensional granular flow is appropriate.

To study this landslide phenomenon, many researchers have studied the failure process of two-dimensional (2D) and three-dimensional (3D) granular-textured slopes. The studies are carried out both by experiments in the laboratory and by numerical simulation models. Researchers who have studied quasi-2D experiment model (in the laboratory and numerical experiment) include Balmforth and Kerswell (2005) used grit, fine glass, coarse glass, and polystyrene as granular materials for experiments with wide channels and narrow slots, Lube et al. (2005) used Fine quartz sand, Coarse quartz sand, Sugar, Rice as materials for experiment within a channel, Lajeunesse et al. (2005) used different diameter Glass beads for experiment in rectangular channel and Trepanier et al. (2010) used granular rod piles as a function of particle length/diameter and pile height/radius aspect ratio for experiment. The above researchers have found the relationship between the initial granular size (the height and width) and the run out-distance of granular flow. In addition to the quasi-2D experiments, the mechanism of granular flow under axisymmetric conditions (i.e., 3D conditions) is often investigated. Typical experiments of this type were done by Lube et al. (2004), Lajeunesse et al. (2004), Lajeunesse et al. (2005) and most recently Warnett et al. (2014) used a limestone particulate with bulk density as material for experiment with different diameter cylinder to identify the relation between the initial cylinder size and the run out-distance of granular flow. Researchers who have studied numerical models to simulate include Bui (2007), Bui

et al. (2006, 2008a, 2008b, 2009) simulate granular flows by application of Lagrangian meshfree particle method (SPH-Smoothed Particle Hydrodynamics) for large deformation and failure flows of geo-material using elastic–plastic soil constitutive model, Trepanier and Franklin (2010) used SPH method to study granular flows, Staron and Hinch (2005) used Discrete Element Methods (DEM) to study the collapse of two-dimensional granular columns. Based on the results of numerical experiments, the researchers pointed out the relation between granular columns' initial sizes with the run out-distance of granular flows.

The studies on the failure of grain columns haven't been performed by many researchers. The studies as published are mainly 3D and quasi-2D. Therefore, in this dissertation, I conduct a series of truly two-dimensional (2D) experiments on the failure of granular columns in order to study the failure mechanism as well as create a basis for testing the numerical model in this case.

Studies on the failure of 2D granular columns by numerical model mainly using the methods based on the platform of grid system such as finite element method (FEM), finite difference method (FDM) etc. Recently, some researchers have used the discrete element methods (DEMs) to investigate the failure mechanisms of granular flows (Cleary and Sawley, 2002; Staron and Hinch, 2005, 2007; Zenit, 2005; Lacaze et al., 2008; Krabbenhoft et al., 2012; Girolami et al., 2012; Guo et al., 2014; Utili et al., 2015; Kermani et al., 2015), the material point method (MPM) (Kumar et al., 2013; Carter et al., 2014), the particle finite element method (PFEM) (Zhang et al., 2014) and the smoothed particle hydrodynamic (SPH) method (Bui et al., 2008a; Nguyen et al., 2013) , etc. The SPH has recently been developed and applied as an alternative to the previous methods with a lot of granular non-grid method's advantages.

In this dissertation, I have studied the failure characteristics and mechanisms of the truly two-dimensional granular columns and retaining wall system both by experiment and numerical simulation for the purpose of mitigating the damages caused by landslides. The experimental results are not only allows me to find out the experiment functions but also to use these functions to verify my numerical model.

In this thesis, The SPH method I choose is Lagrangian particle mesh-free method to study the failure mechanism of the granular columns because it is suitable for solving this problem. Really, solving this problem by using SPH method helps me overcome some difficulties that other methods face. The finite element method (FEM) faces huge difficulties in simulating large deformation and flexible behavior of wall blocks (i.e. full rotational and

translational motions) in the modular-block retaining wall system (MRWs); At present, the discrete element method (DEM) is popular in geotechnical applications. This method can be used to simulate the motion mechanism of modular-blocks in the MRWs. But the accuracy is low due to the difficulty in selecting parameters for contact laws; The discontinuous deformation analysis (DDA) has also been applied to geotechnical applications, but is mainly used for rock engineering; Some other mesh-less methods are proposed to use as the mesh-less Galerkin element method (EFG), material point method (MPM), particle in cell method (PIC), etc. However, they are quite complicated to use because they consist of both interpolation points and the background mesh. Moreover, my studies on numerical model in this thesis, also inherited the results of SPH method for previous simulations of granular flows by Bui et al (2008a).

In this thesis, I have also researched on the failure mechanism of MRWs. The studies were done both in laboratory experiments and in numerical methods. A series of experiments on MRWs' failure mechanism was done. The results also showed me the overall failure mechanisms of MRWs. To get full data for failure simulation of MRWs by numerical model, a series of experimental measurements have been done to determine other needed parameters. My meshfree SPH model was developed based on results of previous researches done by Bui et al. to simulate large deformation and post-failure of the BRW systems.

The dissertation is organized as follows:

Chapter 1: Overview of landslide and its problems study based on failure mechanism of two-dimensional slope, namely two-dimensional (2D) granular columns by both experiments and numerical simulation. This chapter also introduces the organizational structure of the dissertation.

Chapter 2: This chapter provides information on my series of experiments performed in the laboratory in order to study problems of the destructive mechanism of truly two-dimensional granular columns on both hard and soft ground surface. All experiments are recorded by a high speed camera. The experimental results show in detail the failure mechanism. From the series of experimental data on the failure, I have analyzed and found some experiment functions. That can, based on the original size of the granular columns, predict the influence area after failure.

Chapter 3: In this chapter, I focus on improving the SPH approach to forecast the process of landslide. In the SPH approach, I replace the artificial viscosity by combining viscous damping with stress/strain regularisation. This new approach helps reducing the difficulties in specifying the constants used for artificial viscosity. The calculation results show that the improved SPH meshfree approach makes prediction exactly not only in 2D-granular- columns failure mechanism but also in stress distribution during the failure precess.

Chapter 4: In this chapter, I introduce some studying results in failure mechanism of Modular-block retaining wall system through a series of laboratory experiments and numerical simulation applying SPH meshfree method. Modular-block retaining wall system has been modeled in SPH, allowing the motion simulation of these blocks in form of translation and rotation. The interaction between the retaining wall and the inside materials have been also modeled and introduced in detail in this chapter. The numerical simulation results have been proven with the experiment as stated in Chapter 2.

Chapter 5: Present my main conclusions of the SPH improvement to forecast the process of landslide. Besides that, I also point out next study plan based on continuing the study approach that have been implemented in the dissertation, in order to apply SPH meshfree method to forecast the slope landslide in reality.

List of Publications: Lists the published works of my colleagues and me that relate to the content of the dissertation.

REFERENCES

[1] Information from website of NASA about Global Flood and Landslide Monitoring; http://pmm.nasa.gov/trmm/flood-and-landslide-monitoring

[2] Balmforth, N. J. and R. R. Kerswell; "Granular Collapse in Two Dimensions", *Journal of Fluid Mechanics*, **538**, pp. 399–428 (2005)

[3] Bui, H. H., R. Fukagawa, and K. Sako; "Smoothed Particle Hydrodynamics for Soil Mechanics", *Proceedings of the 6th European Conference on Numerical Methods in Geotechnical Engineering*, pp. 278–281 (2006)

[4] Bui, H. H.; "*Lagrangian Mesh-free Particle Method (SPH) for Large Deformation and Post-failure of Geomaterials Using Elasto-plastic Soil Constitutive Models*", Ph.D. Thesis, Ritsumeikan University, Japan (2007)

[5] Bui, H. H., R. Fukagawa, K. Sako and S. Ohno; "Lagrangian Mesh-free Particles Method (SPH) for Large Deformation and Failure Flows of Geomaterial Using Elastic-plastic Soil Constitutive Model", *International Journal for Numerical and Analytical Methods in Geomechanics*, **32**(12), pp. 1537–1570 (2008a)

[6] Bui, H. H., R. Fukagawa, K. Sako and J. C. Wells; "SPH-based Numerical Simulations for Large Deformation of Geomaterial Considering Soil-structure Interaction", *The 12th International Conference of International Association for Computer Methods and Advances in Geomechanics* (IACMAG), pp. 570–578 (2008b)

[7] Bui, H. H., R. Fukagawa, K. Sako, ad J. C. Wells; "Numerical Simulation of Granular Materials Based on Smoothed Particle Hydrodynamics (SPH)", *Powders and Grains, AIP Conf. Proc*. pp. 575–578 (2009)

[8] Carter M. M., Arduino, P., Mackenzie-Helnwein, P., & Miller, G. R.; "Simulating granular column collapse using the Material Point Method", *Acta Geotechnica*, **10**(1), 101-116 (2014)

[9] Cleary, P. W., M. L. Sawley; "DEM modelling of industrial granular flows: 3D case studies and the effect of particle shape on hopper discharge", *Applied Mathematical Modelling*, **26** (2), 89-111 (2002)

[10] Girolami L., Hergault V., Vinay G., and Wachs A.; "A three-dimensional discrete-grain model for the simulation of dam-break rectangular collapses: Comparison between numerical results and experiments", *Granular Matter* **14**(3) 381-392 (2012)

[11] Guo, Y., J. S. Curtis; "Discrete Element Method Simulations for Complex Granular Flows", *Annual Review of Fluid Mechanics*, **47**, 21-46 (2014)

[12] Kermani, E., Qiu, T., & Li, T.; "Simulation of Collapse of Granular Columns Using the Discrete Element Method", *International Journal of Geomechanics*, 04015004 (2015)

[13] Krabbenhoft, K., Lyamin, A. V., Huang, J., & da Silva, M. V.; "Granular contact dynamics using mathematical programming methods", *Computers and Geotechnics*, **43**, 165-176 (2012)

[14] Kumar, K., Soga, K., Delenne, J. Y.; "Multi-scale modelling of granular avalanches", *AIP Conf. Proc* **1542**, 1250-1253 (2013).

[15] Lacaze, L., Phillips, J. C., & Kerswell, R. R.; "Planar collapse of a granular column: Experiments and discrete element simulations", *Physics of Fluids*, **20**(6), 063302 (2008).

[16] Lajeunesse, E., A. Mangeney-Castelnau, and J. P. Vilotte; "Spreading of a Granular Mass on a Horizontal Plane", *Physics of Fluids*, **16**(7), pp. 2371–2381 (2004)

[17] Lajeunesse, E., J. B. Monnier and G. M. Homsy; "Granular Slumping on a Horizontal Surface", *Physics of Fluids*, **17**(10), p. 103302 (2005)

[18] Lube, G., H. E. Huppert, R. S. J. Sparks, and A. Freundt; "Collapses of Two-dimensional Granular Columns", *Physical Review E*, **72**(4), pp. 1–10 (2005)

[19] Lube, G., H. E. Huppert, R. S. J. Sparks and M. A. Hallworth; "Axisymmetric Collapses of Granular Columns", *Journal of Fluid Mechanics*, **508**, pp. 175–199 (2004)

[20] Nguyen, C. T., H. H. Bui, R. Fukagawa; "Two-dimensional numerical modelling of modular-block soil retaining walls collapse using meshfree method", *Int. J. of GEOMATE*, **5** (1), 647-652 (2013)

[21] Staron, L. and E. Hinch; "Study of the Collapse of Granular Columns Using Two-dimensional Discrete-gain Simulation", *Journal of Fluid Mechanics*, **545**, pp. 1–27 (2005)

[22] Staron, L., Hinch, E. J.; "The spreading of a granular mass: role of grain properties and initial conditions", *Granular Matter*, **9**(3-4), 205-217 (2007).

[23] Tran Thuc and Knoos Neefjes, Ta Thi Thanh Huong, Nguyen Van Thang, Mai Trong Nhuan, Le Quang Tri, Le Dinh Thanh, Huynh Thi Lan Huong, Vo Thanh Son, Nguyen Thi Hien Thuan, Le Nguyen Tuong; "*Vietnam Special Report on Managing the Risks of Extreme Events and Disasters to Advance Climate Change Adaptation*", Vietnam Publishing House of Natural Resources, Environment and Cartography (2015)

[24] Trepanier, M. and S. V. Franklin; "Column Collapse of Granular Rods", *Physical Review E*, **82**, p. 011308 (2010)

[25] Utili, S., Zhao, T., and Houlsby, G. T.; "3D DEM investigation of granular column collapse: Evaluation of debris motion and its destructive power", *Engineering Geology*, **186**, 3-16 (2015)

[26] Zhang, X., Krabbenhoft, K., Sheng, D.; "Particle finite element analysis of the granular column collapse problem", *Granular Matter*, **16**(4), 609-619. (2014)

[27] Zenit, R.; "Computer simulations of the collapse of a granular column", *Physics of Fluids*, **17**(3), 031703 (2005).

[28] Warnett, J. M., P. Denissenko and P. J. Thomas; "Scalings of axisymmetric granular column collapse". *Granular Matter*, **16**, pp. 115–124, (2014).

CHAPTER 2

EXPERIMENTAL INVESTIGATION OF LANDSLIDE MECHANISM

2.1. INTRODUCTION

The flow of granular material is commonly observed in engineering applications such as the transport of minerals, powder, or cereals and during geophysical events such as landslides and debris flow. Understanding the mechanisms of granular flow will help to optimize industrial processes and to minimize damage caused by natural disasters. Accordingly, many scientists have been interested in studying this problem both experimentally and by using numerical simulations under two-dimensional (2D) and three-dimensional (3D) conditions.

In the past, most 2D granular flow experiments have been conducted in narrow horizontal flow channels by using 3D materials such as sandy soils or plastic/glass beads. Typical examples of this type of quasi-2D experiment include those of Balmforth and Kerswell (2005), Lube et al. (2005), Lajeunesse et al. (2005), and Trepanier et al. (2010). By using grit, fine glass, coarse glass, and polystyrene as granular materials, Balmforth and Kerswell (2005) reported the following relationship between the final run-out distance and the initial aspect ratio of the granular column: $(d_\infty - d_0)/d_0 \simeq a^{0.9\pm0.1}$ for wide channels, and $(d_\infty - d_0)/d_0 \simeq a^{0.65\pm0.05}$ or $d_\infty/d_0 \simeq a^{0.55\pm0.05}$ for narrow slots, where $a = h_0/d_0$; h_0 and d_0 are the initial height and width of the column, respectively; h_∞ and d_∞ are the maximum final height and width of the column, respectively. In similar experiments using fine quartz sand, coarse quartz sand, sugar, and rice as granular materials, Lube et al. (2005) concluded that $(d_\infty - d_0)/d_0 = 1.2a$ for $a < 1.8$ and $(d_\infty - d_0)/d_0 = 1.9a^{2/3}$ for $a > 2.8$. There was no abrupt break in the

curve $(d_\infty - d_0)/d_0$, within the small transitional region of $1.8 < a < 2.8$ between the linear and power-law ranges. Lajeunesse et al. (2005), through a series of granular flow experiments using glass beads of diameter $d = 1.15$ mm and $d = 3$ mm as the granular materials, suggested that $(d_\infty - d_0)/d_0 \simeq a$ and $(d_\infty - d_0)/d_0 \simeq a^{2/3}$ for $a \leq 3$ and $a > 3$, respectively. Trepanier and Franklin (2010) repeated the experiments by Lube et al. (2005) and Lajeunesse et al. (2005) but with randomly arranged granular rods. They reported that the ratio $(d_\infty - d_0)/d_0$ was given by $a^{1.2\pm0.1}$ and $a^{0.6\pm0.1}$ when $a <$ (1.1 ± 0.3) and $>$ (1.1 ± 0.3), respectively.

In addition to the quasi-2D experiments, the mechanism of granular flow is often investigated under axisymmetric conditions (i.e., 3D conditions). Typical experiments of this type include those by Lube et al. (2004), Lajeunesse et al. (2004), Lajeunesse et al. (2005), and most recently Warnett et al. (2014). Many authors have used the experimental results described above to verify their 2D/3D numerical models, which they then used to study granular flow scenarios that are difficult to model experimentally. Staron and Hinch (2005), Bui (2007), Bui et al. (2006, 2008a, 2008b, 2009), and Trepanier and Franklin (2010) are but a number of authors who have adopted this approach.

As the literature review above shows, most previous 2D granular flow experiments were conducted under quasi-2D conditions. Although such experimental data could be used to validate 2D numerical models, they do not reflect true 2D conditions in the simulations, in plane strain or plane stress conditions. To overcome this knowledge gap, this paper presents the results of a series of column collapse experiments in which aluminum rods are used as the granular materials, i.e., a true 2D condition. To our best knowledge, a true 2D granular column collapse experiment has not yet been conducted in the literature. Herein, we focused on factors that affect the final run-out distance or destruction zone of the granular column, including the characteristics of experimental materials and type of ground contact surface (hard or soft). Notably, we also examined the effect of soil ground quality on the run-out distance and destruction zone of granular columns.

2.2. EXPERIMENTS

2.2.1. Experimental Setup

Figure 2.1 shows a schematic diagram of the initial setup for the true 2D granular column collapse experiments, using aluminum rods as soil models. The full design of the experimental model setup is shown in Figure 2.1(a). However, owing to the symmetrical properties of granular column collapse, only half of the experimental model was considered in the real experiment (Figure 2.1(b)), with the vertical axis (OY) being replaced by a solid wall. The original height and width of the 2D soil layer are h_0 and d_0, respectively. These parameters, however, were changed during the experiment to investigate their effects on the final run-out distance and destruction zone of the granular column.

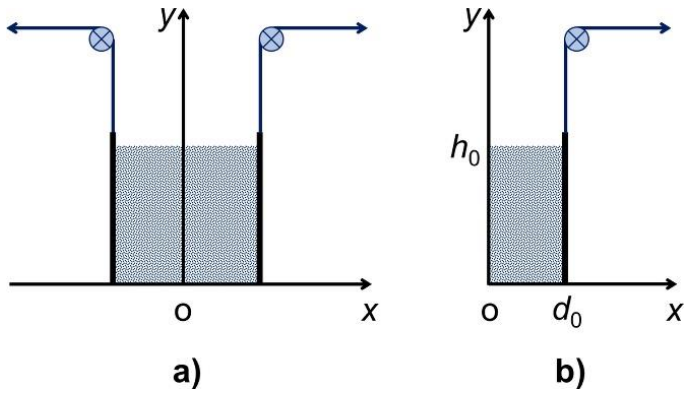

Figure 2.1: *Schematic diagram of the experimental model*

2.2.2. Material

Aluminum rods 5 cm in length and with diameters of 1.6 mm and 3.0 mm, mixed at a ratio of 3:2 in weight, were used as the model ground to simulate the true 2D granular flow experiments (Nakai, 2012). The total unit weight of the model ground after construction is 20.4 kN/m3. The soil shear strength parameters of the model ground, including elastic modulus, friction angle, and cohesion, are obtained by conducting direct shear tests or biaxial tests on the aluminum rods.

These testing results have been reported by the authors in Bui et al. (2008a, 2008b, 2014) and summarized in Table 2.1. Prior to the experiment, the aluminum bars were thoroughly cleaned and dried before being mixed (Nguyen et al., 2013). This was to ensure that the moisture of the model ground was at 0%.

Table 2.1: *Properties of the 2D soil model*

Name	Value	Unit
Density (ρ)	20.4	kN/m3
Friction angle (ϕ)	21.9	deg
Young's modulus (E)	5.84	MPa
Poisson's ratio (ν)	0.3	–
Dilation angle (ψ)	0	deg
Cohesion (c)	0	kPa

2.2.3. Experimental Procedure

A series of experiments were performed at different initial column heights (h_0) of 50, 100, 150, and 200 mm. For each of the initial heights, the following granular column widths (d_0) were considered: 25, 50, 75, 100, 125, 150, 175, and 200 mm. Accordingly, 48 experiments were conducted in total. Each of the experiments was repeated at least twice, with some repeated up to six times.

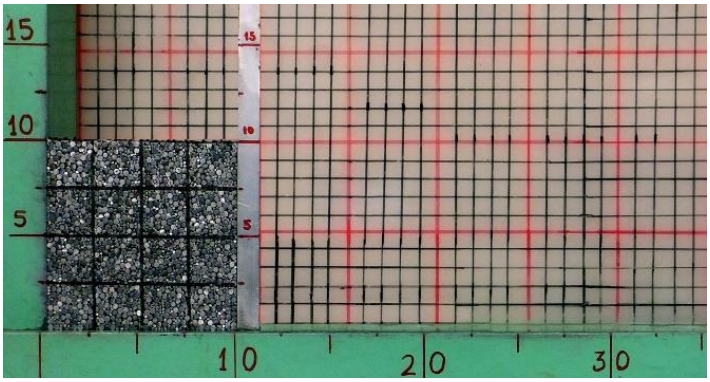

Figure 2.2: *Initial setup for the granular collapse experiment with h0 = 100 mm and d0 = 100 mm*

Figure 2.2 shows the initial setup for the granular column collapse experiments with an initial height and width of 100 mm and 100 mm, respectively. In the experiment, the granular column was constructed by successively placing the ground model in layers of 2.5 cm until the desired initial height was reached. To visualize the failure pattern of the ground model, square grids of 2.5 × 2.5 cm were drawn directly on the soil specimens. In addition, a gridded board was also attached to the steel frame behind the soil sample to allow the visualization of the progressive failure of the granular flow. There was no direct contact between the gridded board and granular rods, neither during nor after the

experiment. Furthermore, the front side was open to enable clear visualization of the granular flow. The above experimental setup represents the true 2D plain-strain conditions due the fact that motions of granular bars in the lateral direction (i.e. direction perpendicular to the vertical and horizontal plane) have been restricted. We acknowledged that some aluminum bar exhibited a non-translational movement in the experiment, especially at the flow front during the later stage of the collapse. However, these affects are not significant in our experiment. Furthermore, bars that were ejected from the flow and underwent independent movement of the collective behavior of the flow were not taken into consideration in the evaluation of the final scaling laws in our work.

In each experiment the following steps were repeated: 1) Ensure the model ground is clean and dry by washing the soil sample with alcoholic solutions and then drying it after each experiment; 2) Construct the granular column according to the required experiment dimensions (i.e., initial height and width) and draw square grids (2.5 × 2.5 cm) on the soil specimens; 3) Quickly remove the right wall to allow granular soil to freely move and collapse (care must be taken to ensure that the aluminum rods do not collide with the wall during the collapse process); 4) Record the failure process of the granular soil using a high speed camera and measure the final run-out distance and final failure pattern. The high-speed camera was a Photron type camera, capable of recording 500 frames/s at a resolution of 1024×512 pixels.

2.3. EXPERIMENTAL OBSERVATION

Two major failure mechanisms were observed from the serial tests on the hard ground contact surface (Figure 2.3). The failure mechanism depended on the initial ratio of the initial height (h_0) to the initial width (d_0); at an initial ratio $h_0 / d_0 > 0.65$, the granular column collapsed and formed a conical shape on the top surface (Figure 2.3(a)). On the other hand, when the initial ratio $h_0 / d_0 \leq 0.65$, there was an undisturbed zone on the top surface of the granular column (Figure 2.3(b)). For tests on the soft ground contact surface (made of the aluminum rods) the same failure mechanisms were observed. However, the final run-out distance was slightly different from that on the hard ground surface. Details of the experimental results are summarized below.

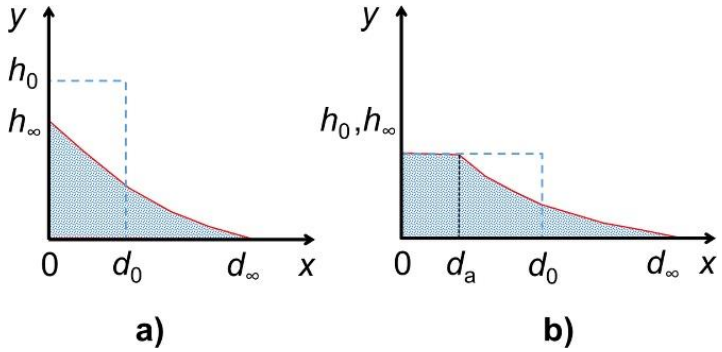

Figure 2.3: *Typical failure mechanism of granular column collapse obtained from experiments*

2.3.1. Results on Hard Ground Contact Surface

For these experiments, I focused on the major failure mechanism of the 2D granular column to determine the relationship between the initial soil height and final run-out distance of the 2D granular column after the collapse.

Figures 2.4 and 2.5 show the progressive collapse of the 2D granular column at several representative time points for the two typical failure mechanisms corresponding to those described in Figure 2.3. The failure mechanism observed in Figure 2.4 corresponds to that of Figure 2.3(a), with a final conical shape on the top surface, whereas that in Figure 2.5 corresponds to the mechanism in Figure 2.3(b) with an undisturbed zone. The failure surface, which separates the failure zone from the undisturbed zone, is highlighted in these figures by a dashed line. Comparing the results, the failure surfaces observed with an initial ratio $h_0 / d_0 \geq 0.65$ (Figure 2.4) remain almost unchanged in shape (i.e., a straight line) from those observed with $h_0 / d_0 < 0.65$ (Figure 2.5). The initial soil height of the former case is markedly that of the latter case, mainly owing to the difference in the initial soil volume.

As for the final run-out distance, the experimental results (Figures 2.6–2.8) show that for $a \leq 0.65$ ($a = h_0 / d_0$) the initial and final heights of the soil column were identical (i.e., $h_0 = h_\infty$). This result is consistent with the quasi-2D experimental data reported by Balmforth Kerswell (2005) and Staron and Hinch (2005). In contrast, for $a > 0.65$, the relationships between the coefficient a and the ratio $(d_\infty - d_0)/d_0$ and between the ratios h_0/h_∞ and d_∞/d_0 were exponential in form. As shown in Figure 2.6, the exponential relationship between a and the ratio $(d_\infty - d_0)/d_0$ changes at a = 1.5, as shown in Equation (2.1) below:

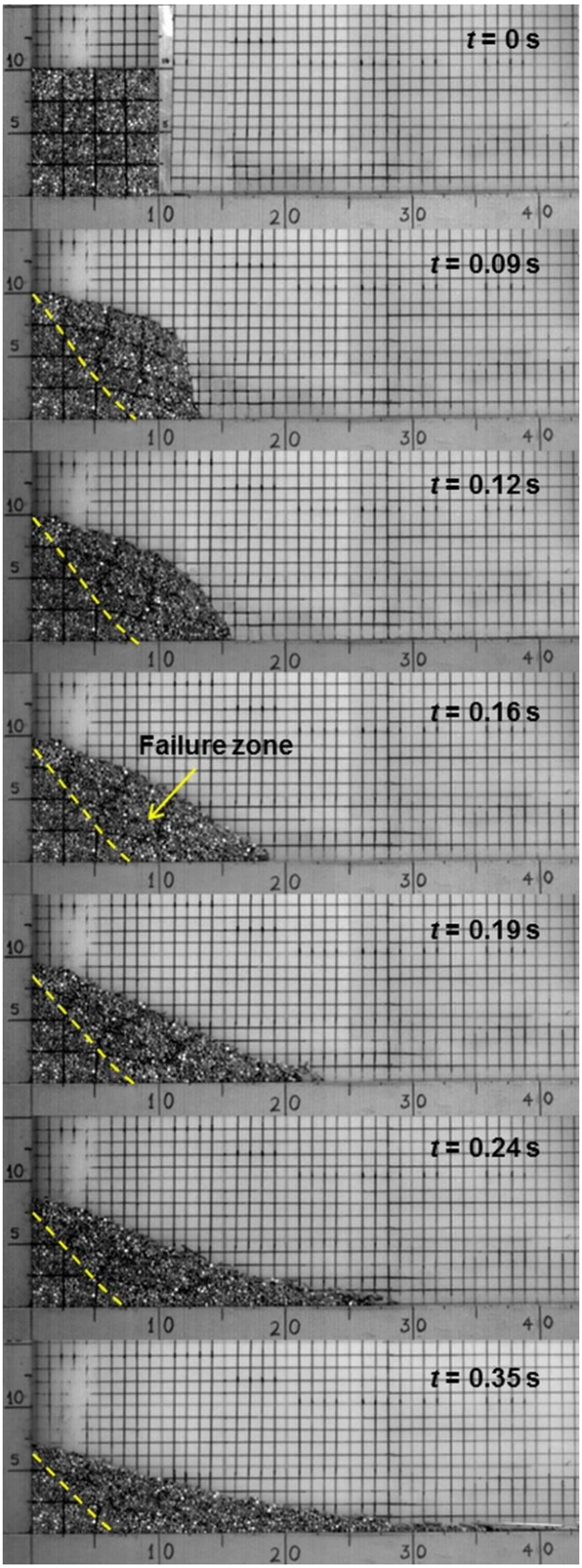

Figure 2.4: *The collapse of the granular column with h_0 = 100 mm and d_0 = 100 mm observed at several times with a high-speed camera*

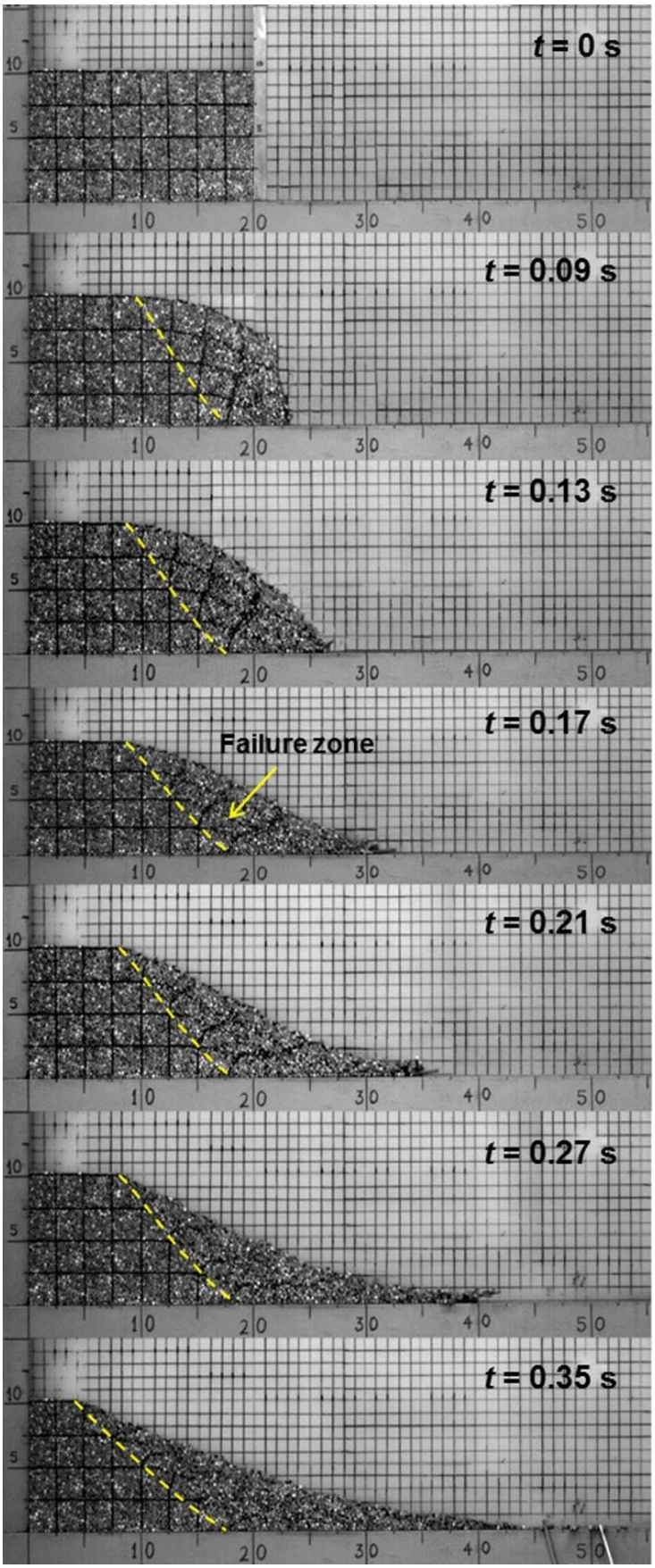

Figure 2.5: *The failure process of the granular column (h_0 = 100 mm and d_0 = 200 mm) at several times obtained by high-speed camera.*

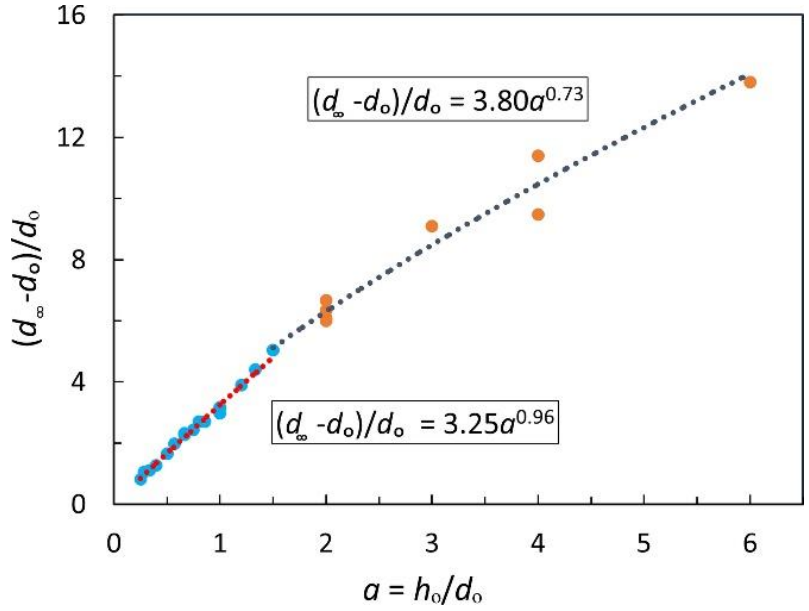

Figure 2.6: *Relation between the coefficient* $(d_\infty - d_0)/d_0$ *and the coefficient* a *compiled from the experiment results*

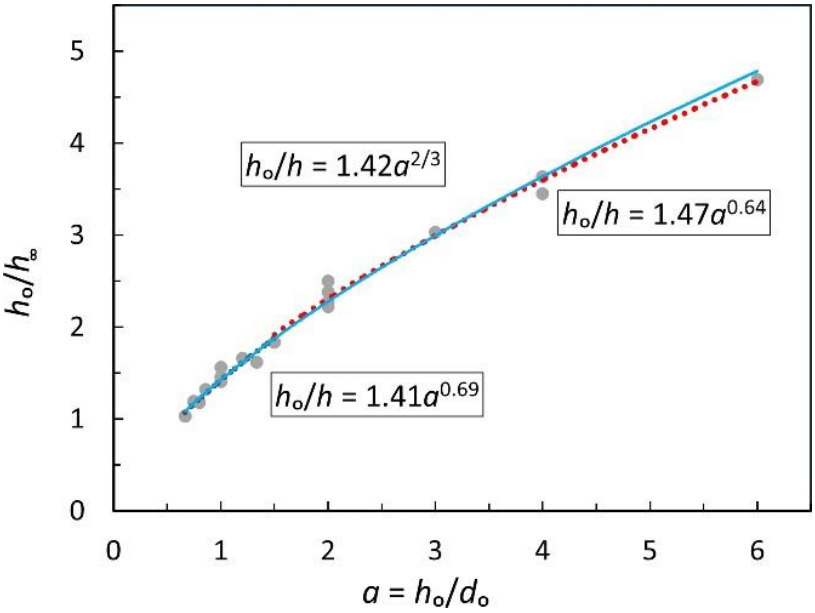

Figure 2.7: *Relation between the coefficient* h_0/h_∞ *and the coefficient* a *compiled from the experiment results*

$$\frac{d_\infty - d_0}{d_0} \approx \begin{cases} 3.25a^{0.96} & a < 1.5 \\ 3.80a^{0.73} & a \geq 1.5 \end{cases} \quad (2.1)$$

The relationship between h_0/h_∞ and a (Figure 2.7) is approximated by using the following exponential equation:

$$\frac{h_0}{h_\infty} \approx 1.42a^{2/3} \quad a \geq 0.65 \tag{2.2}$$

If the experimental data are separated into two data series, consistent with the expression in Equation (2.1), the following exponential equations describe the relation between h_0/h_∞ and a:

$$\frac{h_0}{h_\infty} \approx \begin{cases} 1.41a^{0.69} & a < 1.5 \\ 1.47a^{0.64} & a \geq 1.5 \end{cases} \tag{2.3}$$

Similarly, for the ratio d_∞/d_0 (Figure 2.8), the experimental results also show an overall exponential relationship between this ratio and coefficient$a$, which is:

$$\frac{d_0}{d_\infty} \approx 4.30a^{0.72} \quad a \geq 0.65 \tag{2.4}$$

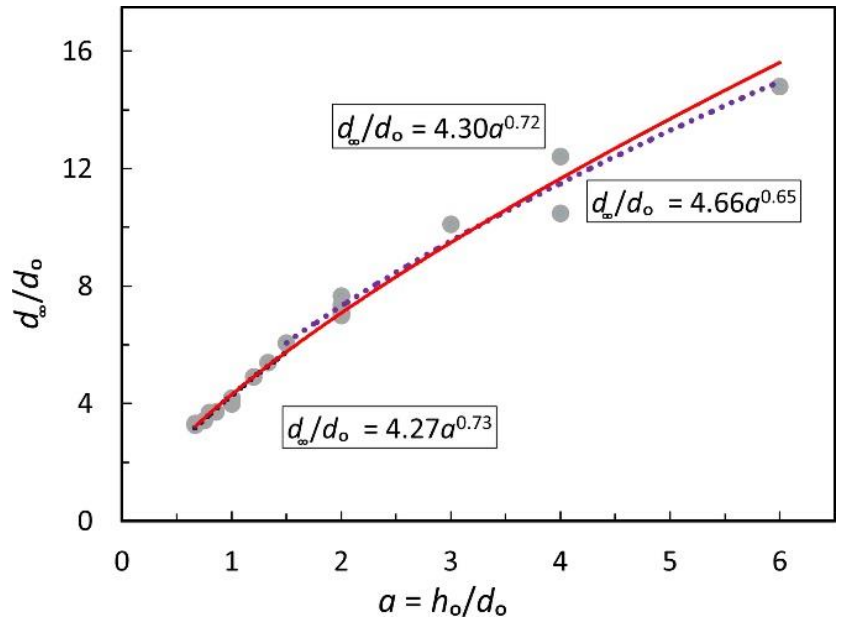

Figure 2.8: *Relation between the coefficient d_∞/d_0 and the coefficient a compiled from the experimental results*

If the data are again separated into two series with a = 1.5 as the breaking point, the following expressions describe the relationship between the ratio d_∞/d_0 and coefficient a:

$$\frac{d_\infty}{d_0} \approx \begin{cases} 4.27a^{0.73} & a < 1.5 \\ 4.66a^{0.65} & a \geq 1.5 \end{cases} \tag{2.5}$$

2.3.2. Results on Soft Ground Contact Surface

To investigate the effect of the ground contact surface on the failure mechanism, 2D granular column collapse experiments were conducted on a soft contact surface. These results were compared with those obtained from the experiments conducted on a hard contact surface.

The initial geometric settings and boundary conditions for the current experiment are shown in Figures 2.9 and 2.10. We only considered the case with a rectangular granular column of h_0 = 100 mm and d_0 = 200 mm. For the experiment on the soft ground surface, the rectangular granular column was placed on a soft ground layer 2.5 mm in height made of the same type of material as the granular column (i.e., aluminum rods), (Figure 2.10). Each experiment was repeated at least six times to confirm the failure mechanism.

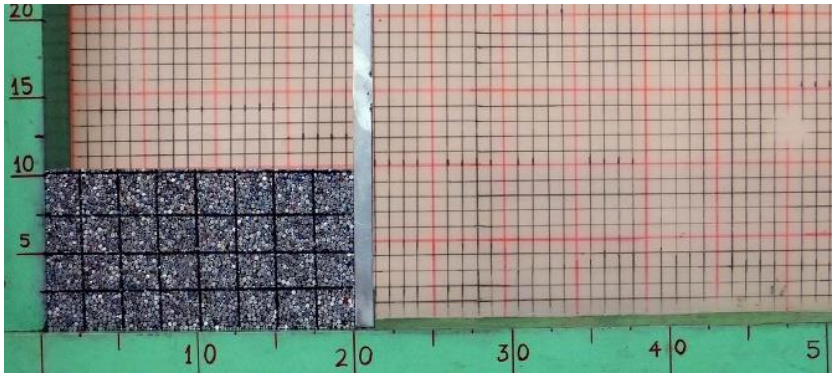

Figure 2.9: *Initial experimental setting for hard ground*

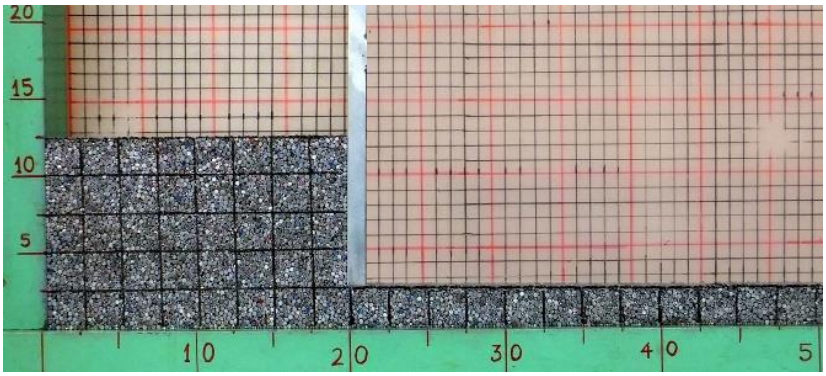

Figure 2.10: *Initial experimental setting for soft ground*

Figure 2.11 shows the collapsing process of the granular column on the soft contact surface at several representative time points. Similar to the results on the hard contact surface, granular soils progressed toward the right after removing the retaining wall. The

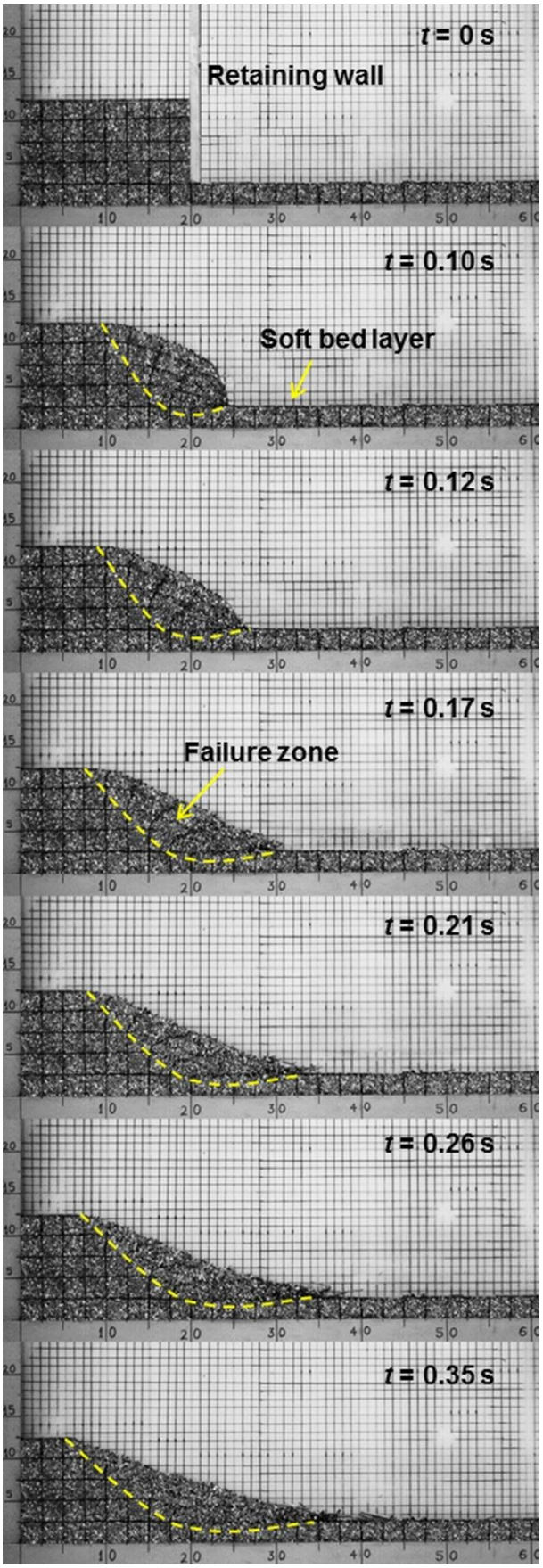

Figure 2.11: *The collapsing process of the granular column on soft ground contact surface*

failure surface was almost a straight line from the ground free-surface to the boundary between the initial rectangular granular column (100 × 200 mm) and the soft bed layer (i.e., 2.5 mm thickness). Beyond this boundary, the failure surface was bent and formed a curved surface inside the granular bed layer. This is similar to what is normally observed in a deep-seated landslide failure.

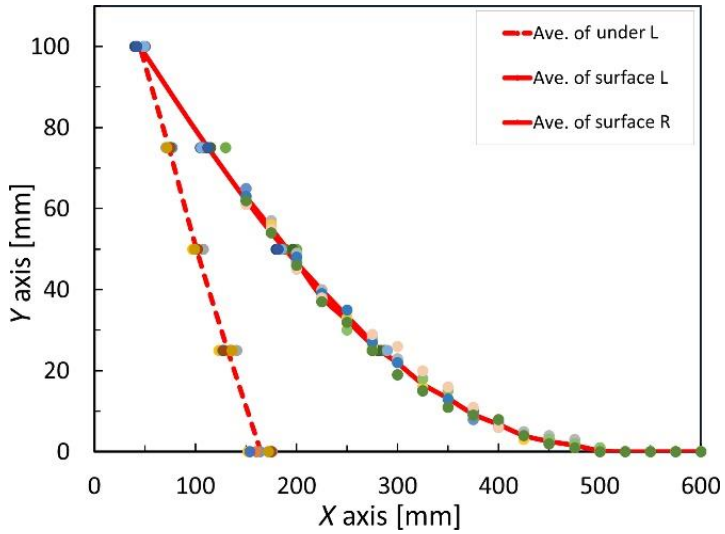

Figure 2.12: *The final shapes of failure surface and ground free-surface of the granular collapse on the hard contact surface*

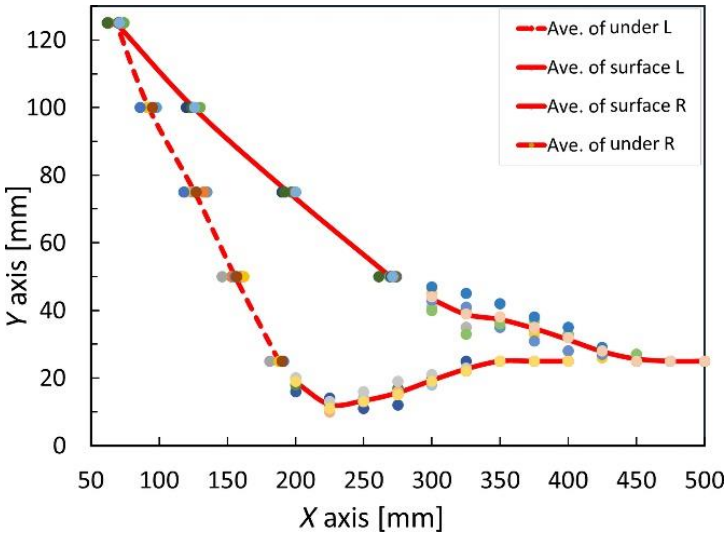

Figure 2.13: *The shapes of failure surface and ground free-surface of the granular collapse on the soft contact surface*

The final configurations of the failure surface and ground free-surface observed in both experiments are repotted in Figures 2.12 and 2.13. Comparing the results, the failure

surface observed on the soft ground contact surface differs from that observed on the hard contact surface. For the soft contact surface, part of the kinetic energy from the granular column collapse is transferred to and causes destruction of the soft bed layer during the collapsing process. In contrast, for the hard contact surface, the transfer of kinetic energy to the ground surface is negligible. This explanation is further supported by comparing the final run-out distance of the two cases. As shown in Figures 2.12 and 2.13, the final run-out distance of the granular column on the hard ground contact surface was approximately 475 mm, whereas that on the soft ground contact surface was approximately 450 mm.

This difference is presumably due to the dissipation of the kinetic energy (from the granular column) into the soft ground surface below. Therefore, I conclude that the ground contact surface plays an important role in the final run-out distance of granular flow.

2.4. DISCUSSION

Several research groups have experimentally investigated the failure mechanism of 2D granular flows. Notable studies include those by Balmforth and Kerswell (2005), Lube et al. (2005), Lajeunesse et al. (2005), and Trepanier and Franklin (2010). However, in all of these studies, the authors adopted quasi-2D models to perform their experiments. In such models, a narrow horizontal channel is typically used with 3D granular materials such as sandy soil, rice, or glass beads to simulate 2D granular flows. Because of the nature of the model and variety of materials used, the reported experimental results for the final run-out distance varied widely across experiments, as summarized below.

In a series of experiments conducted by Balmforth and Kerswell (2005), the authors used grit, fine glass, coarse glass, and polystyrene as the model ground to investigate the failure mechanism of 2D granular flow in a narrow horizontal flow channel with different widths. They found that the final run-out distance of the 2D granular column depends on the width of the flow channel. In particular, they reported the following exponential relationships between the ratio $(d_\infty - d_0)/d_0$ and the coefficient a:

$$\frac{d_\infty - d_0}{d_0} = \begin{cases} \lambda a^{0.9\pm0.1} & \text{for wide slots} \\ \lambda a^{0.65\pm0.05} & \text{for narrow slots} \end{cases} \tag{2.6}$$

where λ is a coefficient depending on the internal friction angle of the used materials and the friction coefficient of the bed contact surface.

Lube et al. (2005) also reported experimental results of 2D granular flow by using a quasi-2D model on fine quartz sand, coarse quartz sand, sugar, and rice. They found the following relationship between $(d_\infty - d_0)/d_0$ and a:

$$\frac{d_\infty - d_0}{d_0} \approx \begin{cases} 1.2a & a < 1.8 \\ 1.9a^{2/3} & a > 2.8 \end{cases} \tag{2.7}$$

In contrast to the result reported by Balmforth and Kerswell (2005), a transition from a linear to exponential relation occurs in the experiments reported by Lube et al. (2005).

In another series of experiments that investigated the granular column collapse mechanism, conducted by Lajeunesse et al. (2005) on glass beads of diameter d = 1.15 mm and d = 3 mm, a narrow horizontal flow channel of 45 mm in width was used. For this series of experiments, the following relationship between $(d_\infty - d_0)/d_0$ and a was found:

$$\frac{d_\infty - d_0}{d_0} \approx \begin{cases} a & a < 3 \\ a^{2/3} & a > 3 \end{cases} \tag{2.8}$$

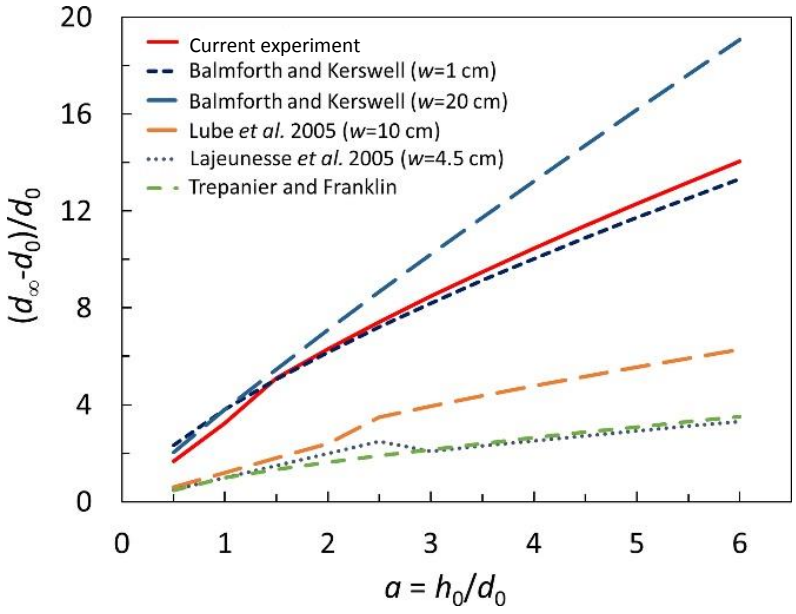

Figure 2.14: *The experimental results of quasi-2D granular flow reported by previous authors and results of our true 2D granular flow experiment*

The result is markedly different from that reported by Lube et al. (2005), although the transition from a linear to exponential relation is also noted. Most recently, Trepanier and Franklin (2010) used granular rods to investigate the failure mechanism of granular columns under 3D conditions. They reported the following relationship for the final run-out distance:

$$\frac{d_\infty - d_0}{d_0} \approx \begin{cases} a^{1.2\pm0.1} & a < 1.1 \pm 0.3 \\ a^{0.6\pm0.1} & a > 1.1 \pm 0.3 \end{cases} \tag{2.9}$$

This result is close to that reported by Trepanier and Franklin (2010), but markedly different from the results of others (Figure 2.14). Overall, the experimental data from 2D granular column collapse experiments that used the quasi-2D granular flow model shared the same form of relationship between the ratio $(d_\infty - d_0)/d_0$ and the coefficient a. These equations can be generalized as follows:

$$\frac{d_\infty - d_0}{d_0} \approx \begin{cases} \lambda_1 a^{\alpha_1} & \text{with } a < a^* \\ \lambda a^{\alpha} & with \ \ a > a^* \end{cases} \tag{2.10}$$

where λ_1 and λ are constants that depend on materials used, and other parameters fall within the following range:

$$\begin{cases} 0.7 < a^* < 3.0 \\ 0.6 < \alpha_1 < 1.3 \\ 0.59 < \alpha < 0.70 \end{cases} \tag{2.11}$$

By comparing my experimental data to the general Equation (2.10), the following parameters are found for true 2D granular flow:

$$\begin{cases} a^* = 1.5 \\ \alpha_1 = 0.96 \\ \alpha = 0.73 \end{cases} \tag{2.12}$$

The coefficients a^* and α_1 obtained from my experiments fall within the range reported by previous authors who used the quasi-2D model. However, the coefficient α is slightly greater than the values reported by other authors.

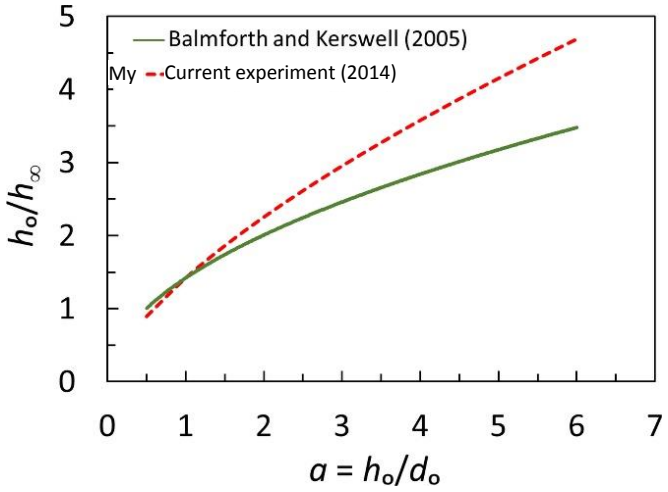

Figure 2.15: *Comparison of the relationship between the ratio h_0/h_∞ and the coefficient a*

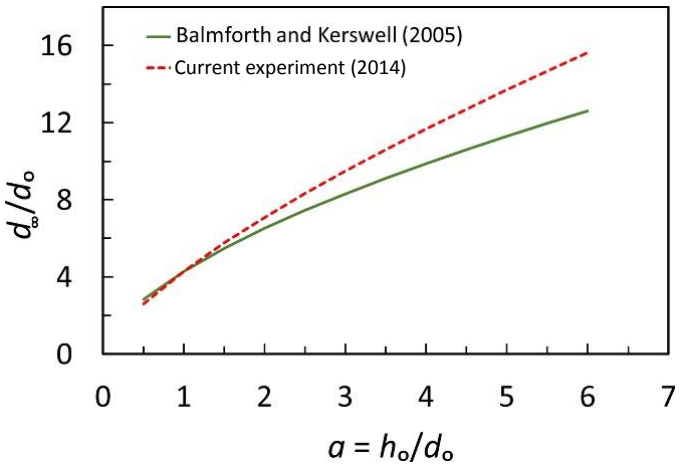

Figure 2.16: *Comparison of the relationship between the ratio d_∞/d_0 and the coefficient a*

Figure 2.14 shows a comparison of the experimental results reported by the different research groups. The solid line represents our experimental data using the true 2D granular model, whereas all other dashed lines show results obtained from quasi-2D granular models. To plot the result reported by Balmforth and Kerswell (2005), I used $\lambda = 3.25$ for $a < 1.5$ and $\lambda = 3.8$ for a $\geq$ 1.5, which were obtained from our experimental data as shown in Equation (1). My experimental data are very close to those reported by Balmforth et al. (2005) for a narrow channel of 1cm width. This suggests that true 2D granular flow is most closely represented by narrower horizontal flow channels when using the quasi-2D approach. However, the data for the true 2D experiment are markedly different from those reported by Balmforth and Kerswell (2005) for a wide flow channel and from other experimental data reported in the literature. These differences can be accounted for by variation of two key reasons across the experiments: 1) the 3D material used and 2) the flow channel width. In all of the quasi-2D experiments

discussed above, the 3D materials differ widely in the size and shape of the particles. In addition, various flow channel widths were adopted in these studies. The wider the flow channel, the larger was the deviation from my experiment.

The empirical relationship between the ratio $(d_\infty - d_0)/d_0$ and the coefficient a reported by Balmforth and Kerswell (2005) for narrow flow channel fits our 2D experiments data quite well. However, other relationships based on a narrow flow channel, such as that between the ratio h_0/h_∞ or d_∞/d_0 and the coefficient a, were markedly different from my data. In particular, Balmforth and Kerswell (2005) reported the following empirical equations:

$$h_0/h_\infty \approx \lambda a^{0.5} \tag{2.13}$$

$$d_\infty/d_0 \approx \lambda a^{0.55\pm0.05} \tag{2.14}$$

which represent the power-law dependencies of h_0/h_∞ and d_∞/d_0 on the initial aspect ratio a. The above empirical equations are consistent with our experimental finding on the true 2D experimental model as expressed by Equations (2.2) and (2.4), which show that the ratios h_0/h_∞ and d_∞/d_0 are exponential functions of the coefficient a. However, the exponential coefficients obtained from true 2D conditions are higher than those obtained from quasi-2D conditions. To further illustrate these differences, Equations (2.13) and (2.14) are plotted in Figures 2.15 and 2.16, using values of λ obtained from my experiment (i.e., $\lambda = 1.42$ and $\lambda = 4.30$, respectively). My data agree with those of Balmforth and Kerswell (2005), in particular for an initial aspect ratio a of less than 1.5. For a higher a value, my data deviate from their equations. Therefore, I conclude that the quasi-2D experimental model does not fully represent the 2D conditions, even for a very narrow horizontal flow channel. Accordingly, care must be taken when validating 2D numerical models with quasi-2D experimental data.

2.5. CONCLUSION

I investigated the failure mechanism of 2D granular flow by using a truly 2D granular flow model (i.e., aluminum rods as the soil model). The results were then compared with experimental data obtained by other researchers who used a quasi-2D granular flow model (i.e., a narrow horizontal flow channel with 3D granular materials).

Interestingly, my experimental findings were markedly different from those reported by previous authors. I also showed that the quality of the ground contact surface affects the destruction zone and final run-out distance of the granular column after collapsing. In particular, for the same ratio of initial height to initial width of a rectangular column, the final run-out distance of the granular column on a soft ground contact surface was less than that on a hard ground contact surface. A deep-seated failure mechanism was observed in the experiment on the soft ground contact surface.

Finally, my thesis provided comprehensive experimental data on the collapsing process of a 2D granular column with full details of the material properties. These data will serve as a useful resource to test 2D numerical models.

REFERENCES

[1] Balmforth, N. J. and R. R. Kerswell; "Granular Collapse in Two Dimensions", *Journal of Fluid Mechanics*, **538**, pp. 399–428 (2005)

[2] Bui, H. H., R. Fukagawa, and K. Sako; "Smoothed Particle Hydrodynamics for Soil Mechanics", *Proceedings of the 6th European Conference on Numerical Methods in Geotechnical Engineering*, pp. 278–281 (2006)

[3] Bui, H. H.; "*Lagrangian Mesh-free Particle Method (SPH) for Large Deformation and Post-failure of Geomaterials Using Elasto-plastic Soil Constitutive Models*", Ph.D. Thesis, Ritsumeikan University, Japan (2007)

[4] Bui, H. H., R. Fukagawa, K. Sako and S. Ohno; "Lagrangian Mesh-free Particles Method (SPH) for Large Deformation and Failure Flows of Geomaterial Using Elastic-plastic Soil Constitutive Model", *International Journal for Numerical and Analytical Methods in Geomechanics*, **32**(12), pp. 1537–1570 (2008a)

[5] Bui, H. H., R. Fukagawa, K. Sako and J. C. Wells; "SPH-based Numerical Simulations for Large Deformation of Geomaterial Considering Soil-structure Interaction", *The 12th International Conference of International Association for Computer Methods and Advances in Geomechanics* (IACMAG), pp. 570–578 (2008b)

[6] Bui, H. H., R. Fukagawa, K. Sako, ad J. C. Wells; "Numerical Simulation of Granular Materials Based on Smoothed Particle Hydrodynamics (SPH)", *Powders and Grains, AIP Conf. Proc*. pp. 575–578 (2009)

[7] Bui, H. H., J. Kodikara, A. Bouazza, A. Haque and P. G. Ranjith; "A Novel Computational Approached for Large Deformation and Post-failure Analyses of Segmental Retaining Wall Systems", *International Journal for Numerical and Analytical Methods in Geomechanics*, **38**(13), pp. 1321–1340 (2014)

[8] Lajeunesse, E., A. Mangeney-Castelnau, and J. P. Vilotte; "Spreading of a Granular Mass on a Horizontal Plane", *Physics of Fluids*, **16**(7), pp. 2371–2381 (2004)

[9] Lajeunesse, E., J. B. Monnier and G. M. Homsy; "Granular Slumping on a Horizontal Surface", *Physics of Fluids*, **17**(10), p. 103302 (2005)

[10] Lube, G., H. E. Huppert, R. S. J. Sparks, and A. Freundt; "Collapses of Two-dimensional Granular Columns", *Physical Review E*, **72**(4), pp. 1–10 (2005)

[11] Lube, G., H. E. Huppert, R. S. J. Sparks and M. A. Hallworth; "Axisymmetric Collapses of Granular Columns", *Journal of Fluid Mechanics*, **508**, pp. 175–199 (2004)

[12] Nakai T.; "*Constitutive Modelling of Geomaterials: Principle and Applications"*, CRC Press, Taylor & Francis Group, USA (2012)

[13] Nguyen, C. T., H. H. Bui and R. Fukagawa; "Two-dimensional Numerical Modelling of Modular-block Soil Retaining Walls Collapse Using Meshfree Method", *International Journal of GEOMATE*, **5**(1), pp. 647–652 (2013)

[14] Staron, L. and E. Hinch; "Study of the Collapse of Granular Columns Using Two-dimensional Discrete-gain Simulation", *Journal of Fluid Mechanics*, **545**, pp. 1–27 (2005)

[15] Trepanier, M. and S. V. Franklin; "Column Collapse of Granular Rods", *Physical Review E*, **82**, p. 011308 (2010)

[16] Warnett, J. M., P. Denissenko and P. J. Thomas; "Scalings of axisymmetric granular column collapse". *Granular Matter*, **16**, pp. 115–124, (2014).

CHAPTER 3

DEVELOPMENT OF SPH TO PREDICT LANDSLIDES

3.1. INTRODUCTION

Granular flows are commonly found in a large number of natural and industrial processes. Thus, the understanding of the mechanisms of granular flows plays an important role in predicting and minimizing natural hazards (e.g. landslides, snow avalanches, soil liquefaction) and in optimizing industrial processes (e.g. mineral processing, ceramic, food processing, pharmaceutical manufacture). Accordingly, the study of granular flows has received much attention from many disciplines of science and engineering (Herrmann et al. 1998; MiDi 2004; Jop et al. 2006; Pouliquen et al. 2006; Forterre & Pouliquen, 2008). In the past decade, a significant number of research works on the flow of granular materials have been conducted using both experimental and numerical modelling techniques. Among a large number of problems defined, the collapse of granular columns on a flat horizontal surface under gravity has been extensively studied for several physical aspects of granular flows. Lube et al. (2004) and Lajeunesse et al. (2004) were the first to conduct experiments of this type using granular columns of cylinders to investigate the mechanisms of granular flow, such as the relationship between the initial aspect ratio (the ratio of initial height to initial width) and the geometrical properties of the final deposit, and the transient free-surface flow occurring during the collapse process. Since then, a large variety of similar problems have been studied for the failure and flow mechanisms of granular materials. These include: columns collapse in a narrow horizontal flow channel (Lube et al., 2005, Balmforth & Kerswell 2005), columns collapse in fluids (Thompson and Huppert 2007,

Rondon et al. 2011), columns collapse of wet granular materials (Artoni and Santomaso 2013), columns collapse on inclined plane (Lacaze et al. 2008, Lube et al. 2011), columns collapsed on eroded beds (Mangeney et al. 2010, Farin et al. 2014), and most recently true 2D columns collapse, in the form of columns made by steel rods moving between two glass walls (Nguyen et al. 2015). In general, the above experimental studies have provided a comprehensive understanding on the mechanism of granular flows from surface observations. However, they hardly provide sufficient details on the internal deformation or the evolution of state variables such as stresses or strains inside the flow, which are important for the understanding of flow properties/mechanisms followed by its generalisation for practical design purposes. In this sense, numerical approaches can be a useful and also less expensive alternative.

In the view point of numerical modelling, the discrete element methods (DEMs) have been extensively used to investigate the mechanisms of granular flows (Cleary and Sawley, 2002; Staron and Hinch, 2005, 2007; Zenit, 2005; Lacaze et al., 2008; Krabbenhoft et al., 2012; Girolami et al., 2012; Guo et al., 2014; Utili et al., 2015; Kermani et al., 2015), and a comprehensive understanding of the flow mechanism (e.g. the initiating general shear failure mechanism, the free fall regime, and the scaling laws between the final run-out distance and the initial aspect ratio) has been achieved. Because the DEMs describe the problem at the particle scale, they are the most suitable method to simulate the kinematics of granular flows. However, for a typical practical problem involving millions of particles, the required computational resource is very demanding, and hence challenging even for a high performance computing server. Therefore, for such field applications, continuum approach is a good alternative.

In the continuum approach, a granular material is assumed to be homogeneous and a constitutive model, which relates stresses to strains, is required to describe the deformation of the material. This material model is then coupled with differential equations describing the motion of the material during flow. Given the characteristics of granular flow in landslides or similar processes, a good continuum approach should be able to capture/predict both stress/failure (e.g. when it fails) and deformation (e.g. run-out distance and final deposit), as these features are important for risk mitigation and design of protective structures. Despite the success of mesh-based continuum approaches in capturing the general behaviour of granular flows and in providing insights of evolution of state variables (Kerswell, 2005; Mangeney-Castelnau et al., 2005; Lacaze et al., 2008; Crosta et al., 2009 and 2015; Lagree et al., 2011; Holsapple, 2013; Ionescu et al,

2015), deformation characteristics such as the final shape of the deposit (e.g. sharp tips/tops, curvature profiles) are however not always well described by mesh-based continuum approaches since these mechanisms are considered as characteristics of discrete behaviours (Crosta et al., 2009; Kermani et al. 2015).

On the other hand, particle-based continuum approaches such as the material point method (MPM) (Kumar et al., 2013; Carter et al., 2014), the particle finite element method (PFEM) (Zhang et al., 2014) and the smoothed particle hydrodynamic (SPH) method (Bui et al., 2008a; Nguyen et al., 2013) offer better capabilities to capture both deformation and failure of granular flows and/or landslides. Among these approaches, SPH is the only numerical method that does not require a global background mesh for the solution of the governing partial differential equations. Although the standard SPH method suffers from a tensile instability issue, which can be overcome using either an artificial stress method (Gray et al. 2001, Bui et al. 2008a) or Taylor-Galerkin SPH model (Blanc and Pastor 2013), the method has been shown to be able to provide a smooth transition between the continuum and discrete behaviours (Morris and Johnson, 2009) and capture well essential characteristics of granular flow (Bui et al, 2008a). Since its invention by Gingold & Monaghan (1977) and Lucy (1977) for astrophysical applications, the SPH method has been successfully applied to a vast range of problems, including fluid mechanics (Monaghan, 1994; Shao & Lo, 2003; Colagrossi et al., 2003; Liu et al. 2004), solid mechanics (Libersky et al., 1993; Randles & Libersky, 1996; Dyka et al., 1997; Gray et al., 2001; Rabczuk et al. 2003, Blanc and Pastor 2012), and geomechanics (Bui et al. 2006, 2008a, 2008b, 2011a, 2011b, 2013, 2014, Pastor et al., 2009, Blanc and Pastor 2013, Hiraoka et al. 2013, Nguyen et al. 2013).

In relation to the present study, the SPH method combined with a granular constitutive model was successfully applied to simulate the collapse of granular columns (Bui et al., 2008a and 2009; Chen and Qiu, 2012) and showed to be a powerful continuum numerical method to simulate the flow behaviour of particulate materials. However, the standard SPH method suffers from unphysical stress/pressure oscillations that need to be stabilised by an artificial viscosity (Gingold & Monaghan, 1982 and 1983). This artificial viscosity requires two unknown parameters whose values greatly influence the simulation stability as well as the accuracy of numerical results. A rigorous method to specify those unknown parameters is yet to be established, and, in most cases, the selection of those parameters results from trial-and-error, and depends on the user's experience. Nevertheless, the standard SPH method using artificial viscosity still suffers

stress oscillations under large shear deformation (e.g. in post-failure process of granular flow) that could both affect the accuracy and reduce the predictive capability of the SPH method.

In this chapter, an attempt is made to improve the overall accuracy and performance of the SPH in simulating granular flows by replacing the standard SPH's artificial viscosity with a viscous damping combined with stress/strain regularisations. The comprehensive validation of the proposed technique demonstrates that it can effectively stabilize SPH simulations i.e. remove the stress oscillations, while providing predictions in very good agreement with experimental and numerical results in the literature. Furthermore, from the kinematic aspects of the granular flow, the combination of viscous damping and stress/strain regularisation technique is equivalent to the standard SPH model with artificial viscosity as both approaches result in the same amount of kinematic energy dissipation. In what follow, the numerical framework of SPH computation for granular flows and the proposed techniques are presented in Section 3.3. The performance of the proposed SPH model is demonstrated in Section 3.4. Section 3.5 describes the validation of the proposed SPH model against experiments and numerical results from the literature. Finally, the contribution of this chapter is summarised in Section 3.6.

3.2. SPH MESH-FREE PARTICLE METHOD

The SPH mesh-free particle method has been described in great detail by some researchers, such as Liu G.R. and Liu M. B. (2004) in the book "Smoothed Particle Hydrodynamics : A mesh-free particle method", and by Bui (2007) in his doctoral thesis, etc. So, in this thesis I would like to present briefly on SPH method and its related problems to my work in this Chapter and next Chapter.

3.2.1. History of The SPH Method

The Smoothed Particle Hydrodynamics (SPH) is a Lagrangian particle method. It was invented by Lucy (1977) and Gingold and Monaghan (1977) to solve astrophysical problems in three-dimensional open space. Since its invention, the SPH method has been extended to various applications such as fluid mechanics (Monaghan, 1994), solid mechanics (Libersky et al. 1993) and geomechanics (Bui 2007, Bui et al. 2008a, 2008b, 2011), etc.

3.2.2. Essential Formulation of SPH

The SPH particle method include two essential formulas for a function and the derivative of a function, namely Equations. (3.3) and (3.2) below.

$$A(\boldsymbol{r}) = \int A(\boldsymbol{r}')W(|\boldsymbol{r}-\boldsymbol{r}'|,h)d\boldsymbol{r}' + O(h^2) \tag{3.1}$$

$$A(\boldsymbol{r}) = \int \frac{A(r')}{\rho(r')}W(|\boldsymbol{r}-\boldsymbol{r}'|,h)\rho(\boldsymbol{r}')dr' + O(h^2) \tag{3.2}$$

$$A(\boldsymbol{r}) \approx \sum_{b=1}^{N}\frac{m_b}{\rho_b}A_b W(|\boldsymbol{r}-\boldsymbol{r}_b|,h) \tag{3.3}$$

$$\nabla A(\boldsymbol{r}) = \frac{\partial}{\partial r}\int \frac{A(\boldsymbol{r}')}{\rho(\boldsymbol{r}')}W(|\boldsymbol{r}-\boldsymbol{r}'|,h)\rho(\boldsymbol{r}')dr' + O(h^2) \tag{3.4}$$

$$\nabla A(\boldsymbol{r}) \approx \sum_{b=1}^{N} m_b \frac{A_b}{\rho_b}\nabla_a W_{ab} \tag{3.5}$$

where A = any variables defined on the spatial coordinate r; W = kernel function which is chosen to be the Cubic-Spline function; and h = smoothing length which specifies the interpolation area Ω (see Figure 3.1); m = mass of particle; b = the quantity evaluated at the position of particle b and

$$\nabla_a W_{ab} \equiv \frac{r_{ab}}{|r_{ab}|}\frac{\partial W_{ab}}{\partial r_a} \tag{3.6}$$

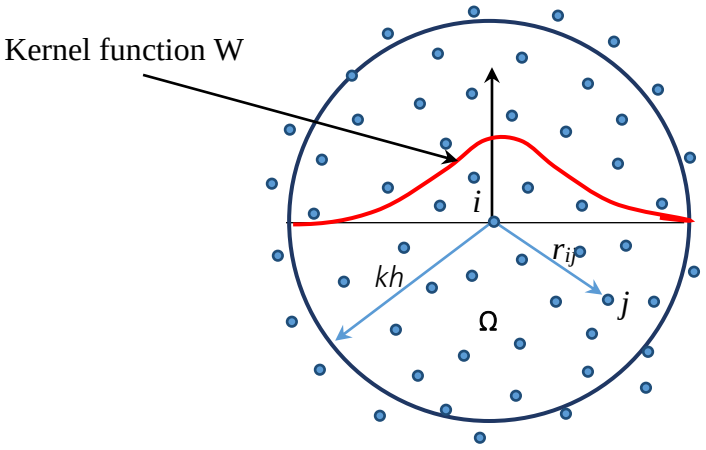

Figure 3.1: *The influence domain Ω with a radius of kh*

The kernel function must be chosen to satisfy at least three conditions. The first condition is called the *normalized condition*

$$\int_{\Omega} W(r-r',h)dr' = 1 \tag{3.7}$$

The second condition is the *delta function property*

$$\lim_{h\to 0} W(r-r',h) = \delta(r-r') \tag{3.8}$$

The third condition is the *compact support condition*

$$W(r-r',h) = 0 \quad when \quad |r-r'| > kh \tag{3.9}$$

Following Monaghan and Lattanzio (1985), the kernel Cubic-Spline function shows as in Equation (3.10)

$$W_{ij} = \alpha_d \times \begin{cases} \frac{2}{3} - q^2 + \frac{1}{2}q^3 & 0 \le q < 1 \\ \frac{1}{6}(2-q)^3 & 1 \le q < 2 \\ 0 & q \ge 2 \end{cases} \tag{3.10}$$

where $\alpha_d = 1/h, 15/7\pi h^2, 3/2\pi h^3$ in one- dimensional, two- dimensional and three-dimensional space; $h = 1.2dx$ ($dx = dy$ is the distance between two particles) and $k = 2$ (in Figure 3.1).

3.3. SPH NUMERICAL FRAMEWORK FOR GRANULAR FLOWS

In his doctoral thesis, Bui (2007) has introduced the detailed application of the SPH method to solve "Elasto- plastic soil constitutive models" problem. Several changing techniques and component approximation for equations of soil by SPH method have been presented very clearly. Moreover, Bui et al (2008a) have introduced detailed SPH algorithms to simulate the granular flow. As introduced in Chapter 1, my thesis inherits the previous study results of granular flow by Bui et al. (2008a). So in this part I only present a brief algorithm of solving granular flow by SPH method basing on SPH studies

by Bui (2007) and Bui et al. (2008a) for my further studies on numerical simulation in my dissertation. My new contributions to the SPH method will be detailed in this chapter and next chapter.

3.3.1. SPH Governing Equations

The governing equations for granular materials consist of the continuity and momentum equations. The continuity equation describes the change in density of granular materials undergoing large deformation, while the momentum equation describes the motion of granular materials subjected to external loadings. These two equations are written as follows:

$$\frac{d\rho}{dt} = -\nabla \cdot \mathbf{v} \tag{3.11}$$

$$\frac{d\mathbf{v}}{dt} = \frac{1}{\rho}\nabla \cdot \boldsymbol{\sigma} + \mathbf{g} \tag{3.12}$$

where $\mathbf{v}$ is the vector velocity; ρ is the density; $\boldsymbol{\sigma}$ is the total stress tensor, taken negative for compression; g is the acceleration vector due to gravity; and $\frac{d}{dt}$ indicates the derivative over time.

Within the SPH framework, the above governing equations are then discretized using several SPH particles, each of which has a constant mass and carries field variables such as density, stresses and strains. The particles move with their own velocities in the updated Lagrangian framework, thus can intrinsically simulate large deformation behaviour of granular materials.

Applying Equation (3.5), the partial differential form of Equations (3.11) and (3.12) can be discretized in the SPH framework in the following way (Bui et al. 2008a),

$$\frac{d\rho_i}{dt} = \sum_{j=1}^{N} m_j \left(\mathbf{v}_i - \mathbf{v}_j\right) \cdot \nabla W_{ij} \tag{3.13}$$

$$\frac{d\mathbf{v}_i}{dt} = \sum_{j=1}^{N} m_j \left(\frac{\boldsymbol{\sigma}_i}{\rho_i^2} + \frac{\boldsymbol{\sigma}_j}{\rho_j^2} \right) \cdot \nabla W_{ij} + \mathbf{g} \tag{3.14}$$

where *i*, *j* indicates the particle (or material point) under consideration; *N* is the total number of "neighbouring particles" (i.e. those within the support domain Ω of particle *i* showed in Figure 3.1); ρ_i and ρ_j are the density of particle *i* and *j*, respectively; m_j is the mass of particle *j*; and *W* is the kernel function taken to be the cubic-spline function (Monaghan & Lattanzio, 1985).

The above equations can be resolved using the standard Leapfrog integration scheme (Liu & Liu, 2004; Bui et al., 2008a) if the stress tensor is known. Thus, it is necessary to select a suitable constitutive relation for granular materials, which will be described in details in the next section.

3.3.2. Constitutive Model for Granular Materials

Any existing constitutive model can be implemented in the SPH method for the calculation of stress due to the movements of particles calculated from the governing differential equations. Although visco-plasticity constitutive models have been showed to be highly suitable to simulate the flow behaviour of granular materials (Jop et al. 2006, Moriguchi et al. 2009, Lagree et al. 2011, Chauchat and Medale 2014, Minatti and Paris 2015, Ionescu et al. 2015), classical rate-independent elasto-plasticity constitutive models have also been demonstrated to be suitable for the predictions of both failure and flow mechanisms of granular materials (Bui et al. 2008a and 2008b, Verghese et al. 2013, Carter et al. 2014, Zhang et al. 2015, Solowski and Sloan 2015). In this thesis, an elasto-plastic constitutive model employing the Drucker-Prager yield criterion is adopted for the calculation of stress during the deformation of granular materials. The stress-strain relation of this constitutive model is derived based on the assumption that the total strain rate which accompanies any change in stress rate can be divided into elastic and plastic components:

$$\dot{\varepsilon} = \dot{\varepsilon}^e + \dot{\varepsilon}^p \tag{3.15}$$

where $\dot{\varepsilon}$ is normally composed; $\dot{\varepsilon}^e$ is elastic strain rate tensor; $\dot{\varepsilon}^p$ plastic strain rate tensor

The elastic strain rate is related to the stress rate via the generalized Hooke's law:

$$\dot{\sigma} = \mathrm{D}\dot{\varepsilon}^e \tag{3.16}$$

with D being the elastic stiffness matrix.

The plastic deformation is computed from the plastic potential g_p that depends on the current stress state:

$$\dot{\varepsilon}^{p} = \dot{\lambda}\frac{\partial g_{p}}{\partial \sigma} \tag{3.17}$$

where $\dot{\lambda}$ is the rate of change of the so-called plastic multiplier λ dependent on the state of stress and gp is the plastic potential function, which specifies the direction to which the

plastic strain develops. If the plastic potential function gp is coincident with the yield function f of the material, the flow rule is then called the associated type; otherwise it is called the non-associated type. The plastic multiplier λ has to satisfy the following conditions of the yield criterion (Bui et al. 2008a):

- $\lambda = 0$ whenever $f < 0$ or $f = 0$ and d$f < 0$ corresponding to elastic or plastic unloading:
- $\lambda > 0$ whenever $f = 0$ and d$f = 0$ corresponding to plastic loading.

The value of plastic multiplier λ can be calculated by using the consistency condition, which states that

$$df = \frac{\partial f}{\partial \sigma^{\alpha\beta}} d\sigma^{\alpha\beta} = 0 \tag{3.18}$$

This equation assures that the new stress state $\sigma^{\alpha\beta} + d\sigma^{\alpha\beta}$ after loading still satisfies the yield criterion:

$$f\left(\sigma^{\alpha\beta} + d\sigma^{\alpha\beta}\right) = f\left(\sigma^{\alpha\beta}\right) + df = f\left(\sigma^{\alpha\beta}\right) \tag{3.19}$$

Substituting the elastic and plastic strain rate tensors obtained from Equations (3.15), Equation (3.16) and Equation (3.17), the total strain rate tensor now can be expressed in the form of stress rate tensor as

$$\dot{\varepsilon}^{\alpha\beta} = \frac{\dot{s}^{\alpha\beta}}{2G} + \frac{1-2v}{3E}\dot{\sigma}^{\gamma\gamma}\delta^{\alpha\beta} + \dot{\lambda}\frac{\partial g_p}{\partial \sigma^{\alpha\beta}} \tag{3.20}$$

The yield function and plastic potential for the Drucker-Prager model used in this study are defined as follows, respectively:

$$f = \alpha_\phi I_1 + \sqrt{J_2} - k_c \tag{3.21}$$

$$g_p = \alpha_\psi I_1 + \sqrt{J_2} \tag{3.22}$$

where I1 and J2 are the first and second invariants of the stress tensor, which are defined by the following equations:

$$I_1 = \delta^{xx} + \delta^{yy} + \delta^{zz} \tag{3.23}$$

and

$$J_2 = \frac{1}{2} s^{\propto\beta} s^{\alpha\beta} \tag{3.24}$$

αϕ and kc are Drucker-Prager constants that are calculated from the Coulomb material constants c (cohesion) and ϕ (internal friction). In plane strain, the Drucker-Prager constants are computed by,

$$\alpha_\phi = \frac{\tan\phi}{\sqrt{9 + 12\tan^2\phi}} \tag{3.25}$$

$$k_c = \frac{3c}{\sqrt{9 + 12\tan^2\phi}} \tag{3.26}$$

The non-associated plastic flow rule specifies the plastic potential function by,

$$g_p = \propto_\psi I_1 + \sqrt{J_2} - constant \tag{3.27}$$

The dilatancy factor α_ψ in equation (3.22) can be related to the dilatancy angle ψ in a fashion similar to that between α_ϕ and friction angle ϕ (Bui et al. 2014).

The combination of equations (3.15), (3.16) and (3.17) in association with the consistency condition, i.e. the stress state must be located on the yield surface during the plastic loading, gives:

$$\dot{\sigma} = \left[\mathrm{D} - \frac{\mathrm{D}\dfrac{\partial g_p}{\partial \sigma}\dfrac{\partial f_y}{\partial \sigma}^T \mathrm{D}}{\dfrac{\partial f_y}{\partial \sigma}^T \mathrm{D}\dfrac{\partial g_p}{\partial \sigma}} \right] \dot{\varepsilon} = \mathrm{D}^{ep}\dot{\varepsilon} \tag{3.28}$$

with D^{ep} being the elasto-plastic stiffness tensor.

When considering a large deformation problem, an invariant stress tensor with respect to rigid-body rotation must be applied to the constitutive relation. Accordingly, the Jaumann rate which gives an objective measure of the stress rate was adopted for the formulation (Libersky et al. 1993, Randles & Libersky 1996, Borja 2013):

$$\dot{\sigma}^J = \dot{\sigma} - \omega\dot{\sigma} - \dot{\sigma}\omega^T \tag{3.29}$$

with ω being the spin rate tensor.

Finally, the above stress-strain relation needs to be discretised onto SPH particles. The detail descriptions of this approach can be found in Bui et al. (2008a, 2014). Here, I only provide the final form of stress-strain relation, which is written in index form as follows:

$$\frac{d\sigma_a^{\alpha\beta}}{dt} = \sigma_a^{\alpha\gamma}\dot{\omega}_a^{\beta\gamma} + \sigma_a^{\gamma\beta}\dot{\omega}_a^{\alpha\gamma} + 2G_a\dot{e}_a^{\alpha\beta} + K_a\dot{\varepsilon}_a^{\gamma\gamma}\delta_a^{\alpha\beta} - \dot{\lambda}_a\left[3K_a\alpha_{\psi a}\,\delta^{\alpha\beta} + (G/\sqrt{J_2})_a s_a^{\alpha\beta}\right] \tag{3.30}$$

with $\dot{\lambda}$ being:

$$\dot{\lambda}_a = \frac{3\alpha_{\phi a}K_a\dot{\varepsilon}_a^{\gamma\gamma} + (G/\sqrt{J_2})_a s_a'^{\alpha\beta}\dot{\varepsilon}_a^{\alpha\beta}}{9\alpha_{\phi a}K_a\alpha_{\psi a} + G_a} \tag{3.31}$$

where α, β and γ denote Cartesian components *x*, *y*, and *z* with Einstein convention applied to repeated indices; $\dot{e}$ is the deviatoric shear strain-rate tensor; $\delta^{\alpha\beta}$ is the Dirac delta function; *K* and *G* are the elastic bulk and shear moduli, respectively; α_ϕ and α_ψ

are the Ducker-Prager constants calculated by fitting the Drucker-Prager yield criterion with the well-known Mohr-Coulomb yield criterion (Bui et al. 2008a; 2008b; 2013a, 2013b). The above constitutive model requires six materials parameters, including cohesion coefficient (c), friction angle (ϕ), dilatancy angle (ψ), Young's modulus (E), Poisson's ratio (υ), and bulk density (ρ). The validations of this constitutive model within the standard SPH framework have been conducted in previous works (Bui et al. 2008a; Bui et al. 2011c), in which an excellent agreement between the SPH method and the FEM for bearing capacity problems has been achieved; therefore, they will not be repeated here.

3.3.3. Standard Approach to Stabilize the SPH Method with Artificial Viscosity

Similar to finite difference methods, when simulating shock or convection dominated flows, the SPH method suffers from numerical instabilities that often result in spurious oscillations of both the velocity and pressure fields and may even lead to incorrect results or termination of the simulation. In order to suppress this numerical instability, a common technique is to add an artificial viscosity term into the momentum equation to smear or damp-out undesirable velocity/stress oscillations. In the SPH method, the following artificial viscosity (Monaghan & Gingold, 1983) is normally adopted:

$$\Pi_{ab} = \begin{cases} \dfrac{-\alpha_\Pi c_{ab}\phi_{ab} + \beta_\Pi \phi^2}{\rho_{ab}} & \mathbf{v}_{ab}\cdot\mathbf{x}_{ab} < 0 \\ 0 & \mathbf{v}_{ab}\cdot\mathbf{x}_{ab} \geq 0 \end{cases} \tag{3.32}$$

in which

$$\phi_{ab} = \frac{h_{ab}\mathbf{v}_{ab}\cdot\mathbf{x}_{ab}}{\left|\mathbf{x}_{ab}\right|^2 + 0.01h_{ab}^2} \qquad c_{ab} = \frac{c_a + c_b}{2} \tag{3.33}$$

$$\rho_{ab} = \frac{\rho_a + \rho_b}{2} \qquad h_{ab} = \frac{1}{2}(h_a + h_b) \tag{3.34}$$

$$\mathbf{x}_{ab} = \mathbf{x}_a - \mathbf{x}_b, \qquad \mathbf{v}_{ab} = \mathbf{v}_a - \mathbf{v}_b \tag{3.35}$$

In the above equations, α_Π and β_Π are two unknown constants, which are usually taken to be 1 (Monaghan, 1992); x is the vector coordinate of the particle; h_a, h_b is the smoothing length which is taken to be $h = 1.2\Delta x$ with Δx being the initial separation between two adjacent particles (at the first time); and c is the speed of sound in granular materials, which is computed from the bulk modulus and density as follows:

$$c_a = \sqrt{E_a / \rho_a} \tag{3.36}$$

The artificial viscosity consists of two contributions: one is linearly proportional to the divergence of velocity, which produces a shear and bulk viscosity; the other one, which is quadratic in the velocity divergence, is substantially analogous to the Von Neumann-Richtmyer viscosity and able to handle high Mach number flows (Monaghan, 1992). The artificial viscosity term is added to the momentum equation as follows:

$$\left(\frac{d\mathbf{v}}{dt}\right)_a = \sum_{b+1}^{N} m_b \left(\frac{\boldsymbol{\sigma}_a}{\rho_a^2} + \frac{\boldsymbol{\sigma}_b}{\rho_b^2} + \Pi_{ab}\mathbf{I} \right) \cdot \nabla W_{ab} + \mathbf{g}_a \tag{3.37}$$

where **I** is the unit tensor. So far, the use of the artificial viscosity term has become essential in most SPH applications. However, the selection of two unknown constants α_Π and β_Π could significantly affect the result of SPH simulations and there is no rigorous method to define these parameters. In addition, these parameters have no direct link to physical material properties.

3.3.4. The SPH Method Without Artificial Viscosity: A New Approach

As addressed in the preceding section, whilst the SPH method has the advantage of simulating large strain plasticity problems, numerical results usually suffer from the well-known zero-energy mode (Zero energy mode or hourglass mode is essentially a spurious deformation mode of a Finite Element Mesh, resulting from the excitation of zero-energy degrees of freedom. It typically manifests as a patchwork of zig-zag or hourglass, where individual elements are severely deformed, while the overall mesh section is unreformed), which results in large stress oscillations that could lead to termination of the SPH computational process. The artificial viscosity is usually adopted to smear out the stress

oscillations over the integral supporting domain of each SPH particle, thus stabilising the SPH model. However, as discussed, the artificial viscosity requires two unknown parameters (α_Π and β_Π) that have no specific link to physical material properties. Therefore, its use in SPH simulations is purely based on the numerical stability needs. Furthermore, the variation of these parameters could significantly alter the failure mechanism of granular materials. Besides, despite its success in the stabilization of the dynamic simulations, the use of artificial viscosity in the SPH cannot completely remove the oscillation of stresses in granular materials under large shear deformation (Johnson G.R., 1996; Bui et al., 2008a). In this chapter, the following two techniques are adopted to both replace the artificial viscosity in SPH simulations and improve the accuracy of the stress distribution.

3.3.4.1. Viscous Damping

In the current SPH numerical framework (Bui et al., 2008a), the motion of granular materials is described using the fully dynamic equation, i.e. Equation (3.15). In the absence of artificial viscosity, SPH particles are subjected to free oscillations due to inertial forces. To damp out this oscillation, a linear viscous damping model, which is commonly used in dynamic simulations of continua, is adopted. The linear viscous damping is modelled as a force antiparallel to velocity of the particle. The damping force per unit mass is defined by:

$$\mathbf{F}_d = -c_d \cdot \mathbf{v} \tag{3.38}$$

Where **v** is vector of velocity (it isn't an absolute velocity); c_d is a damping coefficient which can be formulated using the same approach proposed by Bui and Fukagawa (2013) as follows:

$$c_d = \xi \sqrt{E / \rho h^2} \tag{3.39}$$

with ξ being a non-dimensional damping coefficient that requires calibration for different applications. For the simulation of granular flows, such as the flow of granular column collapse experiments in this thesis, a constant value of $\xi = 5\times10^{-5}$ is recommended. The damping coefficient (c_d) will be then varied depending on the material properties (i.e. E

and ρ) and the initial spacing between two particles (i.e. $h = 1.2\Delta x$). The effects of the viscous damping on SPH simulation results are investigated in Section 3.4 of this chapter, in which it will be shown that the energy loss using this approach is comparable with that due to the artificial viscosity. However, this approach has more physical meaning compared to the artificial viscosity because the damping coefficient is now directly linked to material properties. I acknowledge that there is still a need to calibrate a non-dimensional parameter for the proposed viscous damping model, and this is physically similar to the calibration of two parameters for the traditional use of artificial viscosity in SPH. However, thanks to the direct link with the material properties, once the non-dimensional parameter is calibrated for a certain type of material, the proposed damping coefficient will purely depend on the material properties as seen in Equation (3.39). The viscous damping force is added into the momentum equation as follows:

$$\left(\frac{d\mathbf{v}}{dt}\right)_a = \sum_{b+1}^{N} m_b \left(\frac{\boldsymbol{\sigma}_a}{\rho_a^2} + \frac{\boldsymbol{\sigma}_b}{\rho_b^2}\right) \cdot \nabla W_{ab} + \mathbf{F}_d + \mathbf{g}_a \tag{3.40}$$

3.3.4.2. Stress/Strain Regularisations

While the kinematics of SPH simulation is generally realistic, the stress/pressure fields of SPH particles undergoing large deformation can exhibit large oscillations. This problem is known as the short-length-scale-noise (Monaghan, 2012), and is identified as one of the key challenges of the standard SPH method that needs to be addressed in order to improve the accuracy of SPH simulations. The problem becomes worse when the artificial viscosity is not adopted in SPH simulations, although the viscous damping force could slow down the numerical instability process. To overcome the short-length-scale-noise problem and to stabilise the SPH model without artificial viscosity, this thesis suggests regularising the stresses and strains of each SPH particle over its kernel integral domain after a certain number of computational cycles. Among different approaches, the Moving Least Square (MLS) method (Belytschko et al., 1998; Dilts, 1999) is adopted in this thesis. The method is a first order correction that reproduces exactly the linear variation of stress and strain fields:

$$\langle \boldsymbol{\sigma}_a \rangle = \sum_{b=1}^{N} \boldsymbol{\sigma}_b W_{ab}^{MLS}(x_a)\, dV_b \tag{3.41}$$

$$\langle \boldsymbol{\varepsilon}_a \rangle = \sum_{b=1}^{N} \boldsymbol{\varepsilon}_b W_{ab}^{MLS}(x_a)\, dV_b \tag{3.42}$$

where the corrected MLS kernel function in 2D is evaluated as follows:

$$W_{ab}^{MLS}(x_a) = [\beta_0(x_a) + \beta_1(x_a)(x_b - x_a) + \beta_2(x_a)x_b - x_a)] \cdot W_b(x_a) \tag{3.43}$$

The estimate of coefficients $\beta_k(x_a)$ in Equation (3.43) requires the solution of a (3×3) linear algebraic system of equations for each particle:

$$[\beta_0 \quad \beta_1 \quad \beta_2]^T = A^{-1}[1 \quad 0 \quad 0]^T \tag{3.44}$$

where

$$A(x_a) = \sum_b \begin{Bmatrix} 1 & (x_b - x_a) & (y_b - y_a) \\ (x_b - x_a) & (x_b - x_a)^2 & (x_b - x_a)(y_b - y_a) \\ (y_b - y_a) & (x_b - x_a)(y_b - y_a) & (y_b - y_a)^2 \end{Bmatrix} W_b(x_a) dV_b \tag{3.45}$$

The performance of the stress/strain regularisations is investigated in Section 3.4 by applying the above MLS correction every k steps (k = 2, 5, 10 and 15). Numerical results suggested that the best result for the final run-out distance and stress field predictions could be obtained for k less than or equal to 10 steps. For a larger k value, the numerical results can still experience the oscillations of stress due to insufficient regularisations. In this computation, k = 5 was recommended taking into consideration both the accuracy and computational costs. The comparisons of stress field predicted by the proposed SPH model for different k values are presented in the next section.

3.4. PERFORMANCE OF THE PROPOSED APPROACH

A 2D numerical simulation of granular column collapse is conducted to demonstrate the effectiveness of the proposed SPH model. Three test cases are performed using the same SPH integration scheme and the material constitutive model, but adopting different stabilization techniques. The details of these test cases are summarised as follows: **Case 1** considers the standard SPH simulation, i.e. solving Equations (3.13) & (3.14) without utilising the artificial viscosity; **Case 2** repeats the same SPH simulation with the artificial viscosity (α_Π = 0.1 and β_Π = 0.0) (Bui et al. 2008a); and **Case 3** and

Case 4 incorporate the stress/strain regularisations to the standard SPH simulation (see Section 3.4.4) in which the number of time steps between two consecutive regularisation operations are k = 5 steps. The difference between **Case 3** and **Case 4** is the inclusion of viscous damping: whilst **Case 3** does not consider the viscous damping hence using Equation (3.14) for the momentum equation, **Case 4** introduces the viscous damping with the non-dimensional damping coefficient $\xi = 5\times10^{-5}$ (i.e. the corresponding damping coefficient c_d = 1.55) in the momentum equation, Equation (3.37). Comparison in terms of numerical stability and final stress distribution is then used to evaluate the performance of different test cases.

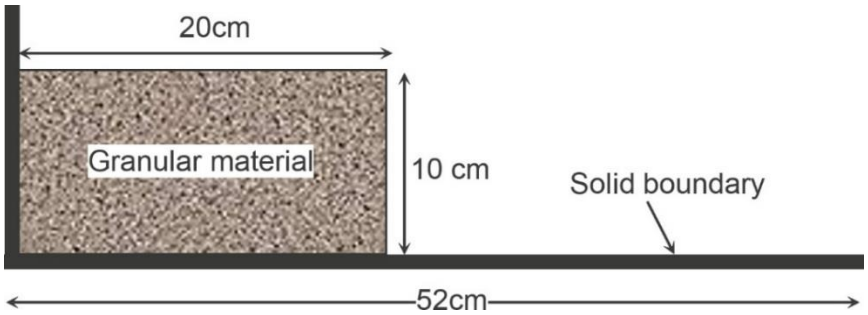

Figure 3.2: *Initial geometry and boundary conditions*

Figure 3.2 shows the initial geometry setting and boundary conditions of a rectangular granular column of 20 cm in length and 10cm in height for the three numerical tests. The assumed boundary conditions are: fully-fixed at the base and free-rolling at the vertical wall. The constitutive model described in Section 3.3.2 is used with material properties and parameters shown in table 3.1.

Table 3.1: *Material parameters for the SPH simulations*

Name	Value	Unit
Gravity Density (ρ)	26.5	kN/m^3
Friction angle (ϕ)	22	deg
Young's module (E)	15	MPa
Poisson's ratio (ν)	0.3	-
Dilation angle (ψ)	0	deg
Cohesion (c)	0	kPa

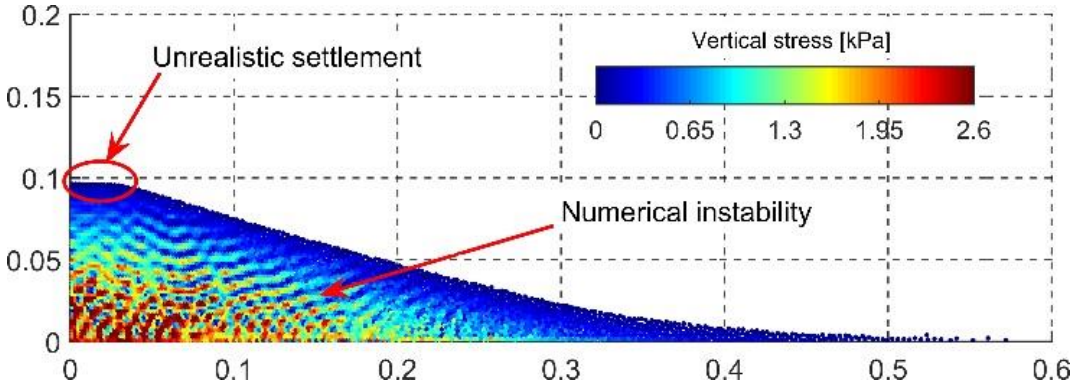

(a) **Case 1**: No stabilisation

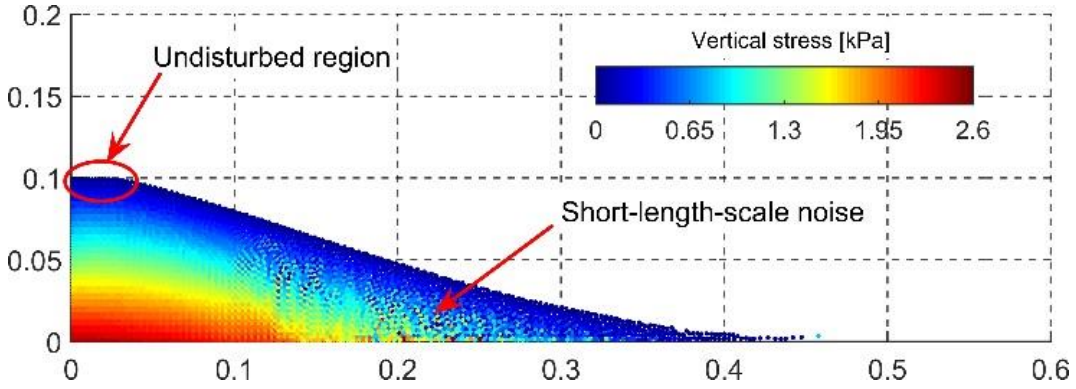

(b) **Case 2**: Stabilisation by artificial viscosity

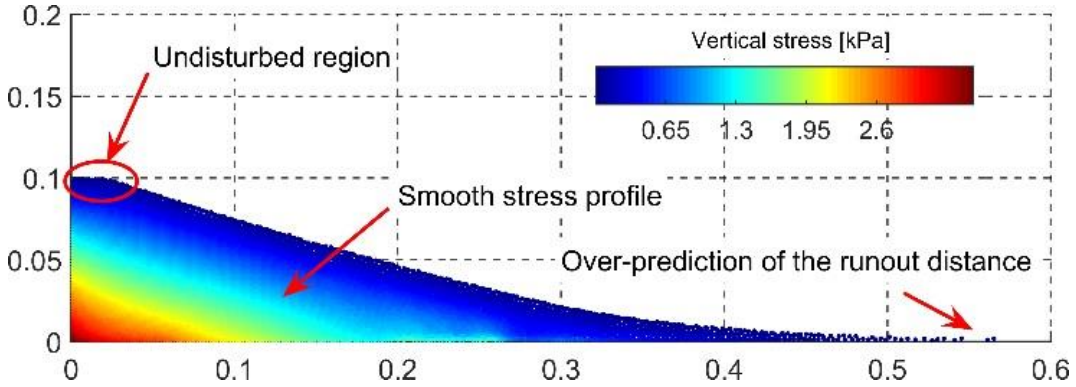

(c) **Case 3**: No stabilisation + MLS (5 steps)

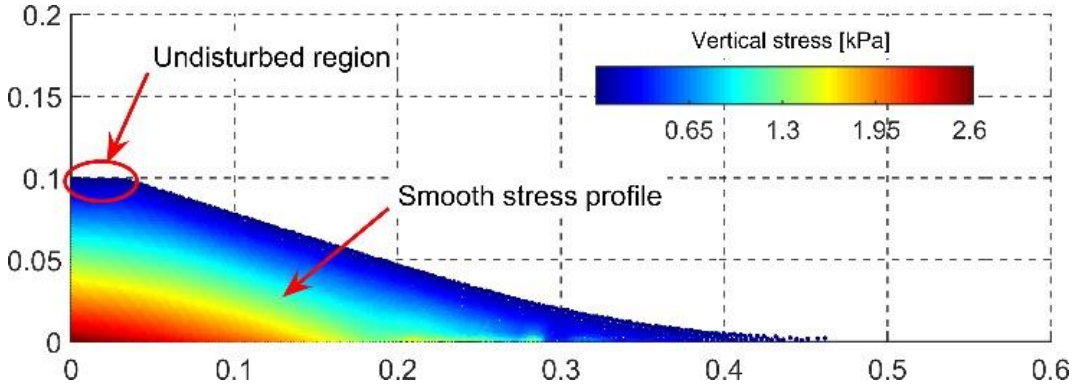

(d) **Case 4**: Viscous damping + MLS (5 steps)

Figure 3.3: *Simulation of the granular column collapse using different stabilization techniques (axes are distances with unit is decimeter)*

In all SPH simulations, 5,000 SPH particles are used to represent the computational domain of the granular material. These particles are arranged in a square lattice with an initial separation of 0.2 cm, and thus smoothing length of 0.24cm. In addition, three layers of SPH particles are located outside the computational granular domain to represent the solid wall. The no-slip boundary condition is enforced at the base to simulate the fully-fixed boundary, while the free-slip boundary condition is applied at the vertical boundary to mimic the free-rolling boundary condition. Details of the implementation of these boundary conditions in SPH can be found in Bui and Fukagawa (2013).

Figure 3.3 shows the comparison of the SPH simulation results from four numerical test cases. In the first case, Figure 3.3 (a) without utilising the artificial viscosity, the distribution of vertical stress predicted by the SPH standard method exhibits large oscillation over the whole computational domain, showing a highly unstable SPH solution. The highly fluctuated stress distribution can be observed in the lower left corner of the granular column where the material undergoes little or almost no deformation during the collapse process. This is physically unreasonable and can be attributed to numerical issues due to zero-energy mode in the SPH method. In addition, the top left corner of the column exhibits vertical settlement which is unrealistic since that region is reported as the undisturbed zone during the collapse of the column (Lube et al., 2004 and 2005; Girolami et al., 2012; Carter et al., 2014). This unrealistic settlement can be explained from the fact that the unstable SPH solution introduces errors to the stress-strain relation which in turn leads to significant errors in the macro behaviour of granular materials.

On the other hand, thanks to the use of the artificial viscosity, the stress distribution was significantly improved in **Case 2**, as shown in Figure 3.3 (b). The noise in the stress profile is only observed in the region where the material undergoes large shear deformation, while a very smooth stress distribution can be observed in the zone experiencing less shear deformation or stationary. The final run-out distance of the granular material is found to be significantly less in **Case 2** compared to that of **Case 1**, indicating that the artificial viscosity dissipates some kinetic energy of granular flows. In fact, the incorporation of the artificial viscosity in the momentum equation will introduce viscous shear stresses to the material flow, thus reducing the final run-out distance. It is obvious from this simulation that the mechanism of granular flow significantly depends on the selection of two unknown parameters in the artificial viscosity and the speed of

sound in granular materials as shown in Equation (3.36). For a constant sound speed, the larger the value of the two unknown parameters in the artificial viscosity is, the higher amount of kinetic energy is dissipated, thus resulting in shorter final run-out distance. The stress noise observed in the region where the material suffers large shear deformation, as seen in **Case 2**, is commonly accepted in most SPH simulations. This problem is often called the short-length-scale-noise (Monaghan, 2012) and does not cause significant error to the overall SPH performance for simulations of granular flows as demonstrated in Bui et al (2008a; 2014), thanks to the kernel approximation nature in the SPH method. However, the short-length-scale-noise may introduce errors if we try to predict stresses at a location where the material experiences large shear deformation. Thus, alternative approaches are being investigated to improve the overall performance of the SPH method.

In contrast, as can be seen from the numerical results of **Cases 3** and **4**, Figure 3.3 (c) and (d), the stress noise is regularised in the SPH simulation after introducing the stress/strain regularisation every 5 steps (k = 5). In both cases, a very smooth stress distribution is achieved over the entire the computational domain, even at locations where the material experiences large shear deformation. Furthermore, the undisturbed zone on the top left corner of the granular column reported in previous studies (Lube et al., 2004 and 2005; Girolami et al., 2012; Carter et al., 2014) can be captured using the proposed SPH model. Comparing the final run-out distance among four cases, the run-out distances of **Case 2** and **Case 4** are comparable, while they are significantly less than those of **Case 1** and **Case 3**. The similarity between **Case 2** and **Case 4** suggests that the viscous damping plays an important role in obtaining realistic run-out predictions of granular flows in SPH simulations, similar to that of the artificial viscosity; however, when combined with the stress/strain regularisation technique, the short-length-scale-noise does not occur anymore. On the other hand, the comparable result of the final run-out distance between **Case 1** and **Case 3** suggests that the stress/strain regularisation does not significant affect the overall behaviour of granular flow. In addition, despite suffering from the short-length-scale-noise issue, the standard SPH model (**Case 1**) is still able to produce results comparable to that of the regularised model (**Case 3**), thanks to the kernel approximation nature in the SPH method.

The robustness of the proposed technique is further examined by varying the non-dimensional damping coefficient in a range of ξ = 3, 4, 5 and 6×10^{-5} hence the corresponding value for c_d is 0.93, 1.24, 1.55 and 1.86. In this investigation, the

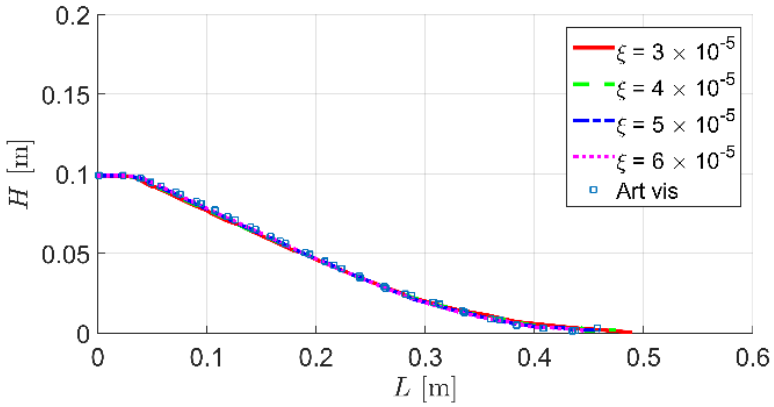

(a) Final shape of the deposit

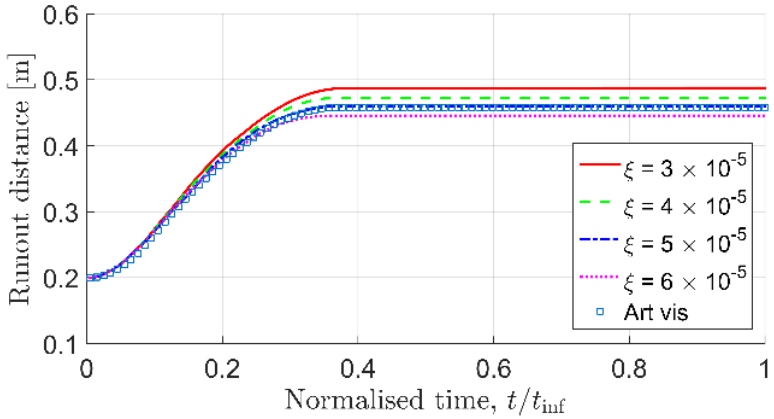

(b) Evolution of runout distance

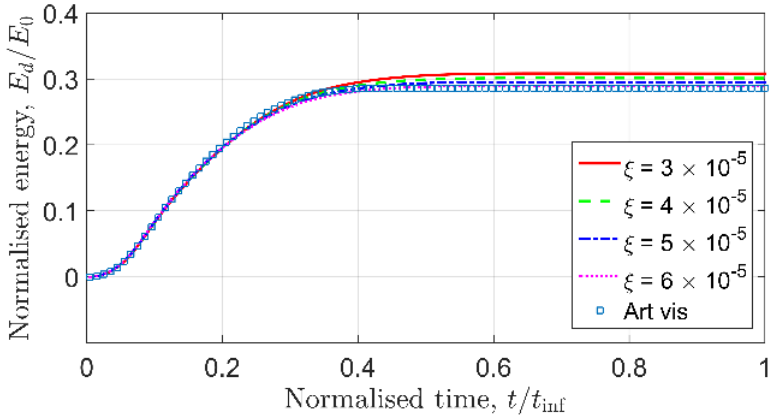

(c) Evolution of dissipated energy

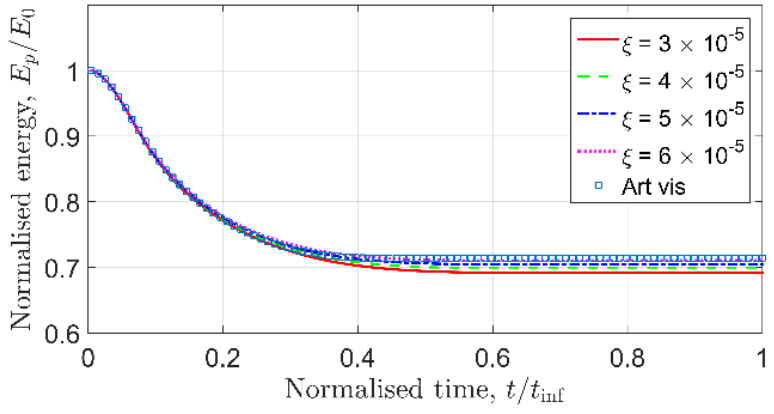

(d) Evolution of potential energy

Figure 3.4: *Influence of the damping coefficient*

stress/strain regularisation is performed every 5 steps (k = 5), and the obtained results are then compared with that of SPH simulations using the artificial viscosity. The final shapes of the deposit and the time evolutions of run-out distance in five simulations (i.e. artificial viscosity and 4 different damping coefficients) are shown in Figure 3.4 (a) and Figure 3.4 (b), respectively. The results are comparable between the standard SPH model and the proposed ones using different damping coefficients. As can be see, the increase of viscous damping shortens the final run-out distance, while the final shapes are more or less similar in all cases. The final run-out distance predicted by the standard SPH model using the artificial viscosity is in between those predicted by the proposed SPH model with damping coefficient $\xi = 4\times10^{-5}$ and 6×10^{-5}.

The comparison of the time evolution of the dissipation energy and the remaining potential energy is shown in Figure 3.4 (c) and Figure 3.4 (d), respectively. The dissipation energy $E_d(t)$ at a given time is calculated from the initial potential energy E_0 minus the current potential energy $E_p(t)$ and the current kinetic energy $E_k(t)$ as follows (Zenit 2005; Utili et al. 2015):

$$E_d(t) = E_0 - E_p(t) - E_k(t) \tag{3.46}$$

in which:

$$E_p(t) = \sum_{i=1}^{N} m_i g h_i(t) \quad \text{and} \quad E_k(t) = \frac{1}{2}\sum_{i=1}^{N} m_i v_i^2(t) \tag{3.47}$$

It can be seen from Figure 3.4 (c) that a larger ξ value (or c_d value) leads to smaller accumulated energy dissipation (E_d). This can be explained due to the fact that the larger the ξ value, the less the final run-out distance as seen in Figure 3.4 (b), and therefore the less potential energy loss. The total energy loss predicted by the standard SPH model using the artificial viscosity is very close to those predicted by the proposed SPH model with non-dimensional damping coefficients between $\xi = 5\times10^{-5}$ and $\xi = 6\times10^{-5}$, as shown in Figure 3.4 (d). Therefore, the proposed technique has been shown to be comparable with the standard SPH with artificial viscosity in controlling the numerical stability and predicting the final run-out distance. However, the most significant advantage of the proposed mode is its capability to produce smooth stress profiles, even at the locations of large shear deformation. The prediction of smooth stress field is essential for SPH simulations of granular materials within the classical plasticity theory because stresses of the granular material are updated at each particle every time step.

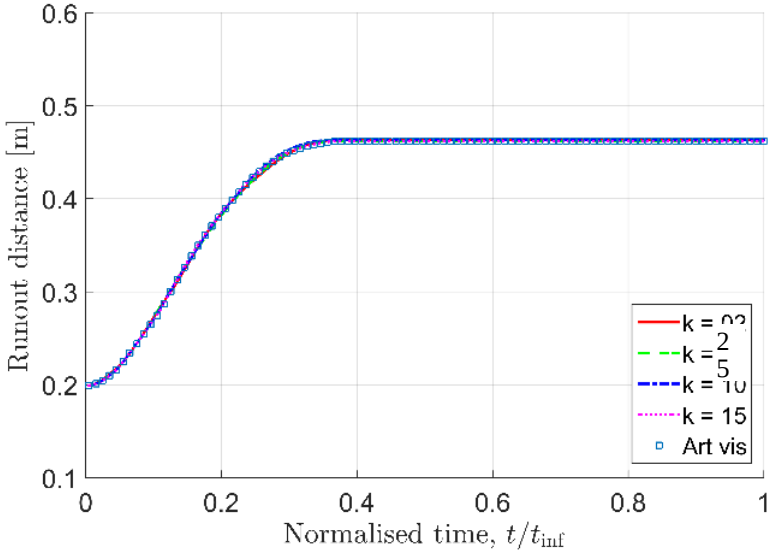

(a) Evolution of runout distance

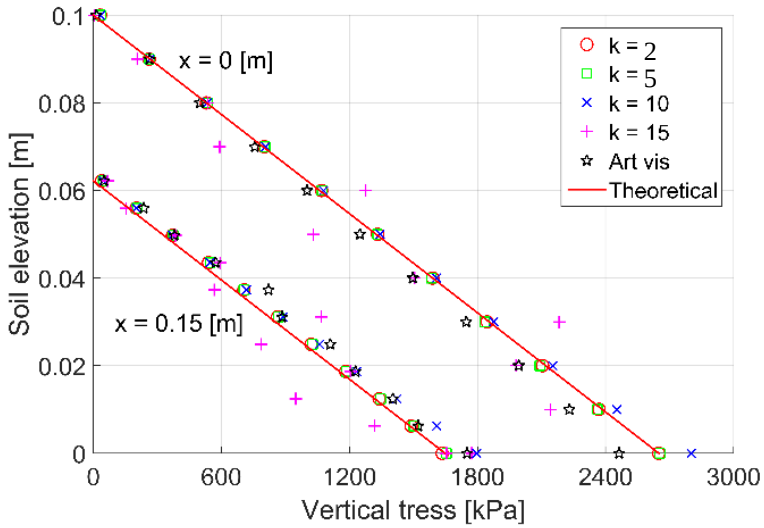

(b) Vertical stress at final stage of collapse

Figure 3.5: *Effect of stress/strain regularisations on SPH simulations*

Finally, the effect of the proposed stress/strain regularisation technique on SPH simulation results is investigated by repeating the proposed SPH model with different intervals between stress/strain regularisation (i.e. k = 2, 5, 10 and 15), whilst keeping the damping coefficient unchanged in all simulations ($\xi = 5\times10^{-5}$). The time evolutions of the run-out distance and the vertical stress profiles predicted at two certain locations of x = 0 and x = 0.15m at the final stage of granular flow are plotted in Figure 3.5, and comparisons is made with the standard SPH model using the artificial viscosity and with

the analytical solution for the vertical stresses. The time evolutions of the run-out distance of granular flow are almost the same in all simulations, as shown in Figure 3.5 (a), indicating that the kinematics of granular flow is not significantly affected by the proposed stress/strain regularisation technique. On the other hand, the effectiveness of the stress/strain regularisation technique is clearly observed when comparing the vertical stress profiles for different SPH simulations. For a k value of less than or equal to 5, the proposed technique could capture quite well the vertical stress profile predicted using the analytical model (i.e. $\sigma = \gamma z$, with γ being the specific weight of granular material and z being the depth from the free-surface).

The slight difference between the SPH model and the analytical solution is explained due to the fact that the bulk density of granular material in SPH simulations is evolved with large deformation, while the analytical solution adopted a constant value of $\gamma = 26.5\text{kN/m}^3$ (see Table 3.1). On the other hand, as the k value increases, there is not enough stress/strain regularisation to stabilise the SPH simulation. As a result, the predicted vertical stress deviates from the analytical solution. The scattered stress distribution for $k = 15$ suggests that the SPH solution in such a case still suffers from the short-length-scale-noise, despite the fact that the runout distance is not significantly affected thanks to the kernel approximation nature in the SPH method. Compared to the standard SPH model with artificial viscosity, the proposed SPH model is more accurate for a k value of less than or equal to 5. To this end, the stress/strain regularisation technique is recommended to be applied every $k = 5$ computational steps to achieve a reasonably accurate solution with acceptable computational cost, while the non-dimensional damping coefficient (ξ) is recommended to be $\xi = 5\times10^{-5}$. It is note that this coefficient may change in a wide range, as shown in Figure 3.4; therefore, it is possible to achieve a better fit in term of the runout distance or energy dissipation for a required particular prediction. As an alternative approach to the viscous damping model, the traditional artificial viscosity has been combined with the stress/strain regularisation technique to reproduce simular outcomes.

3.5. APPLICATION TO THE PROBLEM OF GRANULAR FLOWS

The proposed SPH framework is finally validated with the 2D granular column collapse experiment described in Chapter 2. Figure 3.5 shows the initial geometry and boundary conditions for the experiment with the initial aspect ratio a (the ratio between

the initial height H_0 and the initial width L_0) of 0.5 and 1.0. In the experiments, aluminium rods of 5cm in length were used as the model material to mimic 2D conditions. The aluminium rods had diameters of 1.6mm and 3.0mm and mixed with the ratio of 3:2 in weight to achieve the total unit weight of 20.4kN/m^3 after the mixing. The shear strength parameters for the 2D material model, summarised in Table 3.2 were previously measured using biaxial tests (Bui et al. 2014). To initiate the flow, the supporting wall was quickly removed to allow granular materials to freely collapse. A high speed camera was then used to record the collapse process. For further details on these experimental series see Chapter 2.

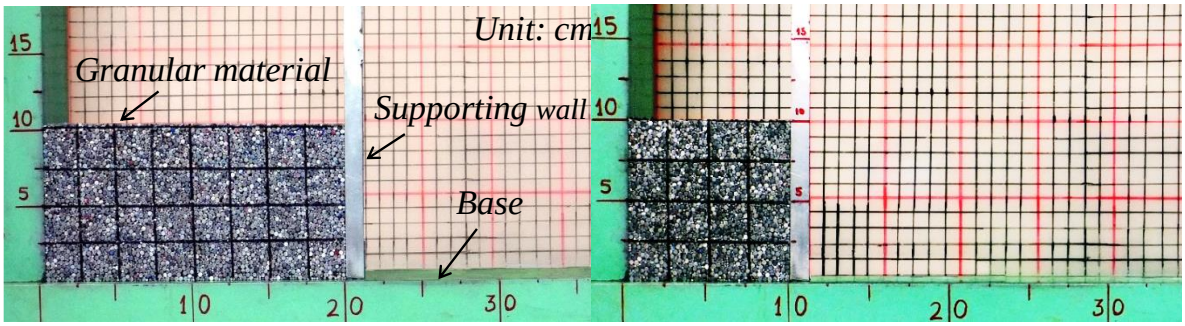

(a) Initial aspect ratio a = 0.5 (b) Initial aspect ratio a = 1.0

Figure 3.6: *Initial setting conditions in experiment*

Table 3.2: *Properties of the 2D material model (aluminium rods)*

Name	Value	Unit
Gravity Density (ρ)	20.4	kN/m^3
Friction angle (ϕ)	21.9	deg
Young's module (E)	5.84	MPa
Poisson's ratio (ν)	0.3	-
Dilatant angle (ψ)	0	deg
Cohesion (c)	0	kPa

In the SPH simulation, a total number of 5,000 and 2,500 SPH particles are used to represent the granular column of (20×10 cm) and (10×10 cm) in the experiments as shown in Figure 3.6, respectively. The SPH particles are arranged in a square lattice with an initial lattice spacing of 0.2cm and an initial smoothing length of 0.24cm. The boundary conditions are assumed to be fully fixed at the bases and the vertical

boundaries. Fixed boundary particles with no-slip boundary condition are then used to simulate these boundary conditions (Bui et al. 2008a; 2014).

Figures 3.7 and 3.8 show the velocity profile of granular flows obtained from the new SPH model at several time intervals. The corresponding free-surface of the deposit extracted from the experiments (i.e. solid-line in red) and the standard SPH model with the artificial viscosity (i.e. dash-line in green) are also superimposed on these Figures to validate the performance of the new SPH algorithm. It can be seen that the results predicted by the new SPH model are almost identical to those predicted by the standard SPH model with artificial viscosity. A minor difference in the time evolution of the run-out distance between the two SPH models can be attributed to the fact that the energy dissipations due to the artificial viscosity and the damping force are different. It is noted that the results obtained from the current case study is different from that observed in Section 3.3. In particular, the final run-out distance predicted by the standard SPH model in the previous section is smaller than that of the new SPH model, unlike the results observed in this section, although the same damping coefficient ($\xi = 5\times10^{-5}$) and the artificial viscosity constants ($\alpha_\Pi = 0.1$ and $\beta_\Pi = 0.0$) are utilised in both simulations. This inconsistency is due to the difference in the material properties that results in different sound speeds, and thus introducing different amounts of artificial viscosity into the material flow, despite the same artificial viscosity constants used.

Regarding the time evolution of the velocity field predicted by the new SPH model, the flow front experiences an acceleration phase, followed by a deceleration phase before full stop at the time $t = 0.607$ s and $t = 0.571$ s for $a = 0.5$ and $a = 1.0$, respectively. Moreover, it can be clearly observed that the interface between the static zone and the flowing zone inside the flow regime migrates progressively from the initial failure surface toward the free-surface and reaches the free-surface when the flow stops completely. These results are consistent with those reported by Girolami et al. (2012) and Crosta et al. (2015).

In comparison with the experiments, both SPH models (i.e. the new SPH model and the standard SPH model with artificial viscosity) predict fairly well the time evolution of surface deformation of the granular column after collapsing. There is a minor difference in the time evolution of the run-out distance between the SPH simulations and the experiment. In particular, the SPH simulations slightly over-predict the experimental results during the early stages of collapse, but are in very good agreement with the experiments in the later stages. This discrepancy can be explained by

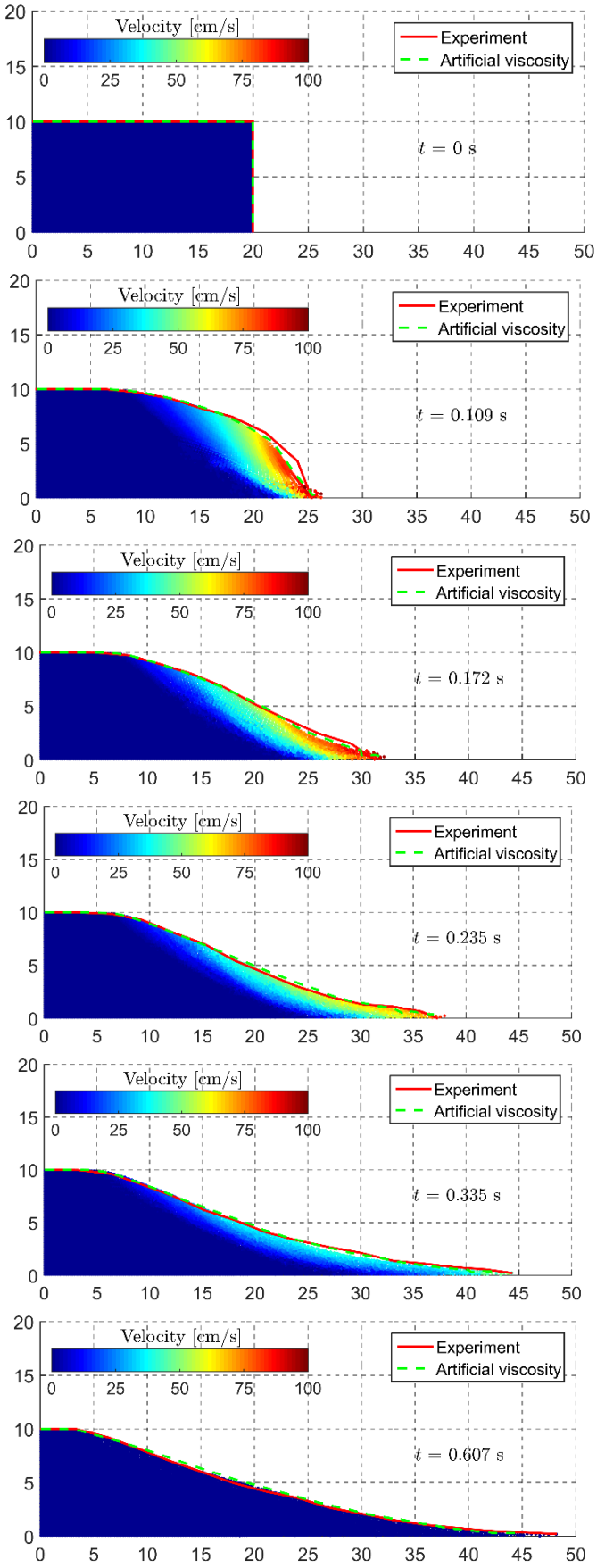

Figure 3.7: *Comparison between the SPH simulation and the experiment for the failure progress of the granular column (a = 0.5)*

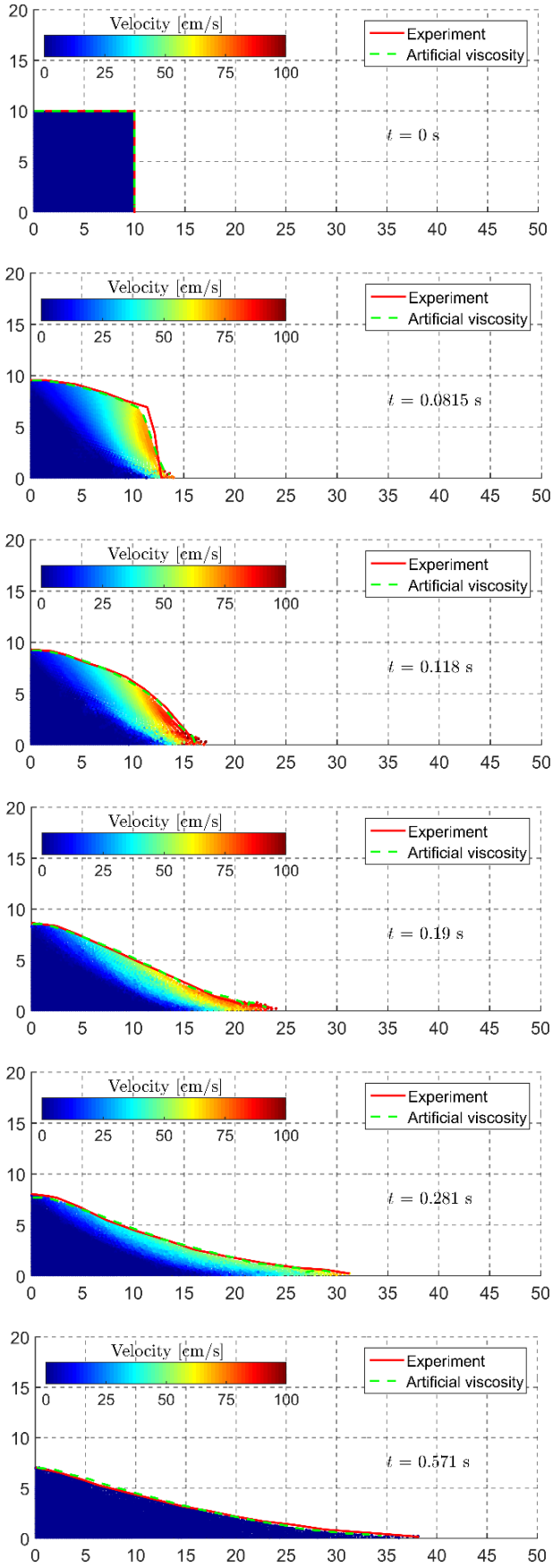

Figure 3.8: *Comparison between the SPH simulation and the experiment for the failure progress of the granular column, a = 1*

friction on the wall and on the bed in the experiment, which is not yet taken into account in the SPH simulations. This friction is not negligible in the early stages of collapse when the momentum of moving particles is large, but can be disregarded in the later stages when the moving particles slow down.

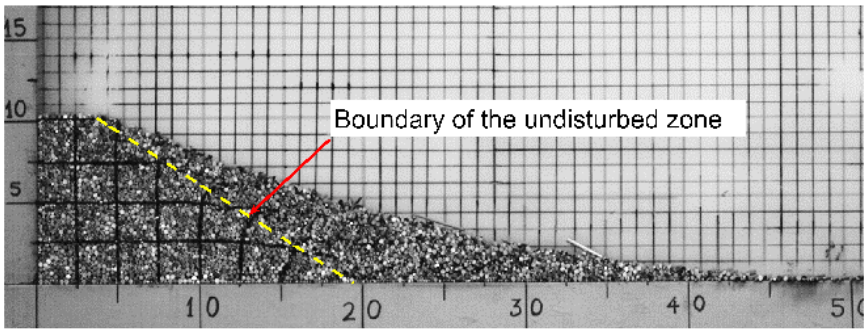

(a) Stationary state

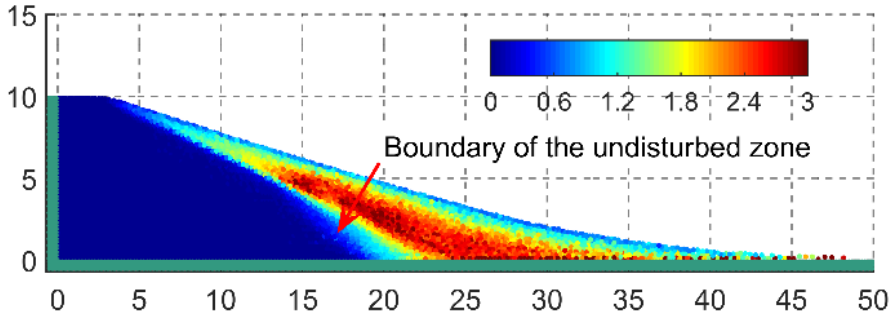

(b) Magnitude of deviatoric plastic strain

Figure 3.9: *Comparison between the SPH simulation and the experiment for the final state (a = 0.5)*

The difference in the failure mechanism between two typical test cases of a = 0.5 and 1.0 observed in the experiments can also be captured in the SPH simulations. As seen in Figure 3.7 (a = 0.5), the failure mechanism consists of the avalanche of the outside column edge, leaving the column inside undisturbed and the final morphology takes a form of a truncated cone. On the other hand, for the case of a = 1.0 (Figure 3.8), the whole granular column collapses completely, resulting in the final deposit of conical shape with the final height smaller than the initial height. In both cases, the granular flow is initiated at the front edge of the column and the collapse mechanism is a general shear failure (Lacaze et al. 2008).

Figures 3.9 and 3.10 show the final stage of the granular column collapse: in sub-Figure (a) the experimental result is given with the dash line representing the boundary of the undisturbed zone; in sub-Figure (b) the distribution of the accumulated deviatoric

plastic strain is given and the boundary of the undisturbed zone is identified as the zone in which the magnitude of the plastic strain is small. Both the experiment and the SPH simulation indicate a similar undisturbed zone which has a width slightly smaller than the initial width of the column and an inclination of about 40 degrees.

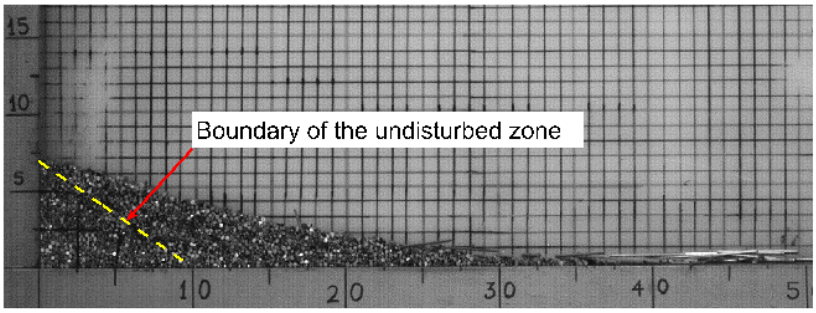

(a) Stationary state

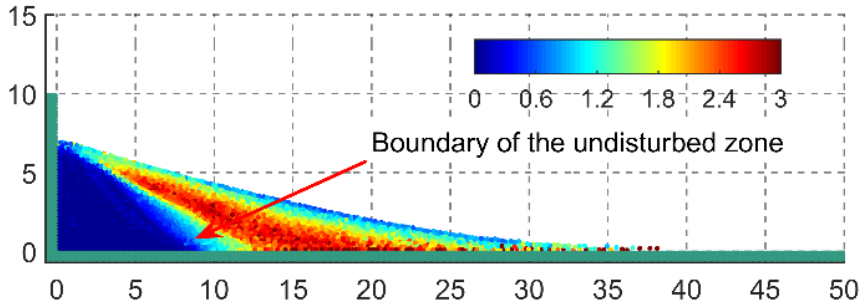

(b) Magnitude of deviatoric plastic strain

Figure 3.10: *Comparison between the SPH simulations and the experiment for the final state (a = 1.0)*

Finally, the proposed SPH model is validated against numerical and experimental data from the literature. Figure 3.11 shows the comparison between the SPH simulations and various results obtained from the literature for the scaling laws of the normalised height and the normalised run-out distance (i.e. the relation to initial aspect ratio). It can be seen that the granular scaling laws for the final height, Figure 3.11 (a), predicted by the new SPH model agrees well with those predicted by the DEM (Staron & Hinch, 2005; Utili et al. 2015) and by the FEM (Crosta et al. 2009) for initial aspect ratio from 0.3 to 10. However, when comparing the new SPH model with experiments (Lajeunesse et al. 2004; Lube et al. 2005), good agreement is only achieved for $a < 0.7$, while the SPH simulations under-predict the scaling laws for final height for $a > 0.7$. As for the run-out distance scaling laws, Figure 3.11 (b), the SPH simulations agree well with some existing DEM simulations (Staron and Hinch, 2005; Utili et al. 2015) for a wide range of a.

However, comparisons of the final height obtained from the SPH simulations, experiments (Lajeunesse et al. 2004; Lube et al. 2005) and the FEM (Crosta et al. 2009) show good agreement for $a < 0.7$, but over-prediction for $a > 0.7$.

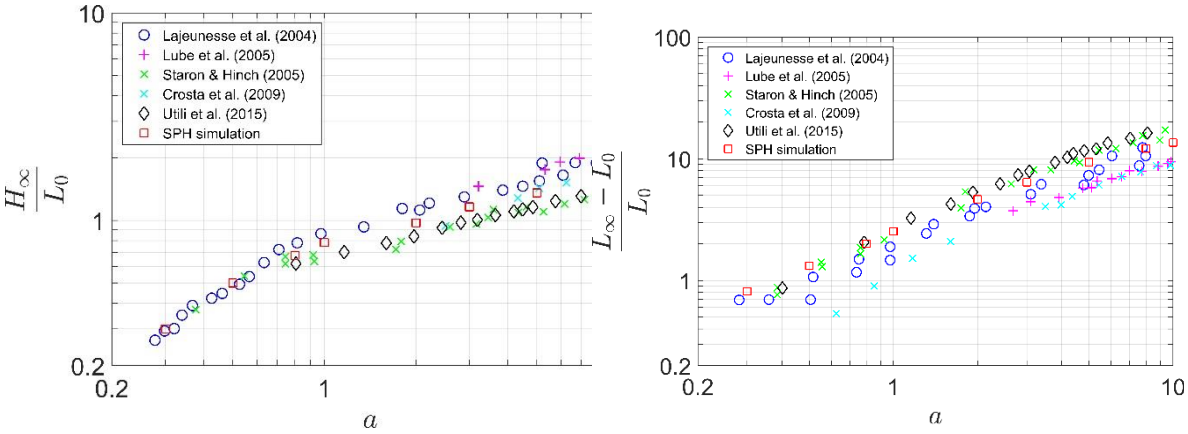

(a) Normalised final height (b) Normalised run-out distance

Figure 3.11: *Comparison between the SPH simulations and results from literatures for the scaling laws*

The similarity in the results between the SPH method and the DEM is expected since both simulations assume plane-strain conditions, thus the kinematic of the problem is identical. This suggests that the SPH method is capable of capturing the discrete behaviour of granular materials. The discrepancy between SPH (this study) or DEM (Staron & Hinch, 2005; Utili et al. 2015) results and experimental ones can be due to different configurations in two- and three-dimensions. In particular, the three-dimensional configuration employed in the experiments by Lajeunesse et al. (2004) and Lube et al. (2005) is presumably different from the two-dimensional kinematics of the DEM simulation by Staron & Hinch (2005), at least when a is large enough (e.g. $a > 0.7$). Due to this difference, the inertia in these three-dimensional cases gradually replaces the general shear failure to become the governing mechanism of the granular flow. Furthermore, the difference of material properties between the present SPH simulations and those experiments also contributed to this discrepancy.

3.6. CONCLUSIONS

This chapter presents a new SPH approach for simulation of granular materials without using the traditional artificial viscosity. The proposed approach adopted a stress/strain regularisation procedure based on the Moving Least Square approach in combination with a linear viscous damping force commonly used in dynamic simulations

of continua. It is employed for the simulations of granular column collapses and results compared with experimental and numerical data available in the literature. The results show that the proposed technique can both replace the artificial viscosity and give better predictions of the flow behaviour of granular materials. Compared to the traditional employment of the artificial viscosity in standard SPH simulations, the usage of the viscous damping requires the calibration of a single parameter for a given material. Furthermore, thanks to the regularisation technique, the short-length-scale-noise, which is normally observed in most SPH simulations using the standard SPH approximation scheme, is removed and smooth stress distribution is obtained even under large shear deformation. The predictions by the new SPH model show good agreement with experimental and numerical results. This recommends that the proposed technique could be considered as a powerful numerical framework to simulate the flow of granular materials.

REFERENCES

[1] Artoni, R., Santomaso, A. C., Gabrieli, F., Tono, D., & Cola, S.; "Collapse of quasi-two-dimensional wet granular columns", *Phys. Rev. E*, **87**, 032205 (2013)

[2] Balmforth, N. J., Kerswell, R. R.; "Granular collapse in two dimensions", *Journal of Fluid Mechanics*, **538**, 399-428 (2005)

[3] Belytschko, T., Krongauz, Y., Dolbow, J., & Gerlach, C.; "On the completeness of meshfree particle methods", *International Journal for Numerical Methods in Engineering*, **43**(5), 785-819 (1998)

[4] Blanc, T., Pastor M.; "A stabilized Fractional Step, Runge Kutta Taylor SPH algorithm for coupled problems in Geomechanics", *Computer Methods in Applied Mechanics and Engineering*, **221–222**, 41-53 (2012)

[5] Blanc, T, Pastor M.; "A stabilized Smoothed Particle Hydrodynamics, Taylor-Galerkin algorithm for soil dynamics problems", *Int. J. Numer. Anal. Meth. Geomech*, **37** (1), 1-30, (2013)

[6] Bui, H. H., Fukgawa R., Sako K.; "Smoothed particle hydrodynamics for soil mechanics", *Proceedings of the 6th European Conference on Numerical Methods in Geotechnical Engineering - Numerical Methods in Geotechnical Engineering*, pp. 278-281, (2006)

[7] Bui, H. H., Sako K. and Fukgawa R; "Numerical simulation of soil–water interaction using smoothed particle hydrodynamics (SPH) method", *J. of Terramechanics,* **44**(5), 339-346, (2007)

[8] Bui, H. H., Fukgawa R., Sako K., and Ohno S.; "Lagrangian mesh-free particle method (SPH) for large deformation and post-failure flows of geomaterial using elastic-plastic soil constitutive model", *Int. J. Numer. Anal. Meth. Geomech.,* **32**(12), 1537 –1570 (2008a)

[9] Bui, H. H., K. Sako, R. Fukagawa and J. C. Wells; "SPH-based numerical simulations for large deformation of geomaterial considering soil-structure interaction", *12th International Conference on Computer Methods and Advances in Geomechanics 2008,* Goa, India, 570–578 (2008b)

[10] Bui, H. H., K. Sako, R. Fukagawa and J. C. Wells; "Numerical Simulation of Granular Materials Based on Smoothed Particle Hydrodynamics (SPH)", *Powders and Grains, AIP Conf. Proc.* 1145, 575 (2009)

[11] Bui, H. H., K. Sako, R. Fukagawa and J. C. Wells; "Slope stability analysis and discontinuous slope failure simulation by elasto-plastic smoothed particle hydrodynamics (SPH)," *Géotechnique*, **61** (7), 565-574 (2011a)

[12] Bui, H. H., and Khoa H.D.V; "Bearing capacity bearing capacity of shallow foundation by smoothed particle hydrodynamics (SPH) analysis", *Proceedings of the 2nd International Symposium on Computational Geomechanics* (COMGEO II), pp.457-468 (2011b).

[13] Bui, H.H., R. Fukagawa; "An improved SPH method for saturated soils and its application to investigate the mechanisms of embankment failure: Case of hydrostatic pore-water pressure", *Int. J. Numer. Anal. Meth. Geomech.*, **37** (1), 31-50 (2013)

[14] Bui, H. H., J. Kodikara, A. Bouazza, A. Haque and P. G Ranjith; "A novel computational approached for large deformation and post-failure analyses of segmental retaining wall systems", *Int. J. Numer. Anal. Meth. Geomech.*, **38**(13), 1321-1340 (2014)

[15] Borja R.I. "Plasticity modelling and computation", Springer-Verlag Berlin Heidelberg (2013)

[16] Carter M. M., Arduino, P., Mackenzie-Helnwein, P., & Miller, G. R.; "Simulating granular column collapse using the Material Point Method", *Acta Geotechnica*, **10**(1), 101-116 (2014)

[17] Chauchat, J., & Médale, M.; "A three-dimensional numerical model for dense granular flows based on the μ (I) rheology", *Journal of Computational Physics*, **256**, 696-712 (2014)

[18] Chen, W.,Qiu, T.; "Numerical simulations for large deformation of granular materials using smoothed particle hydrodynamics method", *International Journal of Geomechanics*, **12**(2), 127-135 (2011)

[19] Cleary, P. W., M. L. Sawley; "DEM modelling of industrial granular flows: 3D case studies and the effect of particle shape on hopper discharge", *Applied Mathematical Modelling*, **26** (2), 89-111 (2002)

[20] Colagrossi, A., M. Landrini; "Numerical simulation of interfacial flows by smoothed particle hydrodynamics", *Journal of Computational Physics*, **191**, 448-475 (2003)

[21] Crosta, G.B., Imposimato, S., Roddeman, D.; "Numerical modeling of 2D granular step collapse on erodible and non-erodible surface", *Journal of Geophysical Research: Earth Surface*, **114**, F03020 (2009)

[22] Crosta, G. B., Imposimato, S., & Roddeman, D.; "Granular flows on erodible and non-erodible inclines", *Granular Matter*, **17**(5), 667-685 (2015)

[23] Dilts, A. G.; "Moving-least-squares-particle hydrodynamics Consistency and stability", *International Journal for Numerical Methods in Engineering*, **44** (8), 1115-1155 (1999)

[24] Dyka, C. T., P. W. Randles, R. P. Ingel; "Stress Points for Tension Instability in SPH", *International Journal for Numerical Methods in Engineering*, **40** (13), 2325-2341 (1997)

[25] Farin, M., Mangeney, A., & Roche, O.; „Fundamental changes of granular flow dynamics, deposition, and erosion processes at high slope angles: Insights from laboratory experiments", *Journal of Geophysical Research: Earth Surface*, **119**(3), 504-532 (2014)

[26] Forterre, Y., O. Pouliquen; "Flows of dense granular media", *Annu. Rev. Fluid Mech.*, **40**, 1–24 (2008)

[27] Gingold, R. A., and J. J. Monaghan; "Smoothed particle hydrodynamics: Theory and application to non-spherical stars", *Mon. Not. R. Astron. Soc.*, **181**(2), 375 – 389 (1977)

[28] Gingold, R. A., & Monaghan, J. J.; "Kernel estimates as a basis for general particle methods in hydrodynamics", *Journal of Computational Physics*, **46**(3), 429-453 (1982)

[29] Girolami L., Hergault V., Vinay G., and Wachs A.; "A three-dimensional discrete-grain model for the simulation of dam-break rectangular collapses: Comparison between numerical results and experiments", *Granular Matter* **14**(3) 381-392 (2012)

[30] Gray JP, Monaghan JJ, Swift RP.; "SPH elastic dynamics", *Computer Methods in Applied Mechanics and Engineering*, **190**:6641–6662. (2001)

[31] Guo, Y., J. S. Curtis; "Discrete Element Method Simulations for Complex Granular Flows", *Annual Review of Fluid Mechanics*, **47**, 21-46 (2014)

[32] Herrmann H. J., S. Luding; "Modeling granular media on the computer", *Continuum Mechanics and Thermodynamics*, **10**, 189-231 (1998)

[33] Hiraoka, N., A. Oya, H. H. Bui, P. Rajeev, R. Fukagawa; "Seismic slope failure modelling using the mesh-free SPH method", *Int. J. of GEOMATE*, **5** (1), 660-665 (2013)

[34] Holsapple, K. A.; "Modeling granular material flows: the angle of repose, fluidization and the cliff collapse problem", *Planetary and Space Science*, **82**, 11-26 (2013)

[35] Ionescu, I. R., Mangeney, A., Bouchut, F., & Roche, O.; "Viscoplastic modeling of granular column collapse with pressure-dependent rheology", *Journal of Non-Newtonian Fluid Mechanics*, **219**, 1-18 (2015)

[36] Johnson G.R.; "Artificial viscosity effects for SPH impact computations", *International Journal of Impact Engineering*, Volume **18**, Issue 5, Pages 477–488 (1996)

[37] Jop, P., Y. Forterre, O. Pouliquen; "A constitutive law for dense granular flows", *Nature*, **441**,727 (2006)

[38] Kermani, E., Qiu, T., & Li, T.; "Simulation of Collapse of Granular Columns Using the Discrete Element Method", *International Journal of Geomechanics*, 04015004 (2015)

[39] Kerswell, R.R.; "Dam break with coulomb friction: a model for granular slumping", *Phys. Fluids*, **17**, 057101 (2005)

[40] Krabbenhoft, K., Lyamin, A. V., Huang, J., & da Silva, M. V.; „Granular contact dynamics using mathematical programming methods", *Computers and Geotechnics*, **43**, 165-176 (2012)

[41] Kumar, K., Soga, K., Delenne, J. Y.; "Multi-scale modelling of granular avalanches", *AIP Conf. Proc* **1542**, 1250-1253 (2013).

[42] Lacaze, L., Phillips, J. C., & Kerswell, R. R.; "Planar collapse of a granular column: Experiments and discrete element simulations", *Physics of Fluids*, **20**(6), 063302 (2008).

[43] Lagree, P.Y., Staron, L., Popinet, S.; "The granular column collapse as a continuum: validity of a two-dimensional Navier-Stokes model with a μ(I)-rheology", *J. Fluid Mech.*, **686**, 378–408 (2011)

[44] Lajeunesse, E., Mangeney-Castelnau, A., & Vilotte, J. P.; "Spreading of a granular mass on a horizontal plane", *Physics of Fluids*, **16**(7), 2371-2381 (2004)

[45] Lajeunesse, E., J. B. Monnier, G. M. Homsy; "Granular slumping on a horizontal surface", *Physics of Fluids*, **17**, 1-15 (2005)

[46] Libersky, L. D., A. G. Petschek, T. C. Carney, J. R. Hipp, F. A. Allahady; "High Strain Lagrangian Hydrodynamics: A Three-Dimensional SPH Code for Dynamic Material Response", *J. Comp. Phys.*, **109** (1), 67-75 (1993)

[47] Liu, G. R., M. B. Liu; *Smoothed particle hydrodynamics: A meshfree particle method*, World Scientific, Singapore (2004)

[48] Lube, G., Huppert, H. E., Sparks, R. S. J., Hallworth, M. A.; "Axisymmetric collapses of granular columns", *Journal of Fluid Mechanics*, **508**, 175-199. (2004).

[49] Lube, G., H. E. Huppert, R. S. J. Sparks, A. Freundt; "Collapses of two-dimensional granular columns", *Phys. Rev. E*, **72**, 041301 (2005)

[50] Lube, G., Huppert, H. E., Sparks, R. S. J., & Freundt, A.; "Granular column collapses down rough, inclined channels", *Journal of Fluid Mechanics*, **675**, 347-368 (2011)

[51] Lucy L.; "A numerical approach to testing the fission hypothesis", *Astronomical Journal*, **82**:1013–1024. (1977)

[52] Mangeney-Castelnau, A., Bouchut, F., Vilotte, J. P., Lajeunesse, E., Aubertin, A., & Pirulli, M. ; "On the use of Saint Venant equations to simulate the spreading of a granular mass", *Journal of Geophysical Research: Solid Earth*, (1978–2012), 110(B9) (2005)

[53] Mangeney-Castelnau, A., Roche, O., Hungr, O., Mangold, N., Faccanoni, G., & Lucas, A.; "Erosion and mobility in granular collapse over sloping beds", *Journal of Geophysical Research: Earth Surface*, (2003–2012), 115(F3) (2010)

[54] MiDi, G. D. R.; "On dense granular flows", *The European Physical Journal* E14.4, 341-365. (2004)

[55] Minatti, L., & Paris, E.; "A SPH model for the simulation of free surface granular flows in a dense regime", *Applied Mathematical Modelling*, **39**(1), 363-382 (2015)

[56] Monaghan, J. J., & Gingold, R. A.; "Shock simulation by the particle method SPH", *Journal of computational physics*, **52**(2), 374-389.

[57] Monaghan, J. J. and J. C. Lattanzio; "A refined particle method for astrophysical problems", *Astron. Astrophys.*, **149** (1), 135-143 (1985)

[58] Monaghan, J.J.; "Smoothed Particle Hydrodynamics", *Annu. Rev. Astron. Astrophys.*, Vol. **30**, 543-574 (1992)

[59] Monaghan, J. J.; "Simulating free surface flows with SPH", J. *Comput. Phys.*, **110** (2), 399-406 (1994)

[60] Monaghan, J. J.; "Smoothed particle hydrodynamics and its diverse applications", *Annual Review of Fluid Mechanics*, **44**, 323-346 (2012)

[61] Moriguchi, S., Borja, R. I., Yashima, A., & Sawada, K.; "Estimating the impact force generated by granular flow on a rigid obstruction", *Acta Geotechnica*, **4**(1), 57-71 (2009)

[62] Morris, J., & Johnson, S.; "Dynamic simulations of geological materials using combined FEM/DEM/SPH analysis", *Geomechanics and Geoengineering: An International Journal*, **4**(1), 91-101 (2009)

[63] Nguyen, C. T., H. H. Bui, R. Fukagawa; "Two-dimensional numerical modelling of modular-block soil retaining walls collapse using meshfree method", *Int. J. of GEOMATE*, **5** (1), 647-652 (2013)

[64] Nguyen, C.T., Bui, H.H., Bui, Fukagawa R.; "Failure mechanism of 2D granular flows: Experiment", *J. Chem. Eng. Japan*, **48** (6), 395-402 (2015)

[65] Pastor, M., B. Haddad, G. Sorbino, S. Cuomo, V. Drempetic; "A depth-integrated, coupled SPH model for flow-like landslides and related phenomena", *Int. J. Numer. Anal. Meth. Geomech.*, **33** (2), 143-172 (2009)

[66] Pouliquen, O., C. Cassar, P. Jop, Y. Forterre, M. Nicolas; "Flow of dense granular material: towards simple constitutive laws", *J. Stat. Mech.*, P07020 (2006)

[67] Rabczuk T. and Eibl J.; "Simulation of high velocity concrete fragmentation using SPH/MLSPH", *International Journal for Numerical Methods in Engineering*, **56** (10), 1421-1444 (2003)

[68] Randles P. W., Libersky, L. D.; "Smoothed Particle Hydrodynamics: Some recent improvements and applications", *Computer Methods in Applied Mechanics and Engineering*, **139** (1), 375-408 (1996)

[69] Rondon, L., Pouliquen, O., & Aussillous, P.; "Granular collapse in a fluid: role of the initial volume fraction", *Physics of Fluids*, (1994-present), 23(7), 073301 (2011)

[70] Shao, S., & Lo, E. Y.; "Incompressible SPH method for simulating Newtonian and non-Newtonian flows with a free surface", *Advances in Water Resources*, **26**(7), 787-800 (2003)

[71] Sołowski, W. T., & Sloan, S. W.; "Evaluation of material point method for use in geotechnics", *International Journal for Numerical and Analytical Methods in Geomechanics*, **39**(7), 685-701 (2015)

[72] Staron, L., Hinch, E. J.; "Study of the collapse of granular columns using two-dimensional discrete-grain simulation", *Journal of Fluid Mechanics*, **545**, 1-27 (2005).

[73] Staron, L., Hinch, E. J.; "The spreading of a granular mass: role of grain properties and initial conditions", *Granular Matter*, **9**(3-4), 205-217 (2007).

[74] Thompson, E. L., & Huppert, H. E.; "Granular column collapses: further experimental results", *Journal of Fluid Mechanics*, **575**, 177-186 (2007)

[75] Utili, S., Zhao, T., and Houlsby, G. T.; "3D DEM investigation of granular column collapse: Evaluation of debris motion and its destructive power", *Engineering Geology*, **186**, 3-16 (2015)

[76] Verghese, S.J., Nguyen, C.T., Bui, H.H.; "Evaluation of plasticity-based soil constitutive models in simulation of braced excavation", *Int. J. of GEOMATE*, **5** (2), 672-677 (2013)

[77] Zhang, X., Krabbenhoft, K., Sheng, D.; "Particle finite element analysis of the granular column collapse problem", *Granular Matter*, **16**(4), 609-619. (2014)

[78] Zenit, R.; "Computer simulations of the collapse of a granular column", *Physics of Fluids*, **17**(3), 031703 (2005).

CHAPTER 4

RETAINING WALL SYSTEM: EXPERIMENTS AND NUMERICAL SOLUTION

4.1. INTRODUCTION

Modular-block retaining walls (MRW) have been used as an effective method to stabilize cuts and fills adjacent to highways, driver-ways, embankment, etc. Because they are flexible structures, modular-block retaining walls can tolerate movement and settlement without causing crack and damage, particularly under seismic loading conditions. Despite of its advantage, very few numerical studies of large deformation of the MRW systems were found in the literature. This is because it is very difficult to simulate large deformation and flexible behaviour of wall blocks (i.e. full rotational and translational motions) in the MRWs system using traditional continuum based numerical methods such as finite element method (FEM) which is suffered from grid distortions. The Discrete Element Method (DEM) proposed by Cundall & Strack (1979) which is an other popular numerical method in geotechnical applications may be applied to simulate dynamic behaviour of the modular-block retaining wall blocks in the MRW system. However, the DEM suffers from low accuracy in predicting soil behaviour due to the difficulty in selecting parameters for contact laws. In addition, the DEM cannot make use of advanced soil constitutive models which have been extensively developed in the literature. The discontinuous deformation analysis (DDA) method proposed by Shi G.H. (1988) has also been applied to geotechnical applications, but is mainly used for rock engineering, etc. In order to overcome the above limitations of traditional numerical methods, continuum based mesh-free methods such as the mesh-free Galerkin element method (EFG) (Belytschko et al., 1994), material point method (MPM) (Sulsky et al.,

1994), particle in cell method (PIC) (Harlow et al., 1964), etc., could be also applied to simulate large deformation of soil. However, these methods are quite time consuming and complicated to implement into a computer code as they consist of both interpolation points and the background mesh. On the other hand, the smoothed particle hydrodynamics (SPH) method, originally proposed by Gingold and Monaghan (1977), has been recently developed for solving large deformation and post-failure behavior of geomaterials (Bui et al., 2007, 2008, 2011a, 2011b; Blanc and Pastor, 2013; Pastor et al., 2009) and represents a powerful way to understand and quantify the failure mechanisms of soil in such challenging problems.

In this chapter, taking into consideration the unique advantage of the SPH method, it is further extended to simulate large deformation and post-failure of the MRW systems. Herein, soil is modelled using the elasto-plastic Drucker-Prager constitutive model (Bui et al., 2008) and wall blocks are assumed rigidity with complete degree of rotation. A linear contact model which is similar to the penalty contact law is proposed and is implemented in the SPH code to simulate interaction between soil and wall blocks, and between wall blocks in the MRW systems. The developed model is then applied to simulate large deformation of the MRW system and comparing to a two-dimensional experiment. Results showed good agreement with the experiment, suggesting that the proposed method is a promising approach for further design of modular-block retaining wall systems subjected to earthquake.

4.2. EXPERIMENTS

4.2.1. Materials

In thoses experiments, I use materials including Alumininum Rods and Aluminium Blocks (Modular-block). Each block is named with a specific ID from 1 to 7. The parameters of 7 aluminium blocks used in our experiments showed in Table 4.1. In the Table 4.1, papameter M is mass of block, L is length dimension of block; W is width of block and H is height of block.

In these experiments I use the same material in chapter 2 with aluminum rods 5 cm in length and with diameters of 1.6 mm and 3.0 mm (Figure 4.1) mixed at a ratio of 3:2 in weight, were used as the model ground to simulate the true 2D granular flow experiments (Nakai, 2012). The total unit weight of the mixed material is 20.4 kN/m^3. Parameters of this soil model showed in Table 4.2.

Table 4.1: *Parameters of Modular-blocks*

ID of Block	M (g)	L (mm)	W(mm)	H(mm)
1	104.028	49.78	31.86	25.01
2	104.054	49.82	31.86	25.02
3	104.016	49.81	31.84	25.02
4	104.053	49.79	31.86	25.01
5	104.046	49.82	31.86	25.02
6	104.047	49.79	31.87	25.02
7	104.047	49.80	31.87	25.02
Average	104.041	49.80	31.86	25.02
≃	104	50	32	25

Table 4.2: *Parameters of soil model*

Name	Value	Unit
Gravity Density (ρ)	20.4	kN/m^3
Friction angle (ϕ)	21.9	deg
Young's modulus (E)	5.84	MPa
Poisson's ratio (ν)	0.3	–
Dilation angle (ψ)	0	deg
Cohesion (c)	0	kPa

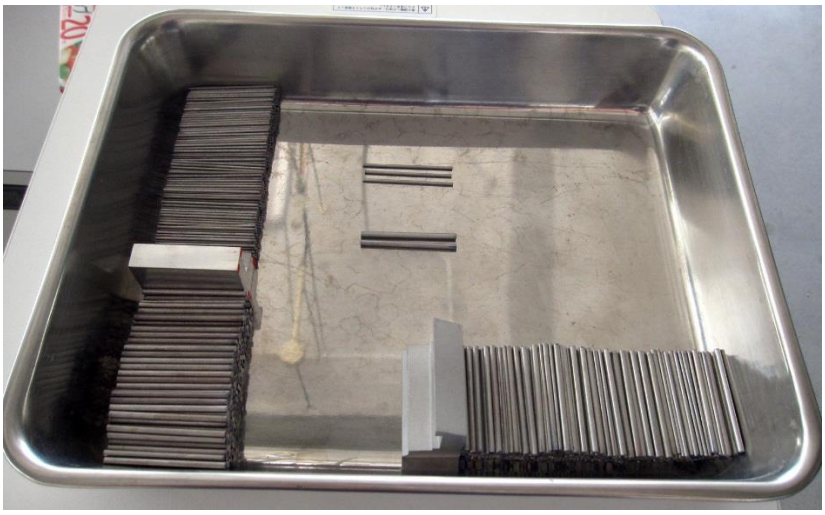

Figure 4.1: *Aluminum rods*

4.2.2. Measuring Friction Coefficients

In addition to the retaining wall collapse experiments, sliding tests were also conducted to measure friction coefficients between the wall blocks, between the soil model and the wall block, and between the block and the bottom solid wall. Outline of these tests are shown in Figures 4.2, 4.3 and 4.4.

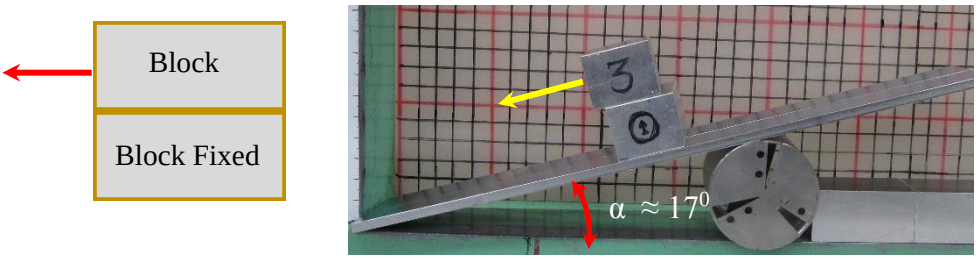

Figure 4.2: *Measuring friction coefficience between retaining wall blocks ($\mu \sim 0.31$)*

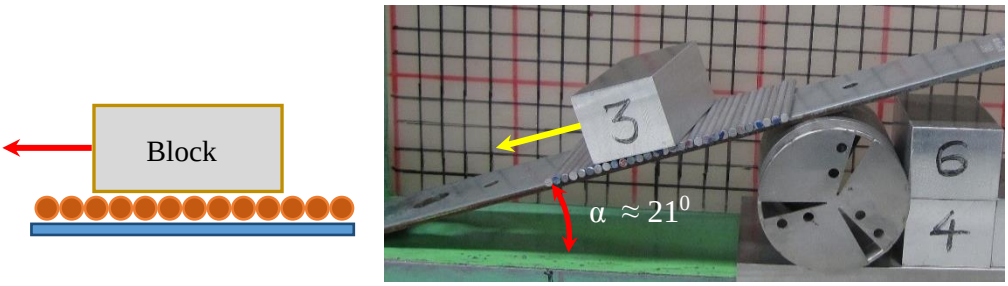

Figure 4.3: *Measuring friction coefficience between the retaining wall block and model ground ($\mu \sim 0.38$)*

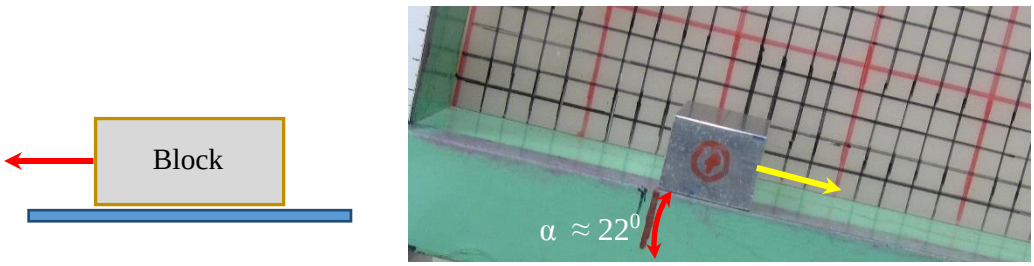

Figure 4.4: *Measuring friction coefficience between wall block and the bottom wall boundary ($\mu \sim 0.40$)*

Based on these experiments, it was found that the friction (μ) between retaining wall blocks is μ ~ 0.31, between the retaining wall block and model ground is μ ~ 0.38, and between wall block and the bottom wall boundary is μ ~ 0.40.

4.2.3. Measuring Displacement of Blocks

4.2.3.1. Experimental Model

This experimental setup is shown in Figure 4.5. The soil box is fixed during conducted time. The overlapping value (Δx) may be changed with each series of experiments.

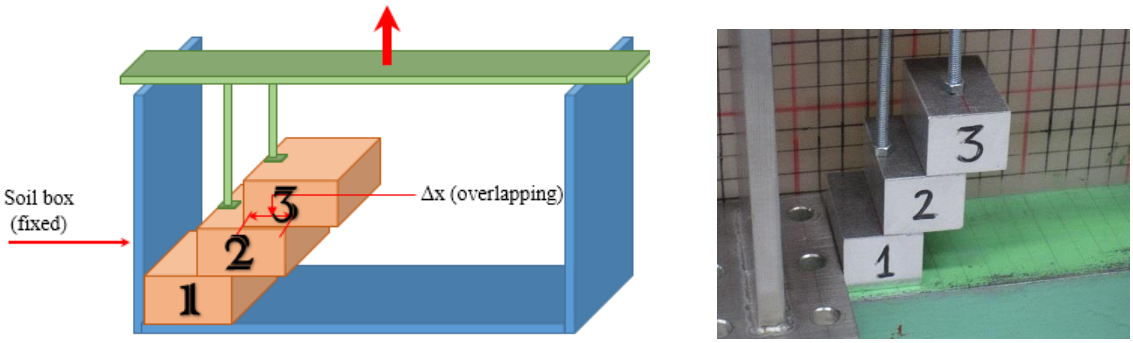

Figure 4.5: *The experimental setup*

4.2.3.2. The First Series of Experiments

The experiments in this series is conducted with the overlapping Δx = 15.64 mm (a haft of block's wide). This experiments is repeated six times. The experimental results shown the position and rotation angle of the blocks after moving on Figure 4.6, and position of blocks (nearest left points and farthest right points) on Table 4.3.

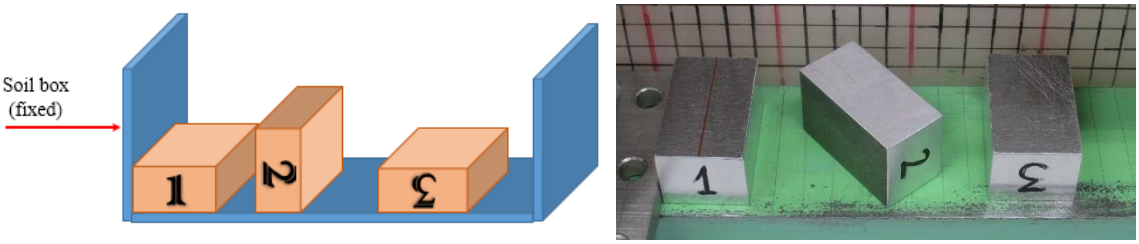

Figure 4.6: *Position and rotation angle of the blocks after moving*

Table 4.3: *Position of blocks (left points and right points) after moving*

Number of Repeat		1	2	3	4	5	6	Average
Left point	Block1	0,00	0,00	0,00	0,00	0,00	0,00	0,00
	Block2	45,20	51,97	53,08	41,16	39,17	32,79	43,90
	Block3	94,96	94,89	98,55	81,36	99,95	82,08	91,97
Right point	Block1	31,00	31,00	31,00	31,00	31,00	31,00	31,00
	Block2	77,58	83,72	82,83	78,98	75,84	71,51	78,41
	Block3	140,89	145,81	131,92	135,56	136,11	122,14	135,41

4.2.3.3. The Second Series of Experiments

The experiments in this series are conducted with the overlapping Δx = 10 mm. As the same as the first series, this experiment is repeated six times. The experimental results show the position and rotation angle of the blocks after moving on Figure 4.7, and position of blocks (nearest left points and farthest right points) on Table 4.4.

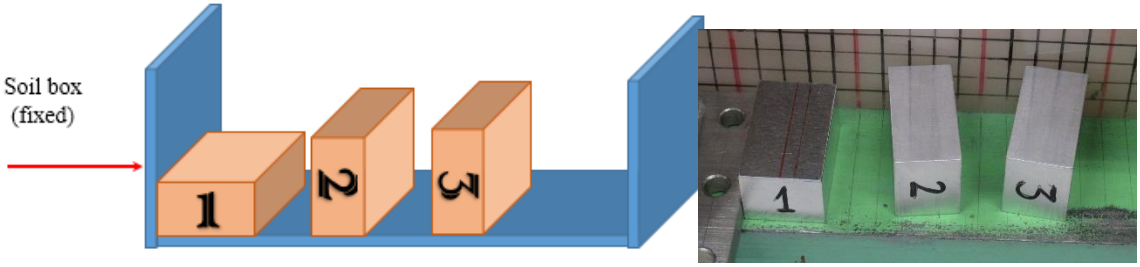

Figure 4.7: *Position and rotation angle of the blocks after moving*

Table 4.4: *Position of blocks (left points and right points) after moving*

Number of Repeat		1	2	3	4	5	6	Average
Left point	Block1	0,00	0,00	0,00	0,00	0,00	0,00	0,00
	Block2	48,22	50,00	46,91	47,29	48,27	53,39	49,01
	Block3	114,32	114,07	111,03	104,93	116,32	106,21	111,15
Right point	Block1	31,00	31,00	31,00	31,00	31,00	31,00	31,00
	Block2	95,15	103,14	98,49	99,15	99,18	103,67	99,80
	Block3	151,40	158,02	146,75	152,16	147,08	153,62	151,51

4.2.3.4. The Third Series of Experiments

This series of experiments are conducted with the overlapping Δx = 15.64 mm (the same the first series). But in this case, the distance between the block ID = 1 with left wall was added in the model setup. This experiment is also repeated six times. The experimental results show the position and rotation angle of the blocks after moving on Figure 4.8, and position of blocks (left points and right points) on Table 4.5.

Table 4.5: *Position of blocks (left points and right points) after moving*

Number of Repeat		1	2	3	4	5	6	Average
Left point	Block1	50,00	50,00	50,00	50,00	50,00	50,00	50,00
	Block2	92,48	98,86	98,91	99,06	104,42	97,62	98,56
	Block3	166,18	161,03	161,01	163,27	168,03	163,42	163,82
Right point	Block1	81,00	81,00	81,00	81,00	81,00	81,00	81,00
	Block2	142,67	138,44	145,87	143,14	130,01	142,28	140,40
	Block3	197,43	197,85	199,42	208,11	197,28	202,14	200,37

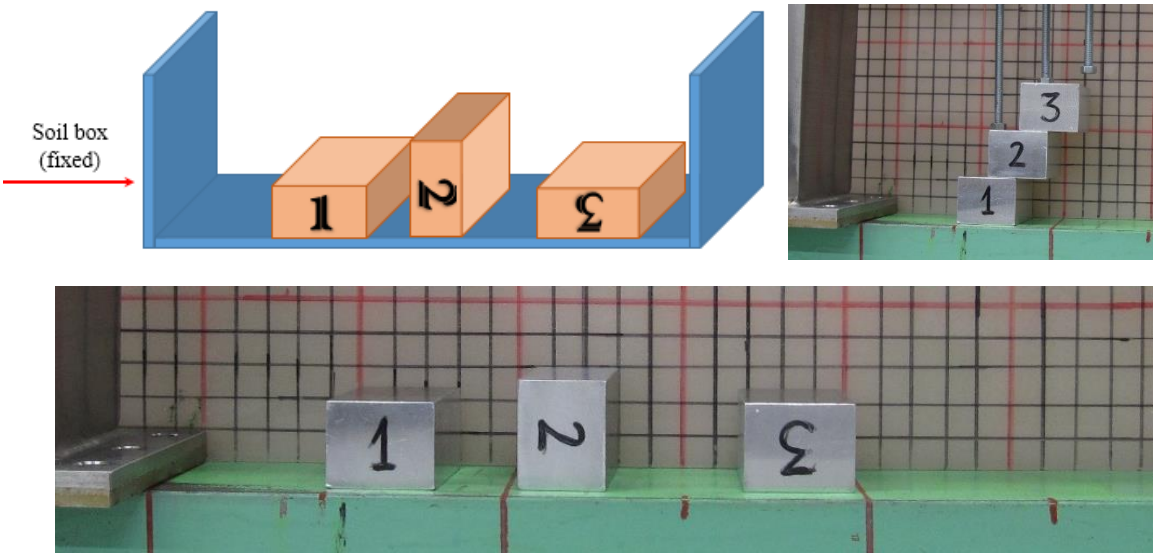

Figure 4.8: *Position and rotation angle of the blocks after moving*

4.2.4. Post-Failure Behavior of Modular-block Retaining Wall System

A series of two-dimensional modular-block retaining wall system collapses were conducted to investigate the failure mechanism of the MRWs and to verify the proposed numerical framework in next sections. Figure 4.9 outlined the initial setting condition of the MRWs which consists of six rectangular wall blocks. The size of the model ground is 15cm in height and 50cm in width at the base. Soil was modelled using aluminum rods of 1.6mm and 3mm in diameters, 50mm in length, and mixed with the ratio of 3:2 in weights. The aluminium wall block is 3.2cm in width, 2.5cm in height, and 5cm in length, which is also manufactured from aluminum. In the experiment, the MRWs was constructed by successively placing one wall block on the top of the other with many value of overlapping (1.2cm, 1.4cm, 1.6cm, 1.8cm, 2.0cm, 2.2cm, 2.4cm, 2.6cm, 2.8cm), followed by filling the model ground at each layer. The MRWs was stabilized by a stopper stand as show in Figure 4.9 and Figure 4.10. To visualize the failure pattern of the model ground after collapse, square grids (2.5×2.5cm) were drawn on the soil specimen. The experiments were initiated by quickly removing the stopper stand and digital photos were taken to record the failure process as well as the final configuration of the MRWs after collapse.

Other series of this experiment were conducted on soft ground surface. The setup for this experiment is show in Figure 4.11.

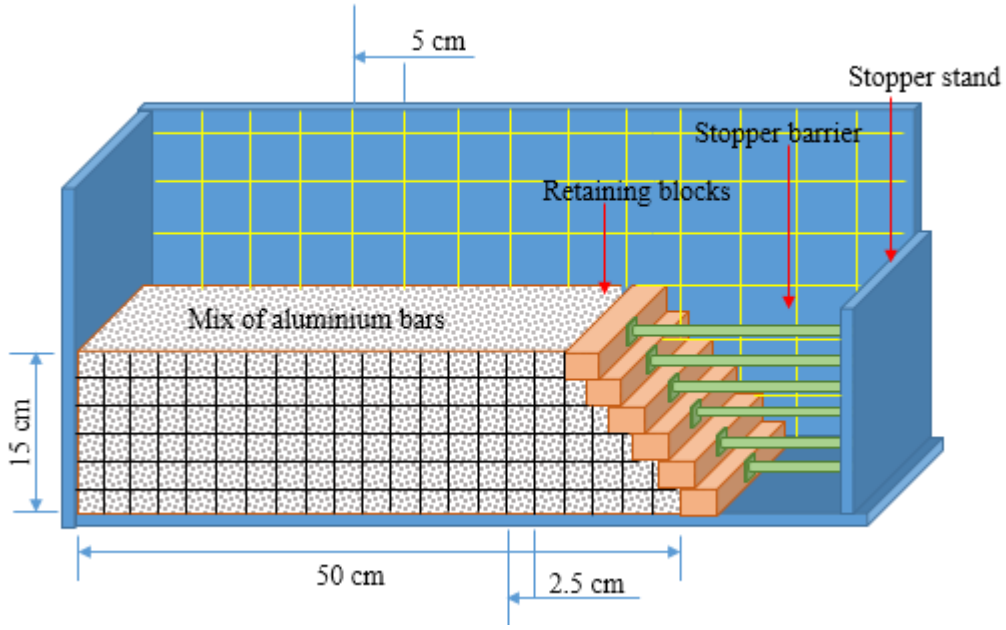

Figure 4.9: *Experimental setup designed*

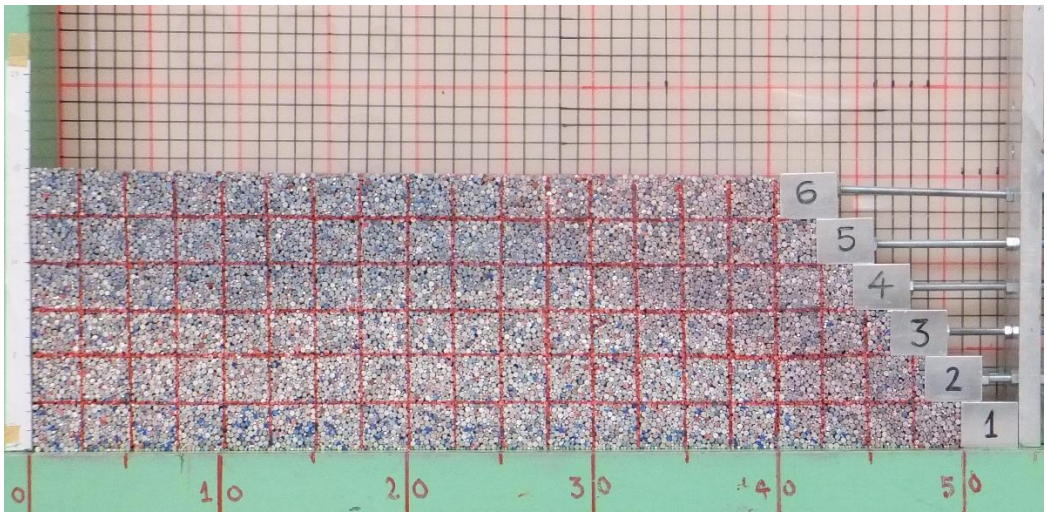

Figure 4.10: *Initial setup of model ground and the retaining wall blocks system*

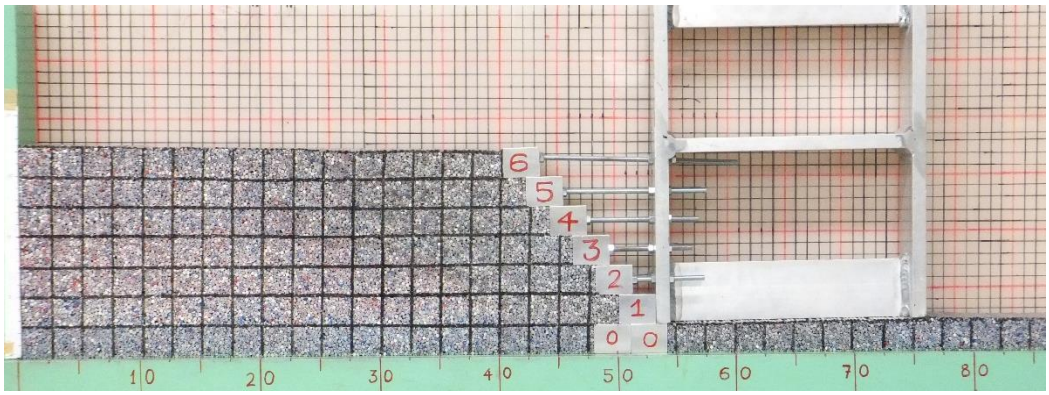

Figure 4.11: *Initial setup of experimental model with soft ground surface*

A series of experiments were conducted starting from one block and then gradually increasing the number of blocks in the BRWs until the retaining wall is collapsed. The experimental evidences consistently showed that the MRW system will collapse when reaching 4 blocks height (with value of overlapping is 1.2cm). Accordingly, a numerical model consisting of six retaining wall blocks and overlapping is 1.2cm will be conducted in the next section to verify the proposed numerical framework. A total of six experiments were conducted to verify the failure mechanism of the MRWs and the final run-out distance of each block in the MRWs. In all experiments, the failure mechanism of the MRW systems was more and less the same as shown in Figure 4.12. The positions of blocks after collapse shown in Table 4.6. Figure 4.13 shows failure zone after the crash downs of box-shape retaining wall

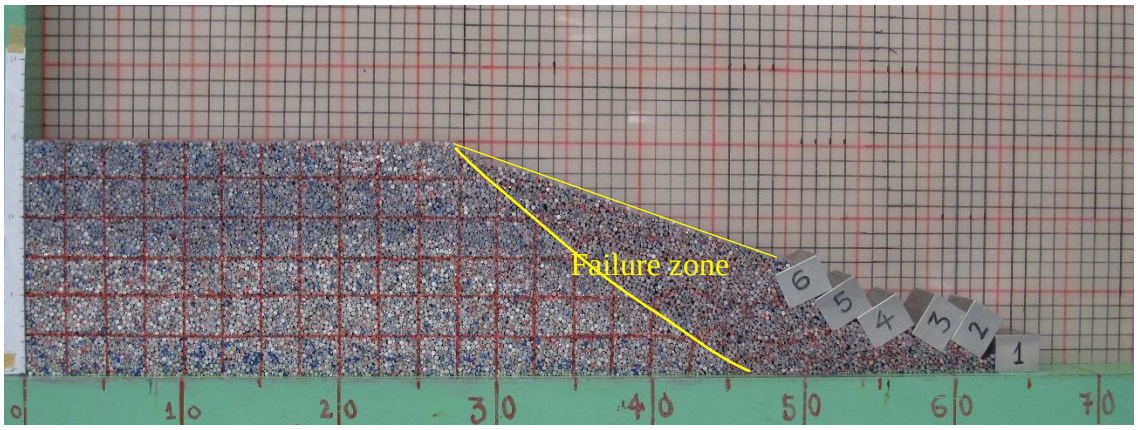

Figure 4.12: *Typical configurations of the MRW system observed in the experiment after collapse*

Table 4.6: *Positions of blocks (left points and right points)*

Number of Repeat		1	2	3	4	5	6	Average
Left point	Block1	64,1	61,0	64,4	65,9	66,9	63,0	64,2
	Block2	60,7	58,4	61,3	62,7	63,9	60,1	61,2
	Block3	57,4	56,2	57,8	59,1	60,8	57,2	58,1
	Block4	53,7	53,1	54,7	55,2	56,0	53,8	54,4
	Block5	51,2	49,7	51,0	51,3	53,0	50,8	51,2
	Block6	47,8	47,3	48,1	49,5	50,0	48,0	48,5
Right point	Block1	67,2	64,1	67,5	69,0	70,0	66,1	67,3
	Block2	64,6	62,3	64,6	66,0	67,1	63,6	64,7
	Block3	61,5	59,7	61,7	63,0	64,0	61,0	61,8
	Block4	57,7	56,8	58,2	59,3	60,0	57,5	58,3
	Block5	55,1	53,6	54,9	55,4	56,8	54,8	55,1
	Block6	52,4	50,4	53,7	52,6	54,0	52,7	52,6

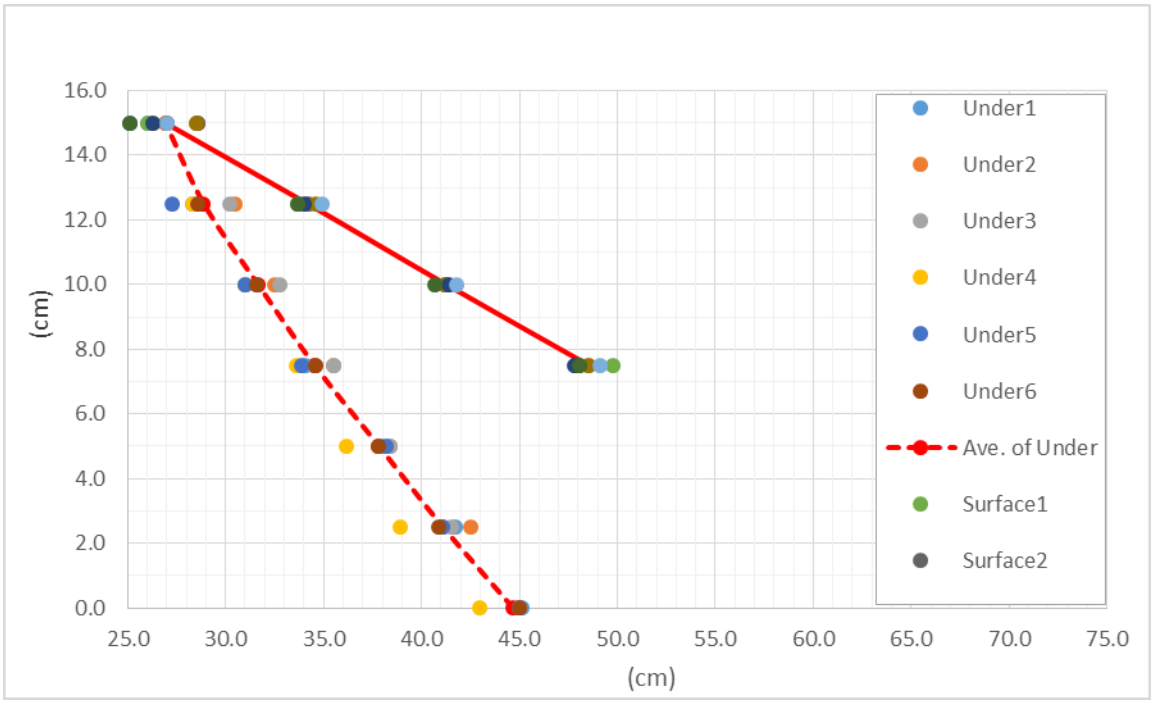

Figure 4.13: *Failure zone after crash downs of box-shape retaining wall*

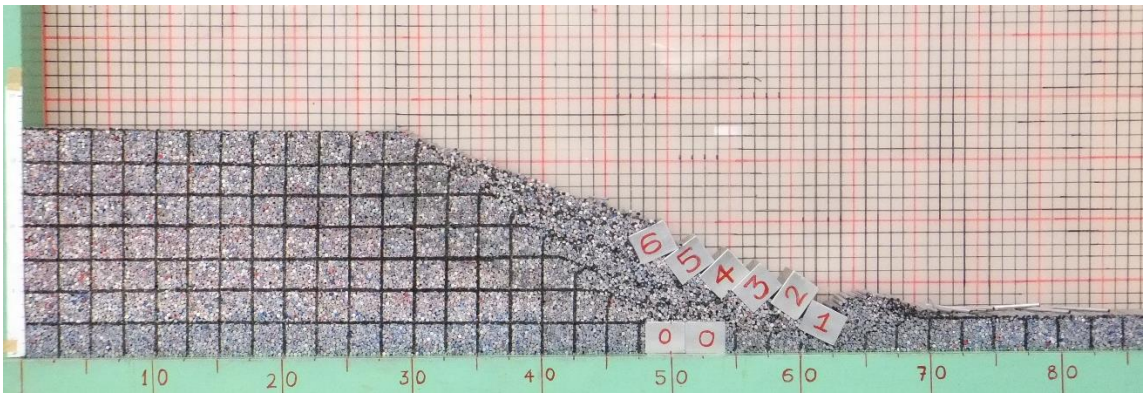

Figure 4.14: *Typical configurations of the MRW system observed in the experiment after collapse with soft ground surface*

The result of experiment with soft ground surface after collapse is shown in Figure 4.14

4.2.5. Analysis of the Failure Mechanism of MRW System

A series of experiments were performed using 4 blocks height at different initial of overlapping value (1.2cm, 1.4cm, 1.6cn, 1.8cm, 2.0cm, 2.2cm, 2.4cm, 2.6cm, and 2.8cm). Accordingly, 9 experiments were conducted in total. Each of the experiments was repeated at least twice, with some repeated up to six times. All the experiments were recorded by high speed camera.

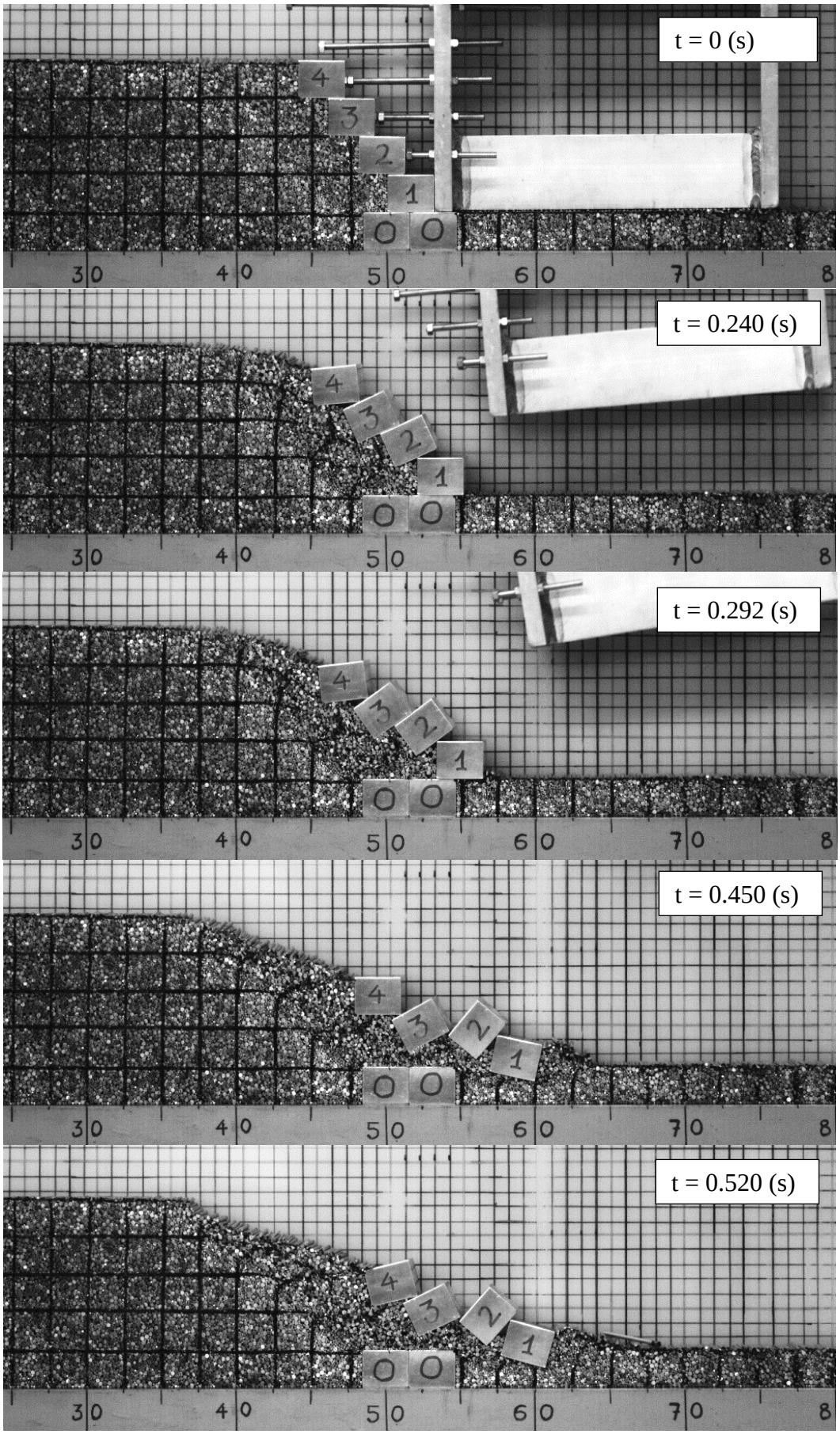

Figure 4.15: *Post-failure behavior of modular-block retaining wall system.* ***Case 1***

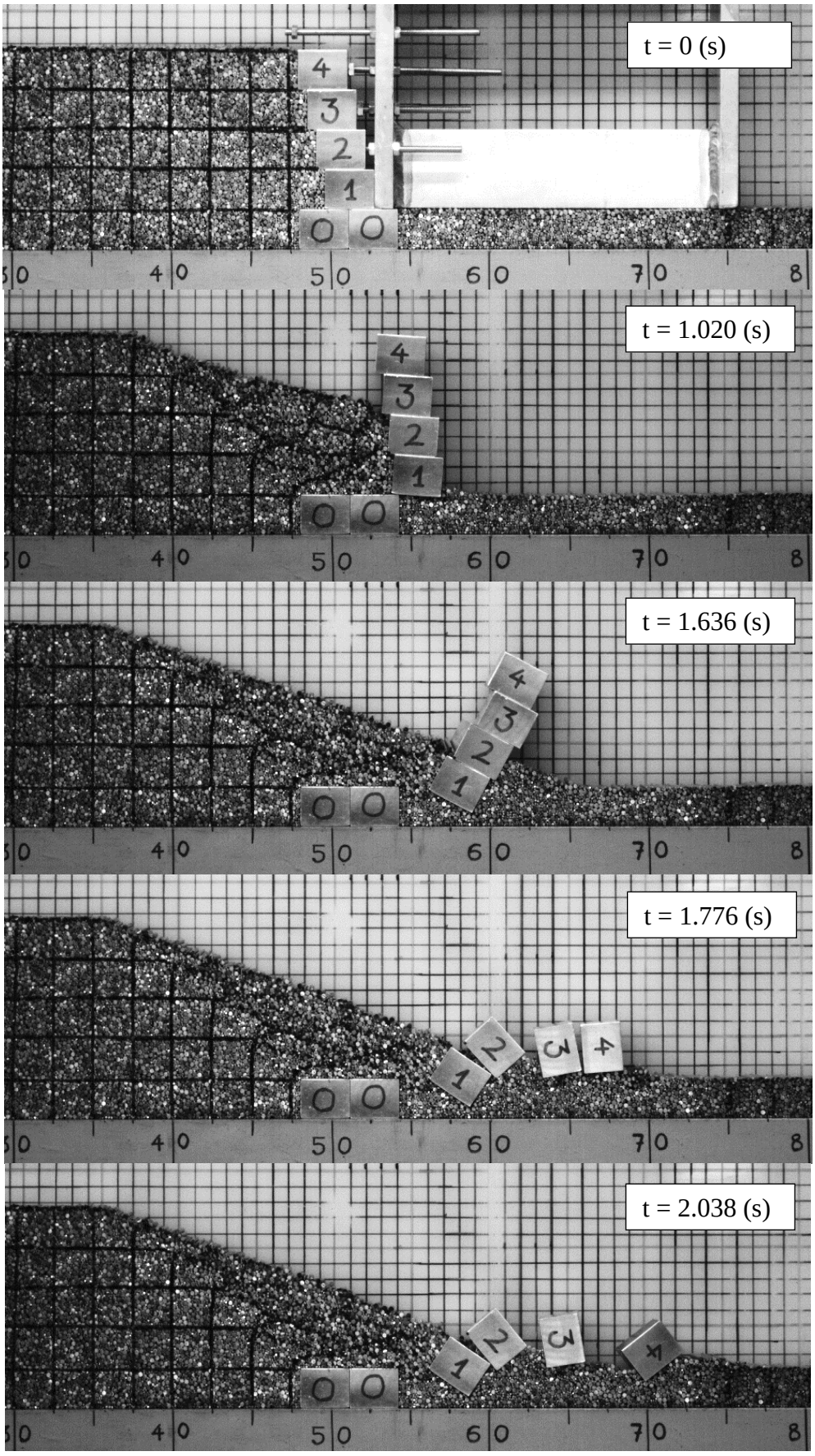

Figure 4.16: *Post-failure behavior of modular-block retaining wall system.* ***Case 2***

The experimental results show that, there are three case of post-failure behavior of modular-block retaining wall system. **Case 1:** shown on Figure 4.15 with overlappping values are 1.2 (cm), 1.4 (cm) and 1.6 (cm); **Case 2:** shown on Figure 4.16 with overlappping values are 2.4 (cm), 2.6 (cm) and 2.8 (cm); **Case 3:** shown on Figure 4.17 with overlappping values are 1.8 (cm), 2.0 (cm) and 2.2 (cm). In this case the retaining wall systems are not destroyed;

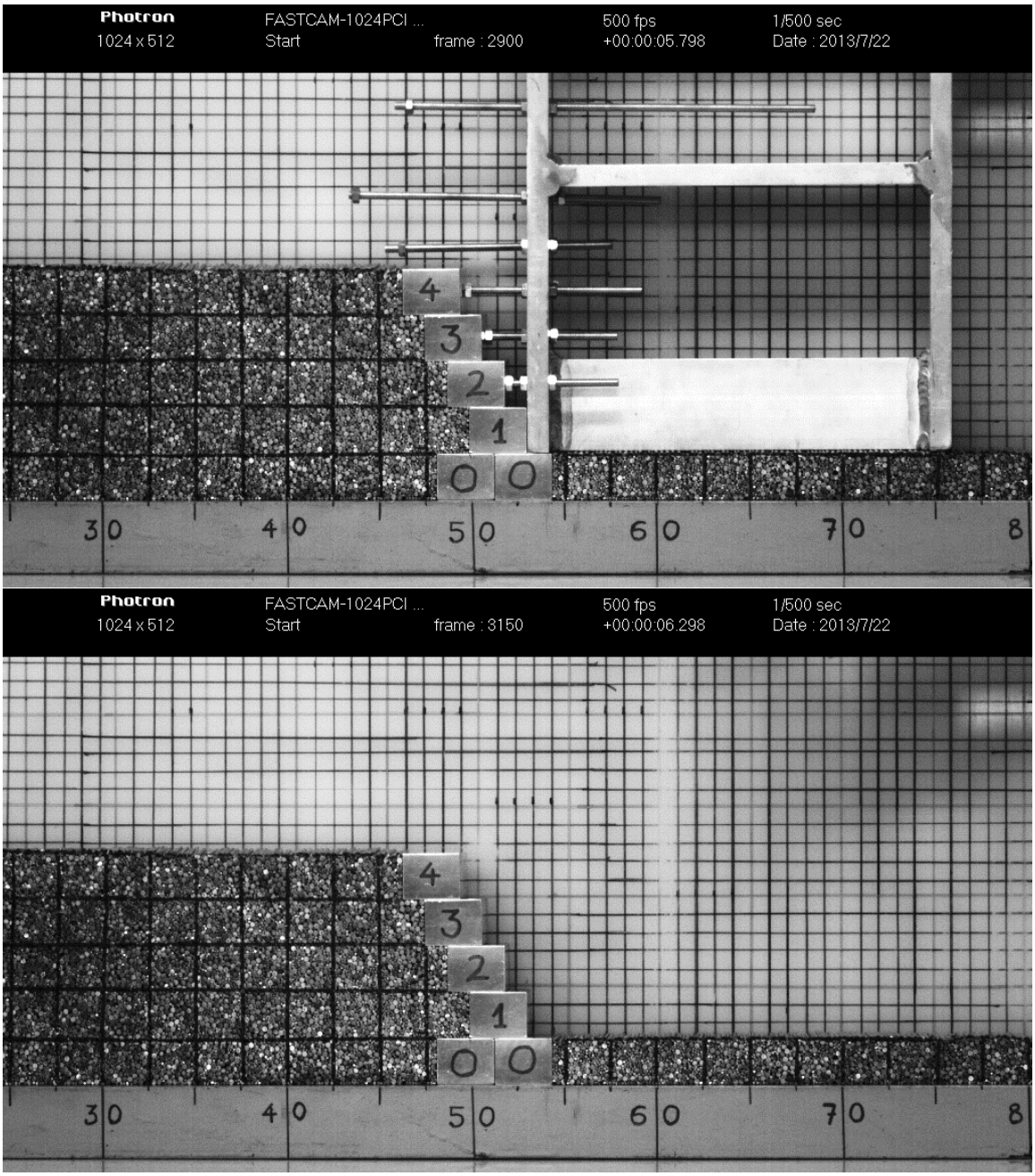

Figure 4.17: *Post-failure behavior of modular-block retaining wall system.* ***Case 3***

4.3. SIMULATION APPROACHES

4.3.1. Simulation of Soil in SPH Framework

The SPH mesh-free particle method was presented in Section 3.2 of this thesis. In the SPH method, motion of a continuum is modeled using a set of moving particles (interpolation points); each assigned a constant mass and "carries" field variables at the corresponding location. The continuous fields and their spatial derivatives are taken to be interpolated from the surrounding particles by a weighted summation, in which the weights diminish with distance according to an assumed kernel function. Details of the interpolation procedure and its application to soil can be found in Bui et al. (2008). The motion of a continuum can be described through the following equation,

$$\rho \frac{d\mathrm{v}}{dt} = \nabla \cdot \sigma + \rho \mathrm{g} + \mathrm{f}_{ext} \tag{4.1}$$

where v is the velocity; ρ is the density; σ is the total stress tensor, where negative is assumed for compression; g is the acceleration due to gravity; and f_{ext} is the additional external force(s). The total stress tensor of soil is normally composed of the effective stress (σ') and the pore-water pressure (p_w), and follows Terzaghi's concept of effective stress. Because the pore-water pressure is not considered, the total stress tensor and the effective stress are identical throughout this paper, and can be computed using a constitutive model.

In the SPH framework, Equation (4.1) is often discretized using the following form (Bui et al., 2008; Blanc et al., 2013),

$$\frac{dv_a^\alpha}{dt} = \sum_{b=1}^{N} m_b \left(\frac{\sigma_a^{\alpha\beta}}{\rho_a^2} + \frac{\sigma_b^{\alpha\beta}}{\rho_b^2} + C_{ab}^{\alpha\beta} \right) \nabla_a^\beta W_{ab} + g_a^\alpha + f_{ext\to a}^\alpha \tag{4.2}$$

where α and β denote Cartesian components x, y, z with the Einstein convention applied to repeated indices; a is the particle under consideration; ρ_a and ρ_b are the densities of particles a and b respectively; N is the number of "neighbouring particles", i.e. those in the support domain of particle a; m_b is the mass of particle b; C is the stabilization term (Bui et al., 2011b); W is the smoothing kernel function which is taken to be the cubic

Spline function (Monaghan , 1985, 2003); and $f_{ext \to a}$ is the unit external force acting on particle *a*.

The stress tensor of soil particles in Equation (4.2) can be computed using any soil constitutive model developed in the literature. For the purpose of soil-structure interaction, the Drucker-Prager model has been chosen with non-associated flow rule, which was implemented in the SPH framework by Bui et al. (2008) and shown to be a useful soil model for simulating large deformation and post-failure behaviour of aluminum rods used in the current paper as model ground. The stress-strain relation of this soil model is driven from the assumption of additive decomposition of the total strain rate tensor,

$$\dot{\varepsilon} = \dot{\varepsilon}^{e} + \dot{\varepsilon}^{p} \tag{4.3}$$

where *a* raised dot denotes the time derivative; $\dot{\varepsilon}$ is the total strain rate tensor; $\dot{\varepsilon}^{e}$ is its elastic component; and $\dot{\varepsilon}^{p}$ is its plastic component. The elastic component is computed using the well-known Hooke's law; while the plastic component can be calculated using the plastic flow rule (Bui et al., 2008),

$$\dot{\sigma} = \mathrm{D}\dot{\varepsilon}^{\mathrm{e}} \tag{4.4}$$

$$\dot{\varepsilon}^{p} = \dot{\lambda}\frac{\partial g_{p}}{\partial \sigma} \tag{4.5}$$

where **D** is the elastic stiffness matrix, $\dot{\lambda}$ is the rate of change of plastic multiplier (see Section 3.3), and g_p is the plastic potential function.

According to the plasticity theory, the plastic deformation occurs only if the stress state reaches the yield surface. Therefore, the plastic deformation will occur only if the following yield criterion is satisfied,

$$f = \alpha_{\phi} I_1 + \sqrt{J_2} - k_c = 0 \tag{4.6}$$

where I_1 and J_2 are the first and second invariants of the stress tensor; and α_ϕ and k_c are Drucker-Prager constants that are calculated from the Coulomb material constants c (cohesion) and ϕ (internal friction). In the plane strain, the Drucker-Prager constants are computed by,

$$\alpha_\phi = \frac{\tan\varphi}{\sqrt{9+12\tan^2\varphi}} \tag{4.7}$$

$$k_c = \frac{3c}{\sqrt{9+12\tan^2\phi}} \tag{4.8}$$

The non-associated plastic flow rule specifies the plastic potential function by (Bui et al., 2011a, 2011b),

$$g_p = \alpha_\psi I_1 + \sqrt{J_2} - \text{constant} \tag{4.9}$$

where α_ψ is a dilatancy factor that can be related to the dilatancy angle ψ in a fashion similar to that between α_ϕ and friction angle ϕ.

Substituting Equation (4.9) into Equation (4.5) in association with the consistency condition, that is the stress state must be always located on the yield surface f during the plastic loading, the stress-strain relation of the current soil model can be written as (Bui et al., 2011b),

$$\begin{aligned}\frac{d\sigma_a^{\alpha\beta}}{dt} &= 2G_a\dot{e}_a^{\alpha\beta} + K_a\dot{\varepsilon}_a^{\gamma\gamma}\delta_a^{\alpha\beta} \\ &\quad - \dot{\lambda}_a\left[3K_a\alpha_{\psi a}\delta^{\alpha\beta} + (G_a/\sqrt{J_{2a}})s_a^{\alpha\beta}\right]\end{aligned} \tag{4.10}$$

where $e^{\alpha\beta}$ is the deviatoric strain-rate tensor; $s^{\alpha\beta}$ is the deviatoric shear stress tensor; and $\dot{\lambda}$ is the rate of change of plastic multiplier of particle a (Bui et al., 2011b),

$$\dot{\lambda}_a = \frac{3\alpha_{\phi a}K_a\dot{\varepsilon}_a^{\gamma\gamma} + (G_a/\sqrt{J_{2a}})s_a^{\alpha\beta}\dot{\varepsilon}_a^{\alpha\beta}}{9\alpha_{\phi a}K_a\alpha_{\psi a} + G_a} \tag{4.11}$$

where the strain-rate tensor is computed by

$$\dot{\varepsilon}_a^{\alpha\beta} = \frac{1}{2}\left(\nabla^\beta \dot{u}^\alpha + \nabla^\alpha \dot{u}^\beta\right)_a \tag{4.12}$$

When considering a large deformation problem, a stress rate that is invariant with respect to rigid-body rotation must be employed for the constitutive relations. In the current study, the Jaumann stress rate is adopted:

$$\hat{\dot{\sigma}}_a^{\alpha\beta} = \dot{\sigma}_a^{\alpha\beta} - \sigma_a^{\alpha\gamma}\dot{\omega}_a^{\beta\gamma} - \sigma_a^{\gamma\beta}\dot{\omega}_a^{\alpha\gamma} \tag{4.13}$$

where $\dot{\omega}$ is the spin-rate tensor computed by

$$\dot{\omega}_a^{\alpha\beta} = \frac{1}{2}\left(\nabla^\beta \dot{u}^\alpha - \nabla^\alpha \dot{u}^\beta\right)_a \tag{4.14}$$

As a result, the final form of the stress-strain relationship for the current soil model is,

$$\begin{aligned}\frac{d\sigma_a^{\alpha\beta}}{dt} &= \sigma_a^{\alpha\gamma}\dot{\omega}_a^{\beta\gamma} + \sigma_a^{\gamma\beta}\dot{\omega}_a^{\alpha\gamma} + 2G_a\dot{e}_a^{\alpha\beta} \\ &+ K_a\dot{\varepsilon}_a^{\gamma\gamma}\delta_a^{\alpha\beta} - \dot{\lambda}_a 3K_a\alpha_{\psi a}\delta^{\alpha\beta} \\ &+ \dot{\lambda}_a(G/\sqrt{J_2})_a s_a^{\alpha\beta}\end{aligned} \tag{4.15}$$

Validation of the elasto-plastic Drucker-Prager soil model with SPH has been extensively documented in the literature (Bui et al., 2007, 2008, 2011a, 2011b), and readers can refer to these references for further details on the validation process.

4.3.2. Motion of Rigid Wall Blocks

The retaining wall system consists of individual rigid wall blocks, each of which is assumed to be a rigid body, has full degrees of freedom and moves in accordance with the Newton's second law. In the computation, the rigid wall block is represented by a set of boundary particles placed uniformly around the boundary. These particles interact with soil particles as well as with particles which belong to different blocks by a contact force model. The technique of replacing moving boundaries by particles was originally

proposed by Monaghan et al. (2003) to simulate a floating body in water. This technique is adopted in this study to simulate soil-structure interaction with a further improvement for simulations of multiple contacts among rigid blocks and blocks and soil. Details of the motion of the rigid wall blocks are described below.

An arbitrary motion of a rigid body can be represented as a superposition of translational motion in which all points of the body, including the centre of mass, move with the same speed along parallel trajectories, and rotation around the centre of mass. Accordingly, the motion of a rigid wall block in the MRW system can be determined by specifying the translational motion of the centre of mass and the rotational motion about its mass central. The equation of motion of the central mass is given as follows (Monaghan et al., 2003),

$$M\frac{d\mathrm{V}}{dt}=\mathrm{F} \tag{4.16}$$

where M is the central mass, V is the velocity vector of the central mass, F is total force vector acting on the body.

The equation of rotation about the central mass is,

$$I\frac{d\Omega}{dt}=\mathrm{T} \tag{4.17}$$

where I is the inertial moment, Ω is the angular velocity which is perpendicular to the plane of the motion, and T is the total torque about the central mass.

In the computation, the rectangular block is represented by the set of boundary particles that are equi-spaced around the boundary. Denoting the force vector acting on each boundary particle i located on the moving block is f_i, Equation (4.16) and Equation (4.17) can be rewritten, respectively, as follows,

$$M\frac{d\mathrm{V}}{dt}=\sum_i \mathrm{f}_i \tag{4.18}$$

$$I\frac{d\Omega}{dt} = \sum_k (\mathrm{r}_i - \mathrm{R}) \times \mathrm{f}_i \tag{4.19}$$

where r_i and R are vector coordinates of boundary particle and central mass, respectively. The rigid body boundary particles move as a part of the rigid body, thus the change on position of boundary particle i is given by,

$$\frac{d\mathrm{r}_i}{dt} = \mathrm{V} + \Omega \times (\mathrm{r}_i - \mathrm{R}) \tag{4.20}$$

The force f_i acting on a boundary particle on the rigid body is due to the surrounding soil particles or boundary particles that belong to different rigid bodies. This force can be calculated using any suitable contact model.

4.3.3. Contact Force Model

The contact force model developed in this study is based on the concept of using a spring-damper system to simulate interaction between two solid objects. The method is similar to that used in the Discrete Element Method, originally proposed by Cundall & Strack (1979) to simulate granular materials; however, it will be the first time this approach is adopted in the SPH framework to simulate soil-structure interaction. In the model, a force-displacement law is calculated by allowing two rigid objects to overlap each other. Linear contact law is assumed for force-displacement relationships, although any other constitutive relations such as Hertz & Mindlin contact theories (Tusji et al.1992; Bui et al. 2009) can be applied. The outline of the proposed algorithm is shown in Figure 4.18. Soil particles (stress points) are labeled by subscript index a; while those particles used to represent the solid boundary are labeled by i. The initial distances between soil particles and between solid particles are denoted by h_a and h_i, respectively. The value of h_a and h_i changes depending on the side discretization of the problem domain and parametric studies have been conducted to identify a suitable mesh-size to be adoped in this study. Based on the above assumption, the radial force acting between two particles can be calculated using the following equation,

$$\mathbf{f}_{a\to i}^{n} = \begin{cases} -k_{ai}^{n}\boldsymbol{\delta}_n - c_n \mathbf{v}_{ai}^{n} & h_a + h_i > 2d_{ai} \\ 0 & h_a + h_i \le 2d_{ai} \end{cases} \tag{4.21}$$

where k_{ai}^{n} is the radial stiffness; δ_n is the allowable overlapping distance between two particles; c_n is the radial damping coefficient; v_{ai}^{n} is the relative radial velocity vector between particle *a* and particle *i*; h_a and h_i are the initial separation between soil particles and between boundary particles, respectively, and $h_a = h_i$ is assumed in this study; and d_{ai} is the distance between particles *a* and *i*.

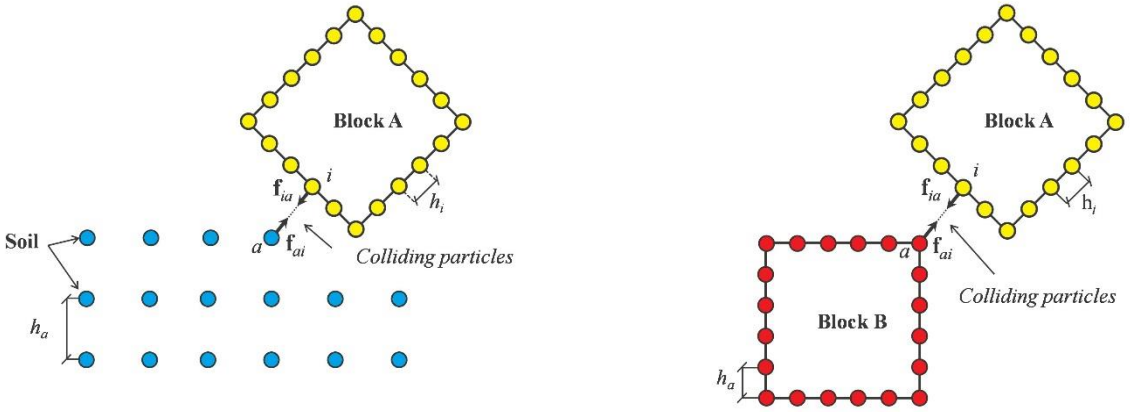

Figure 4.18: *Contact model between soil and retaining wall blocks and between blocks*

The overlapping distance and radial damping coefficient can be calculated using the following relationships,

$$\delta_n = d_{ai} - (h_a + h_i)/2 \tag{4.22}$$

$$c_n = 2\sqrt{m_{ai} k_{ai}^{n}} \tag{4.23}$$

where m_{ai} is the effective mass of soil and solid particles, which is calculated by

$$m_{ai} = (m_a + m_i)/2 \tag{4.24}$$

The contact force in the shear direction which is perpendicular to the radial direction can be calculated in the same manner,

$$\mathbf{f}_{a\to i}^{s} = \begin{cases} -k_{ai}^{s}\boldsymbol{\delta}_s - c_s \mathbf{v}_{ai}^{s} & h_{ai} > 2d_{ai} \\ 0 & h_{ai} \le 2d_{ai} \end{cases} \tag{4.25}$$

where k_{ai}^{s} is the shear stiffness which is taken similar to k_{ai}^{n} (Cundall & Strack, 1979); δ_s is the relative shear displacement between the two particles; c_s is the shear damping coefficient; v_{ai}^{s} is the relative shear velocity vector between particle *a* and particle *i*. The relative shear displacement and shear damping coefficient are,

$$\delta_s = \int \mathrm{v}_{ai}^{s} dt \tag{4.26}$$

$$c_s = 2\sqrt{m_{ai} k_{ai}^{s}} \tag{4.27}$$

The current shear force must satisfy Coulomb's friction law which implies that the shear force must not exceed the maximum resisting force,

$$\mathrm{f}_{a\to i}^{s} \le \mu \frac{\delta_s}{|\delta_s|} \left| \mathrm{f}_{a\to i}^{n} \right| \tag{4.28}$$

where μ is the friction coefficient. The above contact model consists of five parameters: stiffnesses in the normal and shear direction, damping coefficient and friction coefficient. Following the approach proposed by Cundall & Strack (1979), the shear stiffness is taken similar to the normal one; the damping coefficients are specified based on Equations (2.23) and (2.27) with the mass being calculated as the production of the initial particle volume to density. The normal stiffness and friction coefficient are only parameters need to be calibrated. For instance, the friction coefficient can be specified from direct shear test between two blocks or between blocks ad soils; while the normal stiffness should be calibrated from a dropping experiment, in which a block is brought to a certain high and dropped under gravity and numerical is conducted to obtain the same bouncing solution. The damping coefficient can be also adjusted from this test. These forces are finally added to Equation (4.2), Equation (4.18) and Equation (4.19) to progress the motion of soil and wall block.

4.4. SIMULATION OF BLOCK RETAINING WALL COLLAPSE USING SPH

The model test shown in Figure 4.9 was simulated using 11,304 SPH particles arranged in a rectangular lattice with an initial separation of 0.25cm. Rigid blocks were created by placing boundary particles uniformly around the boundary at a constant

distance. In order to simulate the smooth surface, half of particle spacing was chosen for the rigid body boundary particles. Model ground parameters including elastic modulus E = 5.84MPa, Poisson's ratio ν = 0.3, friction angle ϕ = 21.9^o, dilatant angle ψ = 0^o, and cohesion c = 0kPa were taken similar to those measured by Umezaki et al. (Umezaki et al., 2005). The unit weight of the ground model is γ_s = 20.4kN/m3. In addition to the ground parameters, parameters for the linear contact model needed to be specified. In this work, the radial and shear stiffness were assumed to be $k_{ai}^n = k_{ai}^s = 10^9\, N/m$, which is commonly accepted in DEM simulations (Bui et al. 2009). We noted that our numerical results are not sensitive to the stiffness coefficient of higher than 10^9N/s. The friction coefficients between the ground model and the block, between the rigid blocks, and between the block and the bases of the wall boundary were taken similar to those measured in the sliding tests as explained in the experimental section, in which the friction coefficient between wall blocks is taken to be 0.31, between retaining wall blocks and soils is 0.38 and between wall block and the bottom boundary is 0.40 The boundary conditions for the model ground are restrained with a roller boundary at the lateral boundaries and fixed in both directions at the base (Bui et al., 2008).

Figure 4.19 shows the comparison between the experiment and the computation for the final configuration of the MRW system after collapse. It can be seen that the computed result could predict fairly well the behavior of all rigid blocks observed in the experiment after the MRW system was collapsed. The good agreement between experiment and simulation can be attributed to the fact that the complete degrees-of-freedom of the rigid wall was taken into consideration in the simulation and large deformation and post-failure behavior of soil could be simulated well in the current SPH framework.

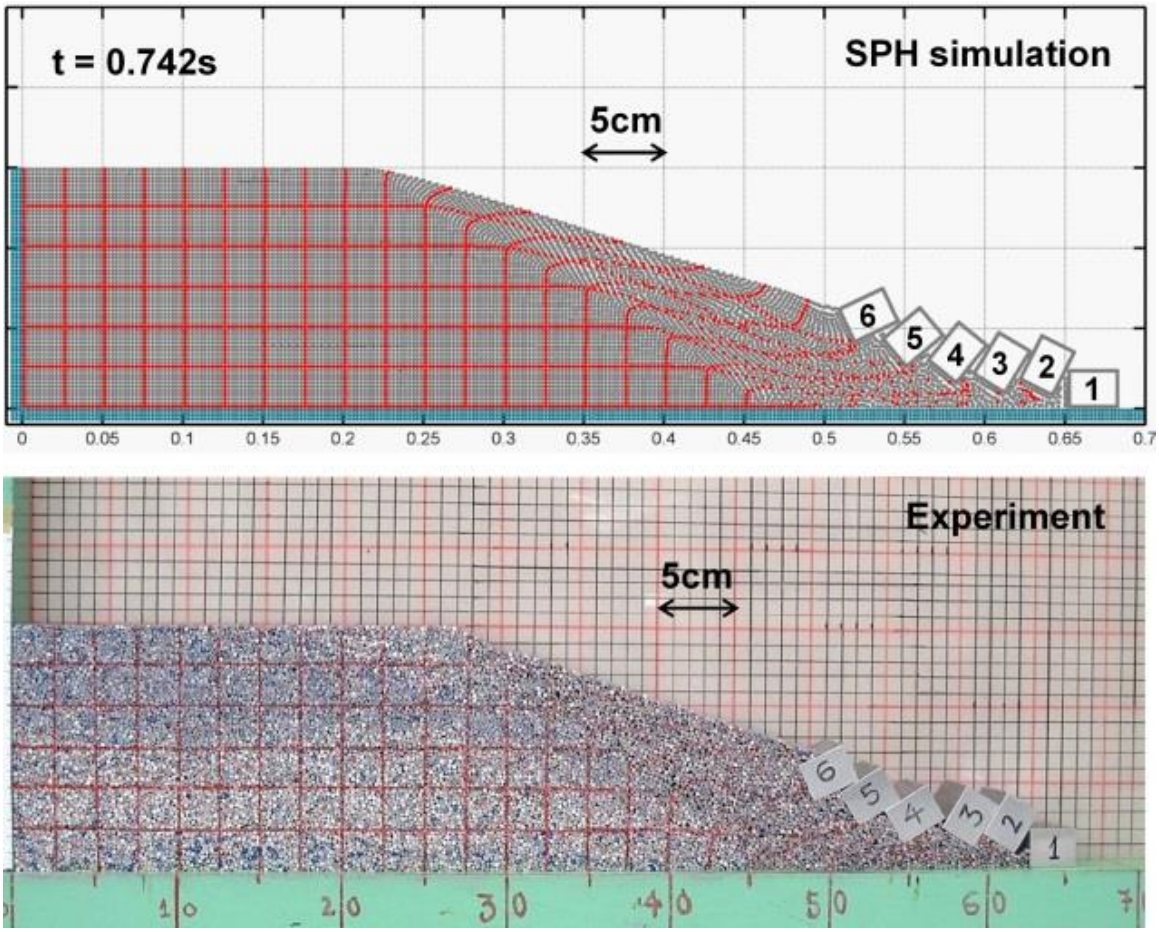

Figure 4.19: *Comparison between the SPH simulation and the experiment for the final configuration of the MRW system.*

Comparing the final run-out distance of each block, for instance Block No.1, it can be seen that the final position (right edge) of Block No.1 in the simulation is approximately ~68.3cm from the left-most solid boundary. This result is in fairly good agreement with that observed in experiment which was approximately ~66.2cm. This suggests that the proposed numerical framework could be applied to simulate the soil-structure interaction in the MRW system. However, further refinement of the contact model should be considered to provide a more theoretical sound framework to specify the parameters for the contact model.

4.5. CONCLUSION

This chapter presents my research on post- failure of MRWs using both laboratory experiments (in section 4.2) and the numerical simulation by using SPH method (in section 3). Series of experimental on post- failure of MRWs was implemented with the

different heights of MRW (The heights are 3, 4, 5 and 6 modular-blocks). With each height of MRW, there are experiments with the overlapping values between modular-blocks are 12, 16, 18, 20, 22, 24, 26 and 28 mm in turn. Each experiment is repeated six times. Most the experimental results are recorded by high speed camera. So the results of my experimental would be a good data to verify numerical models and used to compare with experimental results of other authors. The experimental results also show that the retaining wall's slope (depending on the overlapping value) has a great influence on its stability and destruction mechanisms. Specifically, with the height of 4 modular - blocks, the experimental results show that the retaining wall's stability depends on its slope. Furthermore, this slope also affects the MRWs' destruction mechanism because the slope of retaining wall directly affects the friction force between its blocks as well as lateral earth pressure on the retaining wall. To establish a complete set of data for verifying numerical models, apart from experiments on post- failure of MRWs I have done another series of experiments to determine the friction, bocks jumping coefficient as well as done experiments on motion of the blocks as described in Section 4.2.

Also in this chapter, the first SPH method approach for simulation of large deformation and post-failure of MRW is presented. It was shown that the proposed method provides good agreement with the experimental results. One of the key advantages of the proposed method is that the complete degrees-of-freedom of the retaining wall blocks, which could not be simulated using traditional numerical approaches such as finite element method, can now be simulated in the proposed numerical framework.

The results of numerical simulation correctly reflect the final result of the MRWs' destruction. In the future, I will continue improving this model to simulate correctly the destruction mechanism of MRWs both in space and time as the shown experimental results of 4 modular – blocks height. The purpose of this study is to develop the SPH numerical model to study and optimize the different MRWs helping the design of anti-landslides MRWs. Moreover, in order to broaden the application of the proposed numerical approach in geotechnical engineering, generalized contact model is necessary.

REFERENCES

[1] Belytschko T., Lu Y.Y., and Gu L.; "Element-free Galerkin methods", *Int. J. Numer. Meth. Eng.*, Vol.**37**, pp.229–256 (1994)

[2] Blanc T., and Pastor M.; "A stabilized smoothed particle hydrodynamics, Taylor-Galerkin algorithm for soil dynamics problems", *Int. J. Numer. Anal. Meth. Geomech.*, Vol.**37**, pp.1-30 (2013)

[3] Bui H.H., Sako K., and Fukagawa R.; "Numerical simulation of soil-water interaction using smoothed particle hydrodynamics (SPH) method", *J. Terramecha.*, Vol.**44**, pp.339-346 (2007)

[4] Bui H.H., Fukagawa R., Sako K.. and Ohno S.; "Lagrangian mesh-free particle method (SPH) for large deformation and post-failure of geomaterials using elastic-plastic soil constitutive model", *Int. J. Numer. Anal. Meth. Geomech.*, Vol.**32**, pp.1537–1570 (2008)

[5] Bui H.H., Kobayashi T., Fukagawa R., Wells J.C.; "Numerical and experimental studies of gravity effect on the mechanism of lunar excavations", *Journal of Terramechanics*, Vol.**46**, 115–124 (2009)

[6] Bui H.H., Fukagawa R., and Sako K.; "Slope stability analysis and discontinuous slope failure simulation by elasto-plastic smoothed particle hydrodynamics (SPH)", *Géotechnique*, Vol.**61**, pp. 565-574 (2011a)

[7] Bui H.H. and Fukagawa R.; "An improvement of SPH for saturated soils and its application to investigate the mechanisms of embankment failure: Case of hydrostatic pore-water pressure", *Int. J. Numer. Anal. Meth. Geomech.*, Vol.**37**, Issue 1, pp.31-50 (2011b)

[8] Cundall P.A. and Strack O.D.L.; "A discrete numerical model for granular assemblies", *Géotechnique*, Vol.**29**, pp.47-65 (1979)

[9] Gingold R.A. and Monaghan J.J.; "Smoothed particle hydrodynamics: Theory and application to non-spherical stars", *Mon. Not. Roy. Astron. Soc.*, Vol.**181**, pp.375-389 (1977)

[10] Harlow F.H., Ellison M.A., and Reid J.H.; "The particle-in-cell computing method for fluid dynamics", *Meth. Comput. Phys.*, Vol.**3**, pp.319–343 (1964)

[11] Mindlin RD.; "Compliance of elastic bodies in contact", *Appl. Mech. Trans. ASME*, **16**:259-67 (1949)

[12] Mindlin RD, Deresiewicz H.; "Elastic spheres in contact under varying oblique forces", *J. Appl. Mech. Trans. ASME*, 20:327-44 (1953)

[13] Monaghan J.J. and Lattanzio J.C.; "A refined particle method for astrophysical problems", *Astrono. Astrophys.*, Vol.**149**, pp.135-143 (1985)

[14] Monaghan, J.J., Kos, A., Issa, N.; "Fluid motion generated by impact", *J. Waterway, Port Coastal and Ocean Engng.*, Vol.**129**, 250–259 (2003)

[15] Monaghan J.J.; "SPH elastic dynamics", *Comput. Methods Appl. Mech. Eng.*, Vol.**190**, pp.6641-6662 (2003)

[16] Pastor M., Haddad B., Sorbino G., Cuomo S., and Drempetic V.; "A depth-integrated, coupled SPH model for flow-like landslides and related phenomena", *Int. J. Numer. Anal. Meth. Geomech.*, Vol.**33**, pp.143-172 (2009)

[17] Shi G.H.; "Discontinuous deformation analysis: a new numerical model for the static and dynamics of block systems", Ph.D. Thesis, University of California, Berkeley (1988)

[18] Sulsky D., Chen Z., and Schreyer H.L.; "A particle method for history-dependent materials", *Comput. Methods Appl. Mech. Eng.*, Vol.**118**, pp.179-196 (1994)

[19] Strzalko, J., Grabski, J., Perlikowski, P., Stefanski, A., Kapitaniak, T.: "General Motion of a Rigid Body", *Lect. Notes Phys.*, **792**, 23–39 (2010)

[20] Tsuji Y, Tanaka T, Ishida T.; "Lagrangian numerical simulation of plug flow of cohesionless particles in horizontal pipe", *Powder Technology*, **71**:239-50 (1992)

[21] Umezaki T., Kawamura T., and Ochiai H.; "Increment of Confining Pressure Due To Pull-out of Reinforcement and Modelling of Reinforcing Mechanics", *Geosynth. Eng. J.*, Vol.**20**, pp.241-248 (2005) (in Japanese)

CHAPTER 5

CONCLUSIONS AND FUTURE WORKS

5.1. CONCLUSIONS

This dissertation deeply studies the mechanism of the landslide process and the failure of the anti-landslide blocked retaining system. The studies were conducted by both experimental and numerical simulation methods.

The series of experiments were performed and analyzed to find experimental functions. They were also used to verify our developed and renovated numerical model. The calculation results of renovated mesh-free SPH method truly reflect the failure mechanisms of the slope and retaining wall system. This shows that the numerical model has a high reliability.

The dissertation presents some new research results. These results are mainly focused on the following three basic contents:

- The dissertation has conducted a series of experiments on the failure of 2D granular columns and block retaining wall system. The process of experimental implementation is recorded by high speed camera. This is a good source of data allowing other researchers to compare with their results or verify their numerical models. Based on the results of experiments, the dissertation has found experimental functions. The difference between the functions in my dissertation and by other researchers is that mine is built based on truely two-dimensional experiments while the others are built on the quasi two-dimensional simulation experiments. The results have been published in the Journal of Chemical Engineering of Japan.

- The dissertation has improved the SPH approach for calculating and forecasting the landslide process. Artificial viscosity used to stabilize the numerical model in the SPH approach is replaced by a combining viscous damping with stress/strain regularisation that is proposed for simulations of granular flows. This improvement helps to reduce the difficulties in choosing the unknown parameters when using artificial viscosity. The renovated SPH approach can correctly predict not only the failure mechanism, but also the failure process of slope. The renovated SPH approach has also overcame quite well the interference of stress field that has in previous calculations. The renovated SPH model has been published in Landslide.

- This dissertation also deeply studies the failure mechanism of the MRWs by experiment model and numerical simulation. The experimental results show its characteristics. The SPH numerical model in this dissertation also recommends the interactive mechanism between soil and rigid body. This interaction mechanism allows simulating the movement of rigid body in both transitive and rotational movements. This is a new point of the thesis. Part of research results in this chapter have been published in the International Journal of GEOMATE.

My thesis has achieved some research results on landslide problem. They are the post- flow failure of debris flow and failure mechanism of MRWs. But research in the thesis remains restricted due to no consideration to the effect of pore-water pressure during the post -flow failure. The numerical simulation for MRWs just assessed post-flow failure by only failure mechanism of MRWs. To simulate correctly many failure mechanisms as the experimental results of MRWs both in space and time, I need to continue working on it in the near future.

5.2. FUTURE WORKS

5.2.1. Numerical Experiments

My experiments on the failure of 2D granular columns and the MRWs are performed many times in the laboratory. I have also determined the experimental functions. However, experiments in the laboratory takes time and cost to perform, not mention to many cases that can't perform experimentally or have inaccurate results due to influence of many factors. Therefore next time, I will use the numerical model to do some series of numerical experiments. By this way, I hope to find out correct experiment functions for any size of 2D granular columns. Moreover, with this approach we can

conduct experiments with different materials. From the numerical experiment results, it's highly possible that a new form of suitable empirical functions can be identified for a different material.

Figures 5.1 and 5.2 shows the results of numerical experiments using the improved SPH model to simulate granular flow with different internal friction angle of material.

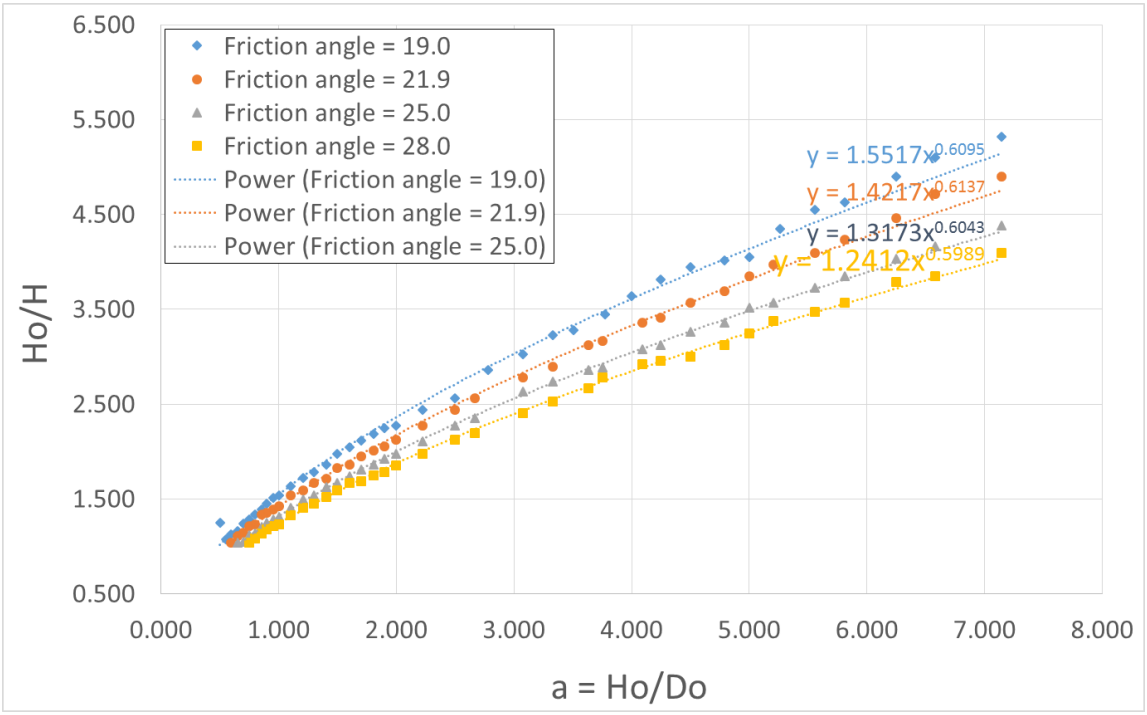

Figure 5.1: *Results of Numerical Experiment*

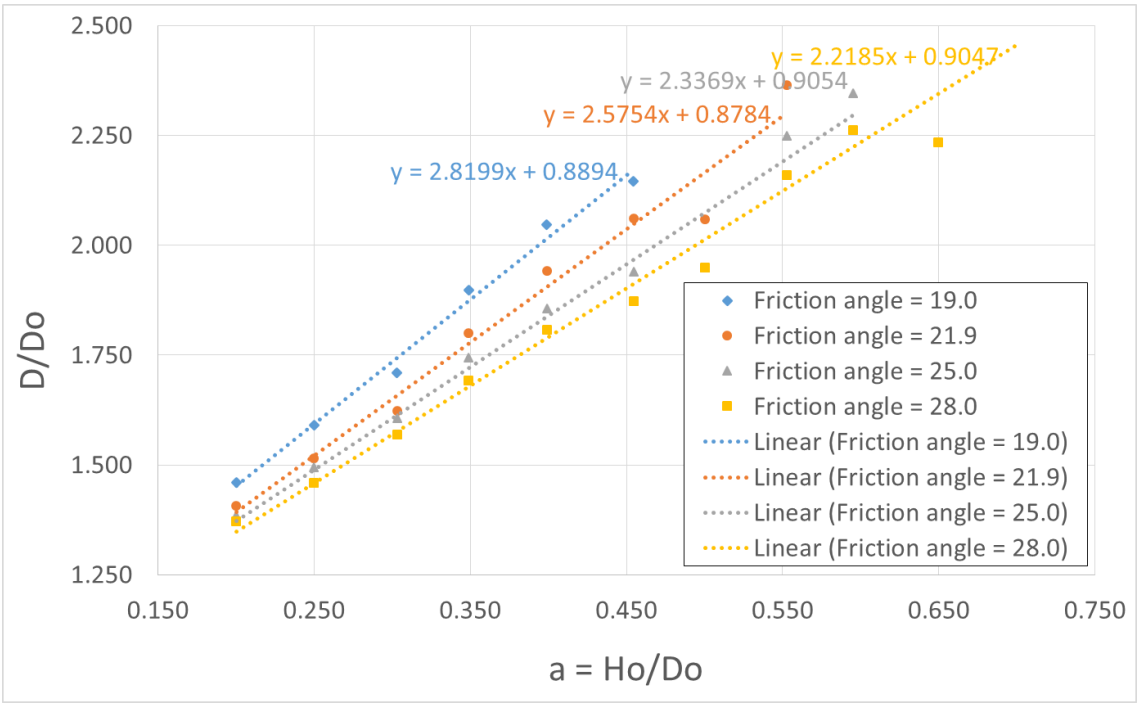

Figure 5.2: *Results of Numerical Experiment*

5.2.2. Extent to study 3D problems

Figure 5.3: *Scene of some landslides*

The 2D experiment results presented in this thesis will be a useful database for other researchers to verify their 2D numerical models under the plain-strain conditions. This is an important step in computational developments to justify an appropriate use of a computational model for geotechnical applications. On the other hand, for real life applications, validations with 3D data field data are required. As per, validations of the proposed SPH framework for granular flows are further needed to be conducted under the 3D field conditions. We can easily see from Figure 5.3 that granular flows in landslide events often tend to expand in the later stage of the the run-out process. The expansion at the toe of granular flows will reduce the run-out distance of granular flows. Furthermore, materials in the real life are often wet materials. Thus, further developments of the proposed SPH framework considering pore-fluid coupling will be undertaken to improve the predictive capability of the SPH model for real life applications. In addition, 3D experiments using wet materials will also need to be conducted to validate the proposed SPH framework at the laboratory scale, before applying the method to larger scales.

In the near future, we will also study the failure mechanism of 3D modular-block retaining wall system (MRWs) by numerical simulation using the prosed SPH method. Therefore, 3D laboratory experiments of MRWs will be conducted to validate the proposed numerical method.

5.2.3. Application of High Performance Computing Techniques

Currently, due to the limitation of computer capacity for calculating big problems, the simulation by mesh-free SPH approach takes lot of time. Therefore, in the near future, besides continuing to improve the existing numerical model, I will study and apply some high-performance computing techniques to speed up the computing of the model and take advantage of computer resources.

The methods of high performance computing today can typically include MPI (Message Passing Interface), OpenMP (Open Multi-Processing) and GPUs (Graphics Processing Units). In which MPI is the computing method based on distributed memory platform, which is used to exploit the potential of computer systems connected together via high speed LAN. OpenMP is a calculating method based on shared memory platform. The advantage of OpenMP is to take full advantage of multi-core technology of current microprocessors. However it can also be restricted to compute on a mainboard. In recent years, a new computing technique based on GPUs graphics technology platform has been applied much in engineering. This technology has an advantage with an ability of good computing despite of its low cost.

Currently, OpenMP technology is used extensively in softwares running on a personal computer or workstation. The super-computers of large computing centers often combines two or all three methods as listed above.

To increase computing performance of SPH approach I will apply two methods as OpenMP and GPUs. The two computing techniques are set in the form of option for users to choose from. In case the high performed graphic card computer is equipped, the GPUs method is activated. In contrast, the OpenMP method will be activated.

PUBLICATIONS

List of Journal Papers:

1. **Cuong T. Nguyen**, Chi T.Nguyen, Ha H. Bui, Giang D. Nguyen, and Ryoichi Fukagawa: "A new SPH based approach to simulation of granular flows using viscous damping and stress regularisation", ***Landslide***, online published 2016, DOI:10.1007/s10346-016-0681-y
   http://link.springer.com/article/10.1007/s10346-016-0681-y

2. **Cuong T. Nguyen**, Ha H. Bui, Ryoichi Fukagawa.; "Failure mechanism of 2D granular flows: Experiment", ***Journal of Chemical Engineering of Japan***, Vol. 48, No. 6, pp. 395–402, 2015
   DOI: http://doi.org/10.1252/jcej.14we358

3. **C.T. Nguyen**, Ha H. Bui, R. Fukagawa: "Two-Dimentional Numerical Modelling of Modular-Block Soil Retaining Walls Collapse Using Meshree Method", ***International Journal of GEOMATE*** (ISSN: 2186-2982(P), 2186-2990(O)), Vol.5, No1, pp.647-652, 2013.
   http://www.geomatejournal.com/sites/default/files/articles/647-652-3329-Cuong-sept-2013.pdf

4. **Nguyen Tien Cuong**, Bui Hong Ha, Ryoichi Fukagawa : "Failure Mechanism of Two-Dimensional Granular Columnns: Numerical Simulation and Experiments", ***Vietnam Journal of Mechanics***, VAST, Vol. 37, No. 4, 2015
   DOI: 10.15625/0866-7136/37/4/5844

5. Samuel J. Verghese, **Cuong T. Nguyen**, Ha H. Bui: "Evaluation of Plasticity-Based soil constitutive models in simulation of Braced excavation", ***International Journal of GEOMATE*** (ISSN: 2186-2982(P), 2186-2990(O)), Vol.5, No2, pp.672-667, 2013.
   http://www.geomatejournal.com/sites/default/files/articles/672-677-3328-Ha%20Bui-Dec-2013.pdf

List of Refereed Conference Papers:

1. **Cuong T. Nguyen**, Ha H. Bui and R. Fukagawa; "Experimental study of the two-dimensional granular column collapse", ***The 3rd International Conference on Engineering Mechanics and Automation*** - ICEMA 3 (ISBN: 978-604-913-367-1), pp.132-139, 2014.

2. **C.T. Nguyen**, Ha H. Bui, L.V. Hoang, R. Fukagawa: "A SPH model for simulation of Seepage flow through rigid porous media", ***Proceedings of The 14th Asia***

Congress of Fluid Mechanics - 14ACFM (ISBN: 978-604-913-145-5), Vol. 1, pp.383-388, 2013.

3. **C.T. Nguyen**, Ha H. Bui, A. Oya, N. Hiraoka, R. Fukagawa: "Box-Shape Retaining Wall system: Experiment and Numerical Prediction", ***Geotechnique, Construction Materials and Environment*** (ISBN: 978-4-9905958-2-1 C3051), Vol.3, No.1, pp.298-303, 2013.

4. Ha H. Bui, **C.T. Nguyen**, K. Sako, R. Fukagawa: "An investigation of riverbank failure due to water level changes using two-phase flow SPH model", ***The 13th International Association for Computer Methods and Advance in Geomechanics*** (IACMAG), Volume 1, pp.116-123, 2011.

5. Ha H. Bui, **C.T. Nguyen**, K. Sako, R. Fukagawa: "A SPH model for seepage flow through deformable porous media", ***The 6th International Smoothed Particle Hydrodynamics European Research Interest Community (SPHERIC)***, pp.164-171, 2011.

List of Conference Presentations:

1. **C. T. Nguyen**, H. H. Bui and R. Fukagawa: "An improvement of SPH method to Simulate Failure mechanism of 2D Franular flows", ***Proceedings of the 5th Vietnam/Japan Joint Seminar on Geohazards and Environmental Issues***, Kusatsu, Shiga, Japan, March 13, 2015.

2. L. V. Hoang, **C. T. Nguyen** and R. Fukagawa: "Dyke systems in Vietnam and Some problems for Sustainable development", ***Proceedings of the 5th Vietnam/Japan Joint Seminar on Geohazards and Environmental Issues***, Kusatsu, Shiga, Japan, March 13, 2015.

3. **C. T. Nguyen**, H. H. Bui, L. V. Hoang and R. Fukagawa: "Two dimensional experiments about collapse of soil columns and box-shape retaining wall system", ***Proceedings of the 4th Vietnam/Japan Joint Seminar on Geohazards and Environmental Issues***, Ho Chi Minh city, Vietnam, March 12, 2014.

4. L. V. Hoang, **C. T. Nguyen** and R. Fukagawa: "Reservoir Regulation and some related problems in Red river system", ***Proceedings of the 4th Vietnam/Japan Joint Seminar on Geohazards and Environmental Issues***, Ho Chi Minh city, Vietnam, March 12, 2014.

5. Ha H. Bui, **C.T. Nguyen,** R. Fukagawa: "Coupled DEM-SPH modelling of two phase fluid solid mixture: A potential approach for study riverbank erosion at the grain scale", ***Proceedings of the 3rd Vietnam/Japan Joint Seminar on Geohazards and Environmental Issues***, Sendai city, Japan, March 14, 2013.

6. **C.T. Nguyen,** L.V. Hoang, Ha H. Bui, and R. Fukagawa: "Situation of landslide and river bank erosion in Vietnam and some studies to control morphology of river channel", ***Proceedings of the 3rd Vietnam/Japan Joint Seminar on Geohazards and Environmental Issues***, Sendai city, Japan, March 14, 2013.

7. Ha H. Bui, J. Kodikara , **C.T. Nguyen,** K. Sako, R. Fukagawa: "An improvement of SPH to correctly predict riverbank failure", ***Proceedings of the 2nd Vietnam/Japan Joint Seminar on Geohazards and Environmental Issues***, Ho Chi Minh city, Vietnam, March 13, 2012.

8. Ha H. Bui, K. Sako, R. Fukagawa, **C.T. Nguyen**: "A two-phase flow SPH model and its application to simulate seepage induced embankment failure", ***Proceedings of the 1st Vietnam/Japan Joint Seminar on Saigon Riverbank Erosion***, Kusatsu, Shiga, Japan, March 08, 2011.